



# THE UNIVERSITY *of* EDINBURGH

This thesis has been submitted in fulfilment of the requirements for a postgraduate degree (e. g. PhD, MPhil, DClinPsychol) at the University of Edinburgh. Please note the following terms and conditions of use:

- This work is protected by copyright and other intellectual property rights, which are retained by the thesis author, unless otherwise stated.
- A copy can be downloaded for personal non-commercial research or study, without prior permission or charge.
- This thesis cannot be reproduced or quoted extensively from without first obtaining permission in writing from the author.
- The content must not be changed in any way or sold commercially in any format or medium without the formal permission of the author.
- When referring to this work, full bibliographic details including the author, title, awarding institution and date of the thesis must be given.

**SCHOOL OF CHEMISTRY**  
**THE UNIVERSITY OF EDINBURGH**



---

**Synthesis of Novel Polymers of Intrinsic Microporosity  
for Gas and Vapour Adsorption**

---

Thesis submitted for the degree of Doctor of Philosophy by:

**Wan Ting (Emily) Xu**

**Supervisor: Neil B. McKeown**

**2024**

## Declaration

### **Statement 1**

This work has not been submitted in substance for any other degree or award at this or any other university or place of learning, nor is it being submitted concurrently in candidature for any degree or other award.

Signed ..... (candidate)

Date .....

### **Statement 2**

This thesis is being submitted in partial fulfilment of the requirements for the degree of Doctor of Philosophy.

Signed ..... (candidate)

Date .....

### **Statement 3**

This thesis is the result of my own independent work/investigation, except where otherwise stated. Other sources are acknowledged by explicit references. Any views expressed are my own.

Signed ..... (candidate)

Date .....

### **Statement 4**

I hereby give consent for my thesis, if accepted, to be available for photocopying and for inter-library loan, and for the title and summary to be made available to outside organisations.

Signed ..... (candidate)

Date .....

## Acknowledgment

First and foremost, I would like to express my gratitude to my supervisor, Professor Neil McKeown, for offering me the opportunity to take on this project and for his extensive guidance and support throughout my PhD study. I would also like to thank DTRA for funding my project. Additionally, my heartfelt appreciation goes to my post-docs, John and Dominic, for their extensive support especially during my write-up period. A very special thank you to Chun Chun for helping me regain my confidence and motivation during difficult times. I would also like to express my gratitude to the former group members of MCK, for all the chemistry helps as well as the great parties.

I am also thankful for those who were present in my life during the 5 years of my PhD study, making this experience as memorable as it was. A special appreciation goes to Kimia who has started and finished this special journey alongside of me. I will forever cherish all the memories we created together, including those slightly demoralising 'all-nighter' sessions in the lab! I would also like to express my appreciation for Anli, for always being there for me during the most stressful time of this journey. I don't think I could have survived my final year without the emotional support and cheering up from her. Additionally, a huge thank you goes to all my friends outside the research group, especially my former flatmates: Weiwei for those midnight city strolls during the lockdown, cooking sessions that always lasted way too long, and chatting sessions that lasts through dusk and down; Rob and Ayushi for being the best 3-in-1 combo (flatmates/colleagues/friends) I could have ever asked for, who have turned my otherwise daunting part-time residential assistant job into an enjoyable activity. Those short and long kitchen chats after a long day have always helped me recharge and will always remain as one of the biggest highlights during my time in Edinburgh. Moreover, I'd like to thank Ayesha for all the fun demonstration session banter and being my designated Japanese food/bubble tea/baking buddy!

Finally, I would like to thank my mum and dad, and friends back home, who has been the most strong and reliable support network I could ever dream of. Most importantly, my late granddad who was the one that ignited a spark in the young me to become a Doctor and have always encouraged me to achieve my dreams. Furthermore, a wee thank you (and apologies) for my guinea pigs Cotton and Charcoal, for putting up with me at very random hours and adapt to my hectic schedule. Appreciation also needs to go to hexane, for always being the solvent that saves the day for me. And lastly, I would like to send a special message to my dog Beibei who has sadly passed away just a few months before I finished my PhD, it's such a shame that I didn't get to say goodbye to you, and that I can no longer share my joys with you, but I hope you are having a great time in doggy heaven right now!

## Lay Summary

Adsorption is a powerful process that helps capture and remove substances from different environments, which plays a crucial role in many areas of technology. The ability to efficiently capture and remove pollutants, contaminants, and toxic substances from air, water, and industrial processes, alongside its ease of operation and low cost, makes the adsorption technology pivotal, especially for environmental remediation, which is an issue that is becoming increasingly significant as our society continues to advance.

Given their significant importance in various applications, there is a growing demand for the development of cost-effective and highly efficient adsorbent materials. Within the broad spectrum of materials available for adsorption, polymers of intrinsic microporosity emerge as particularly promising adsorbents. This class of microporous organic polymers possesses excellent surface area and a narrow range of pore sizes, ensuring high adsorption capacity and enhanced selectivity. While adaptable nature of this class of polymers makes it easy to customise their characteristics for specific purposes. Additionally, PIMs exhibit features highly desirable for commercialization, such as superb solution processability and high chemical and thermal stability, granting the material excellent recyclability. This project aims to explore ways through which the adsorption performances of PIMs can be further enhanced, specifically for applications such as the capture of CO<sub>2</sub>, through incorporating additional functionalities, and the development of structural units designed to strengthen PIMs performance in specific areas.

## Abstract

Polymers of intrinsic microporosity (PIMs) are a class of highly porous polymeric materials, within which the microporosity originates from the inability of the rigid and contorted polymeric chains to pack efficiently. PIMs exhibit outstanding solution processability, large surface areas and great structural tunability, which makes them promising materials for a range of applications, such as gas separation, catalysis and sensors. Furthermore, their highly porous nature, along with gas separation performances, makes PIMs excellent materials for gas adsorption applications, which includes the capturing and storage of CO<sub>2</sub>, and the deactivation of chemical warfare agents (CWAs), as they can efficiently store a significant volume of adsorbate in their pores, which are flexible due to the lack of a covalent network structure. Additionally, their macromolecular structures can be tailored to show special selectivity towards the target gases.

The project described in this thesis explored ways to further enhance the gas adsorption properties of PIMs, via three approaches. First, the incorporation of additional basic, and nucleophilic functionality onto PIMs was investigated to induce additional acid-base interactions with acidic gases such as CO<sub>2</sub>, and the potential catalytic reactivity towards electrophilic compounds such as organophosphorus-based CWAs. A PIM containing pyridine units was synthesised, and further functionalised with amidoxime groups. The effect of the basic and nucleophilic functional groups incorporation on PIMs were studied by comparing their polymer properties, and performances in areas such as CO<sub>2</sub> adsorption, CWA deactivation, and gas separation of the synthesised polymers against that of related PIM-1 and AO-PIM-1. Secondly, the synthesis of the extremely bulky and rigid structural unit, naphthopleiadene (NP), with in-built amine functionalities was explored to enhance the porosity of PIMs, and to increase the affinity of polar gases such as CO<sub>2</sub> towards PIMs. Finally, the synthesis of some -CF<sub>3</sub> containing monomers were attempted. These fluorinated PIMs were expected to minimise interactions between polymeric chains, thus offering the possibility of altered solubility, and reducing the impact of weak interchain interactions on the porosity, and further enhance the hydrophobicity of PIMs to increase their selectivity of the target gas molecules over water vapours.

## Abbreviations

|              |   |
|--------------|---|
| <b>3D</b>    | Three dimensional                                 |
| <b>AC</b>    | Activated carbon                                  |
| <b>AO</b>    | Amidoxime   |
| <b>BET</b>   | Braunauer-Emmett-Teller                           |
| <b>COFs</b>  | Covalent Organic Frameworks                       |
| <b>CWAs</b>  | Chemical warfare agents                           |
| <b>DCM</b>   | Dichloromethane                                   |
| <b>DIC</b>   | diisopropylcarbodiimide                           |
| <b>DMAP</b>  | 4-dimethylaminopyridine                           |
| <b>DMF</b>   | Dimethylformamide                                 |
| <b>DMNP</b>  | Dimethyl-4-nitrophenylphosphate                   |
| <b>DMP</b>   | Dimethyl phosphate                                |
| <b>DMSO</b>  | Dimethyl sulfoxide                                |
| <b>EA</b>    | Ethanoanthracene                                  |
| <b>fmoc</b>  | 9-fluorenylmethyloxycarbonyl                      |
| <b>FT-IR</b> | Fourier-transform infrared spectroscopy           |
| <b>GD</b>    | Soman   |
| <b>GPC</b>   | Gel Permeation Chromatography                     |
| <b>h</b>     | Hour  |
| <b>HCl</b>   | Hydrochloric Acid                                 |
| <b>HCPs</b>  | Hyper-Crosslinked Polymers                        |
| <b>HD</b>    | Mustard gas                                       |
| <b>IMFV</b>  | Internal Molecular Free Volume                    |
| <b>ITM</b>   | Institute on Membrane Technology                  |
| <b>IUPAC</b> | International Union of Pure and Applied Chemistry |
| <b>M4NP</b>  | Methyl-4-nitrophenyl phosphate                    |
| <b>MOFs</b>  | Metal-Organic Frameworks                          |
| <b>Mp</b>    | Melting point                                     |
| <b>MS</b>    | Mass Spectrometry                                 |
| <b>NLDFT</b> | Non-local density functional theory               |
| <b>NMR</b>   | Nuclear magnetic resonance                        |
| <b>NP</b>    | Naphthopleiadene                                  |
| <b>PCPs</b>  | Porous Coordination Polymers                      |
| <b>PI</b>    | Polyimides  |
| <b>PIMs</b>  | Polymers of intrinsic microporosity               |
| <b>Py</b>    | Pyridine  |
| <b>r.t</b>   | Room Temperature                                  |
| <b>SA</b>    | surface area                                      |
| <b>SBF</b>   | Spirobifluorenes                                  |
| <b>SBI</b>   | Spirobisindane                                    |
| <b>SEM</b>   | Scanning electron microscopy                      |
| <b>TB</b>    | Tröger's base                                     |
| <b>TBAF</b>  | Tetrabutylammonium fluoride solution              |
| <b>TEM</b>   | Transmission Electron-Microscopy                  |

|                          |  |
|--------------------------|--|
| <b>TFPCN</b>             | 2,3,5,6-tetrafluoro-4-pyridinecarbonitrile                       |
| <b>TFTPN</b>             | Tetrafluoroterephthalonitrile                                    |
| <b>THF</b>               | Tetrahydrofuran  |
| <b>TMS</b>               | Trimethylsilyl   |
| <b>TMSCF<sub>3</sub></b> | Trifluoromethyltrimethylsilane                                   |
| <b>Trip</b>              | Triptycenes  |
| <b>TTSBI</b>             | 5,5',6,6'-Tetrahydroxy-3,3,3',3'-tetramethyl-1,1'-spirobisindane |



## Table of Contents

|   |    |
|---|----|
| Declaration.....  | 2  |
| Acknowledgment .....  | 3  |
| Lay Summary.....  | 4  |
| Abstract.....   | 5  |
| Abbreviations.....  | 6  |
| Table of Contents.....  | 8  |
| Chapter 1: Introduction .....                                 | 10 |
| 1.1    Porous Materials.....                                  | 10 |
| 1.2    Background Theory.....                                 | 10 |
| 1.2.1    Adsorption Mechanism .....                           | 10 |
| 1.2.2    Determination of Surface Area .....                  | 12 |
| 1.3    Microporous Materials .....                            | 13 |
| 1.3.1    Activated Carbons .....                              | 14 |
| 1.3.2    Zeolites .....                                       | 15 |
| 1.3.3    Metal-Organic Frameworks.....                        | 16 |
| 1.3.4    Covalent Organic Frameworks .....                    | 16 |
| 1.3.5    Hyper-Crosslinked Polymers .....                     | 17 |
| 1.4    Polymers of Intrinsic Microporosity .....              | 18 |
| 1.4.1    Current PIMs .....                                   | 20 |
| 1.4.2    Properties and Applications of PIMs.....             | 23 |
| Chapter 2 Project Aims .....                                  | 25 |
| Chapter 3 Amidoxime Functionalised Polymers .....             | 26 |
| 3.1    Synthesis of Model Compounds.....                      | 27 |
| 3.2    Polymer Synthesis.....                                 | 30 |
| 3.3    Polymer Analysis.....                                  | 31 |
| 3.4    Solution Processability.....                           | 34 |
| 3.5    Gas Separation Measurements .....                      | 37 |
| 3.5.1    Background of PIMs for Gas Separation Membranes..... | 37 |
| 3.5.2    Analysis of Gas Permeability Data.....               | 38 |
| Chapter 4 Naphthopleiadene-Based Monomers.....                | 42 |
| 4.1    Monomer Synthesis.....                                 | 44 |
| 4.1.1    Synthesis of 2,7-diaminonaphthalene.....             | 44 |
| 4.1.2    Protected 2,7-Diaminonaphthalene Derivatives.....    | 45 |
| 4.1.3    Amine-Containing Naphthopleiadenes.....              | 46 |

|   |   |     |
|---|---|-----|
| 4.2   | Polymer Synthesis.....  | 48  |
| 4.3   | Polymer Analysis.....   | 51  |
| Chapter 5 Synthesis of Fluorinated PIM Precursors ..... |   | 56  |
| 5.1   | Synthesis of Tetra(trifluoromethyl) Spirobisindane Monomers .....         | 57  |
| 5.1.1   | Synthesis of tetra(trifluoromethyl) precursors .....                      | 58  |
| 5.1.2   | Attempted Synthesis of Target Monomers.....                               | 59  |
| 5.2   | Alternative Routes to Tetra(trifluoromethyl) Incorporation.....           | 63  |
| 5.2.1   | Synthesis of Carbonyl-Containing Precursors for Trifluoromethylation..... | 64  |
| 5.2.2   | Attempted Trifluoromethyl Incorporation with TMSCF <sub>3</sub> .....     | 66  |
| 5.4   | Synthesis of Bis(trifluoromethyl) Monomer.....                            | 67  |
| 5.5   | Polymer Synthesis.....  | 69  |
| 5.5   | Polymer Analysis.....   | 71  |
| Chapter 6 Future Work .....                             |   | 75  |
| 6.1   | Amine-containing structural units.....                                    | 75  |
| 7.2   | Continuation of fluorinated monomer and polymer synthesis.....            | 77  |
| Chapter 7 Conclusion .....                              |   | 78  |
| Chapter 8: Experimental .....                           |   | 80  |
| 8.1   | Techniques.....   | 80  |
| 9.2   | General Procedures .....  | 81  |
| 9.3   | Amidoxime-functionalised polymers.....                                    | 82  |
| 9.4   | Amine-containing monomer and polymer synthesis .....                      | 86  |
| 9.5   | Fluorinated monomer and polymer synthesis .....                           | 94  |
| 9.6   | Future work .....   | 100 |
| References .....  |   | 104 |

## Chapter 1: Introduction

### 1.1 Porous Materials

Any solid materials which contain cavities, channels or interstices, where the depth of the free spaces is larger than their width can be described as porous. Porous materials are further classified into the following three sub-categories based on their predominant pore sizes, as defined by the International Union of Pure and Applied Chemistry (IUPAC):<sup>1</sup>

- i) Microporous – pores with a diameter of less than 2 nm.
- ii) Mesopores – pores with diameter between 2 to 50 nm.
- iii) Macropores – pores with a diameter of more than 50 nm.

Aside from their width, pores can also be categorised based on their shapes and accessibility to external fluids and gases. When a pore is completely isolated from its surroundings, it is described as a closed pore (**Figure 1.1 – a**). These pores impact the macroscopic properties such as the bulk density, mechanical strength and thermal conductivity. In contrast, an open pore has unhindered access to external fluids and gases (**Figure 1.1 – b-f**), which influence processes such as fluid flow and gas adsorption. There are several types of open pores, some have only one open end, which are described as blind pores, and can be of either an ink bottle shaped (**b**) or cylindrical (**f**). Pores with two open ends are described as through pores, they can be cylindrical (**c**), funnel shaped (**d**) or slit shaped (**e**).

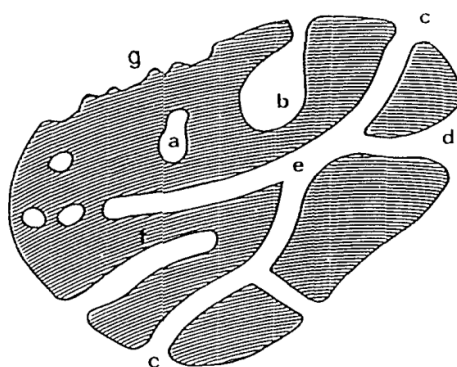


**Figure 1.1** Schematic cross-section of a porous solid.<sup>1</sup>

### 1.2 Background Theory

#### 1.2.1 Adsorption Mechanism

From removal of dyes and heavy metals in water sources to the capture of volatile organic compounds and CO<sub>2</sub> gas, adsorption is an important process that plays a key role in many industries.<sup>2-4</sup> The basic concept of adsorption is a mass transfer process where the substances accumulates at the interface of

two phases (*i.e.* liquid-liquid, gas-liquid, gas-solid).<sup>5</sup> The driving force of adsorption is the attraction between the adsorbates and the adsorbent material.

Depending on the nature of the interactions, the process of adsorption can be further categorised into two classes – physisorption and chemisorption. When the adsorbate molecules adsorb onto the surface of adsorbent, or into the pores of the adsorbent via weak, reversible intermolecular forces such as van der Waals interactions, the process is known as physisorption. The pore size and surface area of the adsorbent are important factors that controls physisorption. Due to the weak interactions between the adsorbent/adsorbates, physisorption is a reversible process where adsorbates bound to the material can be partially released; this phenomenon is known as desorption, which can occur at relatively low temperatures due to the weak interactions involved.<sup>6</sup> In contrast to physisorption, chemisorption is a process where the adsorbates interact with the adsorbent surface in a manner than resembles the formation of a chemical bond. This is especially prevalent for adsorbates that demonstrates acidic/basic properties, such as CO<sub>2</sub>, where they have the potential to form acid/base interactions with the adsorbent material. Unlike physisorption, the process of chemisorption is not easily reversible.<sup>7</sup>

The adsorption capacity of a material can be measured by determination of its adsorption isotherm, which defines the relationship between the quantity of adsorbed material and the amount of adsorbate remaining in the surrounding environment.<sup>8</sup> The adsorption capacity of the material for gaseous molecules is determined by measuring the amount of gas adsorbed by a known amount of adsorbent material, with increasing pressure over time at a constant temperature, until the maximum set pressure is reached. Adsorption is believed to occur as a layering process, where the adsorbates first occupy the material in a single layer, and as the pressure increases, multilayers of adsorbates will be formed. Many mathematical models are available to describe the adsorption process, and while most of these operate on the assumption that adsorbates occupy only a single layer on the material, a few take into consideration the formation of multilayers, out of which the Braunauer-Emmett-Teller (BET) model is one of the most widely used.<sup>8,9</sup> From the information obtained, other details such as the surface area of the material can then be calculated using the chosen calculation model, which will be discussed in more detail in the coming section.

Different types of porous materials will provide different adsorption isotherms due to the unique ways each type of material interact with the adsorbates. The various isotherms of porous materials can be summarized into six types according to IUPAC (**Figure 2.1**).<sup>10</sup> Type I isotherm is generally observed for microporous materials, where a combination of high surface area and multi-wall interactions offered by micropores enables large gas uptake at low partial pressure. After the initial

uptake, the curve flattens due to the coverage of the first monolayer, and the curve rises again upon additional layers being filled by adsorbates until saturation point is reached. Type II, III and VI isotherms are typically observed in nonporous and macroporous materials, whereas isotherms type IV and V are representative of mesoporous materials.<sup>11</sup>

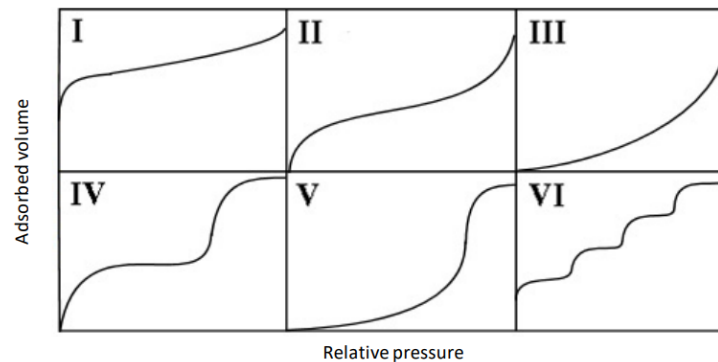
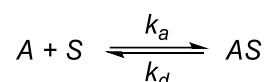


**Figure 2.1** The six types of isotherms for porous materials classified by IUPAC.<sup>10</sup>

### 1.2.2 Determination of Surface Area

Multiple methods of surface area determination for materials exist, for example optical methods,<sup>12</sup> and porosimetry with a non-wetting liquid (*e.g.* mercury).<sup>13</sup> However, the most widely used technique in modern research is that based on gas adsorption. The underlying principle of this technique is the reversible physisorption of gas molecules onto internal and external surfaces. If a known volume of gas molecules (adsorbate), such as N<sub>2</sub>, whose cross-sectional area are also known, is adsorbed onto the internal and external surface areas of the material until the formation of a monolayer, the apparent surface area can then be calculated. For the simplicity of discussion, N<sub>2</sub> will be used as the representative adsorbate for this section.

A number of mathematical models exist for the calculation of surface areas, the Langmuir model is the simplest isotherm model available, which assumes the ideal gas behaviour of the adsorbate. In a measurement, the free N<sub>2</sub> molecules (*A*) adsorb onto the accessible surfaces of the material (*S*) to form a volume of adsorbed species (*SA*) at rate  $k_a$ ; the N<sub>2</sub> molecules only interact with the material *via* weak intermolecular forces, which can then be easily reversibly desorbed at rate  $k_d$ :



The surface coverage of the material ( $\theta$ ) can be expressed as a fraction of the volume of gas adsorbed over amount of gas in one monolayer:

$$\theta = \frac{\text{Sites occupied}}{\text{Sites available}} = \frac{V_a}{V_m}$$

The rate of adsorption  $k_a$  is dependent on the pressure applied to the system (P), and the amount of uncovered surfaces of the material ( $N(1-\theta)$ ), and the rate of desorption is related to only the amount of covered surfaces ( $N\theta$ ). At equilibrium, the surface coverage of the material ( $\theta$ ) can be defined as:

$$\theta = \frac{KP}{1 + KP}, \text{ where } K = \frac{k_a}{k_d}$$

The above equation can be rearranged to the linear form of  $y = mx + c$ , which then enables the calculation of  $V_m$  from linear plots:

$$\frac{1}{V_m} = \frac{1}{KV_m} \left( \frac{1}{P} \right) + \frac{1}{V_m}$$

The Langmuir model alone is not an adequate method to calculate the surface of microporous materials, as the model operates on the assumptions that (i) the adsorption of gas occurs only as monolayer coverage, (ii) all accessible surfaces in the material are equal in size, (iii) there are no interactions between the adsorbate molecules, and (iv) that the adsorbate molecules do not move once adsorbed onto the material.<sup>14</sup> Using the Langmuir model as a foundation, the BET model, created by Brunauer, Emmett and Teller make an improvement on the accuracy of surface area prediction by introducing additional assumptions to the calculation:

- 1) gas molecules can physically adsorb onto the material in infinite layers,
- 2) the individual gaseous layers do not interact with each other, and
- 3) each individual gaseous layers obey the Langmuir theory.

The final form of BET surface area ( $S_{BET}$ ) calculation is the relationship between cross-sectional area of adsorbate molecule ( $\sigma$ ), mass of the sample ( $M$ ), the volume of gas in one monolayer ( $V_m$ ), and the volume occupied by adsorbate at standard temperature and pressure ( $V_{STP}$ ):

$$S_{BET} = \frac{V_m N_A \sigma}{MV_{STP}}, \text{ Where } N_A \text{ is Avogadro's constant}$$

BET theory does not always give accurate values for the surface area of microporous materials due to the complexity of the porous structure of the materials, but also due to the inaccuracies in the BET measurement itself. Factors such as error in sample weighing, and the capillary actions causing inclusion of excess volume of gas.

### 1.3 Microporous Materials

Porous materials, in particular microporous materials, have been utilised into a vast range of applications such as heterogeneous catalysis, gas separation, energy storage and ion exchange.<sup>15-19</sup> Due to their huge technological potential, microporous materials are still a rapidly growing field. Aside from well-established microporous solids such as activated carbon and zeolites, numerous new

functional materials have emerged in the past two decades, including polymers of intrinsic microporosity (PIMs).<sup>17</sup>

### 1.3.1 Activated Carbons

Activated carbons (ACs) are amorphous solids with a hierarchy of pore sizes.<sup>20</sup> ACs can be produced from a wide range of raw materials such as nutshells,<sup>21</sup> coals,<sup>22</sup> and wood biomass,<sup>23</sup> followed by an activation step using either physical or chemical activation. Commercial production processes typically involve two steps, pyrolysis of raw materials followed by physical activation using steam, carbon dioxide or hot air mixtures, at temperatures ranging from 800 to 1100 °C. Chemical activation requires the raw materials to be firstly treated with acids, bases or other chemicals followed by heating at 400-900 °C.<sup>24</sup>

Although being one of the oldest known microporous materials with a long history of commercial applications, the structure of ACs still remains a topic of discussion. It is believed that the structures of ACs are related to that of graphite, consisting of layers of fused hexagonal rings.<sup>25</sup> Recent studies utilising transmission electron-microscopy (TEM) has found that ACs also contain curved fragments of pentagonal and heptagonal rings similar to fullerenes (**Figure 1.2**), which also contributes towards the high porosity of ACs.<sup>26,27</sup>

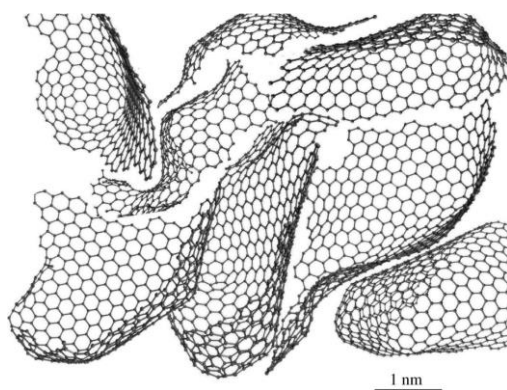


**Figure 1.2** Illustration of a model structure of AC containing hexagonal and non-hexagonal rings.<sup>27</sup>

The highly porous nature of ACs give rise to their well-known exceptional surface areas of over 1000 m<sup>2</sup> g<sup>-1</sup>, with many commercially available activated carbons offering a surface area in the range of 700-2200 m<sup>2</sup> g<sup>-1</sup>,<sup>28</sup> which makes ACs excellent adsorbents. ACs have a wide range of commercial applications such as heavy metal and toxic gas removal, wastewater treatment and carbon dioxide capture.<sup>29-32</sup> However, the high surface area of ACs arises from its wide distribution of pore sizes, which hinders their potential to be used in size selective applications.

### 1.3.2 Zeolites

Zeolites are another class of well-established microporous material that could be found naturally as well as synthetically produced under laboratory conditions. Natural zeolites were first discovered by Swedish mineralogist Axel Fredrick Cronstedt in 1756, who named the naturally occurring minerals based on the Greek terms *zein* which means 'to boil' and *lithos* meaning 'stone', after observing the material producing large amount of steam upon heating.<sup>33</sup> Currently, more than 50 types of natural zeolites has been discovered, and there are more than 150 varieties of synthetic zeolites available.<sup>34</sup>

Due to their crystallinity, zeolites boast well-ordered and defined microporous cage-like frameworks, which also consist of sub-structures to form interconnected channels through the material, that are roughly 1-20 Å in diameter. These sub-structures are also known as supercages ( $\alpha$  cage) and sodalite cages ( $\beta$  cage). Typical zeolites are comprised of  $[\text{SiO}_4]^{4-}$  and  $[\text{AlO}_4]^{5-}$  tetrahedral units bridged through oxygen atoms, although alternative compositions also exist (Figure 1.3).<sup>35,36</sup>

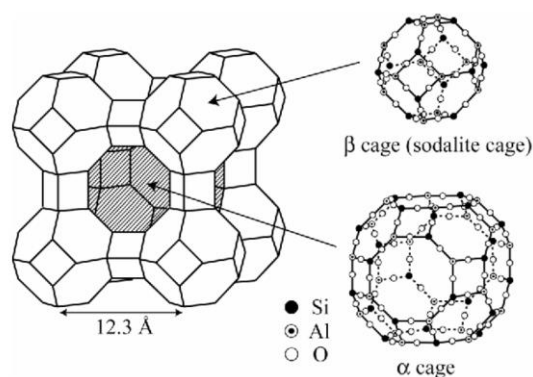


**Figure 1.3** An illustration of Zeolite-A structure highlighting supercages ( $\alpha$  cage) and sodalite cages ( $\beta$  cage) and their chemical composition.<sup>37</sup>

Zeolites commonly have an overall negative charge due to the presence of  $[\text{SiO}_4]^{4-}$  and  $[\text{AlO}_4]^{5-}$  units, which enables a variety of cationic species, such as  $\text{Na}^+$ ,  $\text{K}^+$ ,  $\text{Mg}^{2+}$  and  $\text{Ca}^{2+}$ , to be present in the cavities of the framework. These cations could then be easily exchanged with other organic and inorganic cationic species in solution, granting zeolites the ability to freely undergo ionic exchange. This property, along with good sorption abilities, has made zeolites a useful material in many commercial applications such as water softening<sup>38-41</sup> and wastewater treatment.<sup>42-44</sup> Further to the aforementioned applications, zeolites have also been proven useful in many other areas such as catalysis<sup>45-47</sup> and molecular sieving,<sup>47-49</sup> owing to their high surface area, catalytic active sites and their crystallinity resulting in their pores having fixed shapes and sizes.



### 1.3.3 Metal-Organic Frameworks

Metal-organic frameworks (MOFs), also known as porous coordination polymers (PCPs), are becoming another well-established class of microporous materials. Although other organic-inorganic hybrid materials had been previously studied, the term MOF was first introduced by Yaghi and co-workers in 1995.<sup>50</sup>

The structures of MOFs are constructed of a network of metal ions or metal clusters, joined together by organic linking molecules, giving rise to a crystalline 3D structure. A classic example being MOF-5, developed by Yaghi *et al.* (**Figure 1.4**), which demonstrated good structural stability towards high temperatures, and was able to maintain its crystallinity after the complete removal of guest molecules from its pores.<sup>51</sup> To date, many reported MOF structures have shown even greater stability under harsh conditions.<sup>52,53</sup>

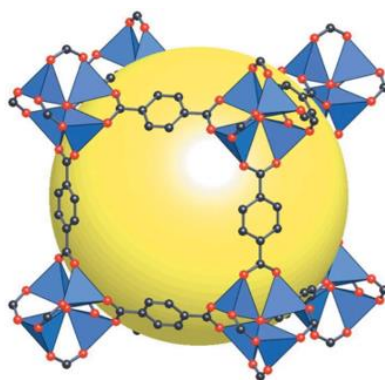


**Figure 1.4** An illustration of MOF-5, demonstrating  $ZnO_4$  metal clusters (blue) joined by benzene dicarboxylates as organic linkers and the porosity created within the frame (yellow).<sup>54</sup>

The incorporation of organic linkers has greatly enhanced the versatility of MOFs compared to purely inorganic zeolites. This modular nature of MOFs allow the pore structure, topologies and functionality of the material to be specifically controlled.<sup>55</sup> Thus since their establishment, MOFs has quickly attracted major research interest, and the field has been extensively studied, with more than 100,000 MOF structures being reported.<sup>56</sup> Typically, MOFs have surface area ranging from 1,000-10,000  $m^2 g^{-1}$ , far exceeding zeolites and carbon-based porous materials.<sup>57</sup> Although commercial applications have been slow to develop, currently MOFs are being studied for a wide range of applications including catalysis,<sup>58-60</sup> gas separation and storage,<sup>61,62</sup> drug delivery<sup>63-65</sup> and sensing.<sup>66-68</sup>

### 1.3.4 Covalent Organic Frameworks

Covalent organic frameworks (COFs) are another class of crystalline microporous material made up of units consisting of solely light elements (H, B, C, N, Si and O), which are linked *via* covalent bonds.<sup>69</sup>

Very similar to MOFs, reported COFs also exhibit similar properties such as large surface area, tuneable features (pore sizes etc.) and great structural diversity, though their skeletal structures are distinctly less dense. This class of material was developed by Yaghi *et al.* in 2005, one of the structures reported being COF-5 (**Figure 1.5a**).<sup>69</sup> This particular structure was synthesised from the condensation reaction between benzene-1,4-diboronic acid and hexahydroxytriphenylene, resulting in a 2D layer and a material with a surface area of 1590 m<sup>2</sup> g<sup>-1</sup>. Other COFs with a 3D structure (**Figure 1.5b**) were subsequently reported via the incorporation of both triangular and tetrahedral linkers such as hexahydroxytriphenylene (triangular) and tetra(4-dihydroxyborylphenyl)methane.<sup>70</sup>

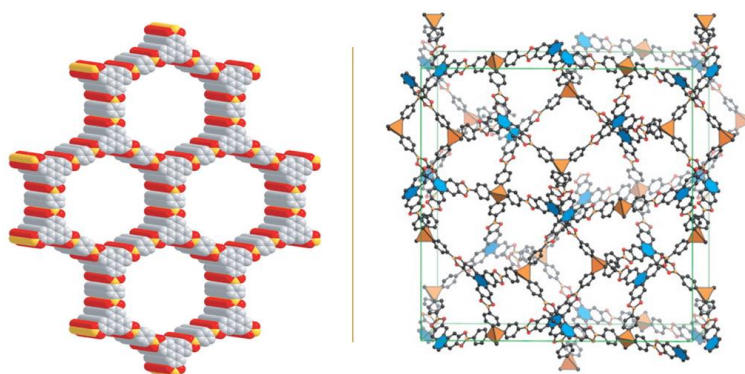


**Figure 1.5** (a) Structural representation of COF-5 with a 2D framework<sup>69</sup> and (b) structural representation of COF-105 with a 3D framework.<sup>70</sup>

In addition to applications in fields such as gas storage and separation,<sup>71,72</sup> catalysis<sup>73,74</sup> and sensing<sup>75,76</sup> similar to MOFs, 2D structured COFs also exhibit electronic and optical properties owing to the transportation of charges through pre-organised  $\pi$ -conjugated pathways.<sup>77,78</sup>

### 1.3.5 Hyper-Crosslinked Polymers

Most polymers exhibit adequate flexibility and rotational freedom in their backbones, which allows the polymeric chains to rearrange in space, so that they can pack in an efficient manner in space, resulting in materials with only a small amount of unconnected free volume. Hyper-crosslinked polymers (HCPs) were the first polymeric material with well-defined micropores, which were developed in the early 1970s by Tsyurupa and Davankov.<sup>79</sup> HCPs are prepared by the complete dissolution or swelling of a loosely crosslinked polystyrene-based precursor, in a suitable solvent in the presence of a Lewis acid catalyst, leading to the extensive crosslinking of the polymers. The resulting network of covalent bonds locks the polymer into a confined conformation and immobilises the polymer from twisting and collapsing to minimise free volume, resulting in large amount of interconnected porosity (**Figure 1.6**).<sup>80,81</sup>

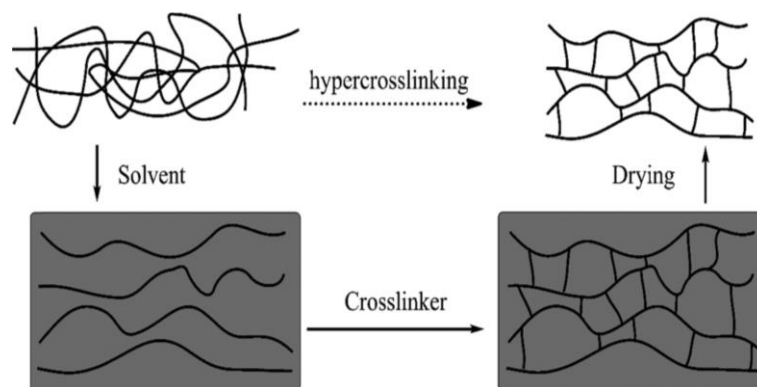


**Figure 1.6** Diagrammatic illustration of HCP formation process.<sup>81</sup>

Furthermore, post-polymerisation functionalisation can be carried out on HCPs to introduce additional properties which can be customised for specific applications.<sup>82,83</sup> Today, HCPs have found many applications in technology such as water purification,<sup>84,85</sup> catalysis,<sup>86,87</sup> and CO<sub>2</sub> capture.<sup>88,89</sup>

#### 1.4 Polymers of Intrinsic Microporosity

Polymers of intrinsic microporosity (PIMs) are a relatively new class of amorphous organic microporous material that contains a continuous network of interconnected intermolecular voids.<sup>90</sup> Unlike other microporous polymers such as HCPs, PIMs have microporosity as an inherent feature due to the presence of contorted and rigid molecular units in their structure, joined in a manner that fixes the polymeric chain in a 2D or 3D conformation, causing the polymer to pack inefficiently in space.<sup>91</sup>

The concept of intrinsic microporosity is closely related to that of internal molecular free volume (IMFV), a theory introduced by Swager *et al.*<sup>92</sup> IMFV can be defined as the unoccupied volume of a concaved molecule, in relation to their total volume.<sup>91,92</sup> A typical example of concaved molecule is triptycene (**Figure 1.7**) with a highly rigid structure made up of a system of fused rings. This locks the molecule conformation in place and gives rise to cavities surrounding the molecule. The development of PIMs utilises this concept by incorporating similarly concaved molecules into their polymeric structures, which results in the polymer chains packing inefficiently in space. The intrinsic microporosity of PIMs thus arises from both IMFV of the cavities present on the molecular building blocks themselves, as well as the awkward packing of the polymer chains.

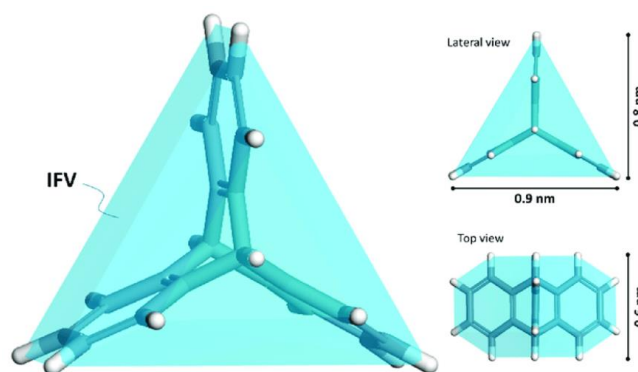


**Figure 1.7** 3D illustration of a triptycene unit, with its corresponding IMFV highlighted.<sup>93</sup>

The first polymer of this class, PIM-1, was reported in 2004 by McKeown and Budd.<sup>90</sup> The polymer was synthesised *via* a nucleophilic aromatic substitution reaction between cheap, commercially available materials 5,5',6,6'-tetrahydroxy-3,3,3',3'-tetramethyl-1,1'-spirobisindane (SBI) and 2,3,5,6-tetrafluoro-1,4-dicyanobenzene (TFTPN) (**Figure 1.8**). PIM-1 was reported to have a surface area of 860 m<sup>2</sup> g<sup>-1</sup>, and a total pore volume of 0.68 ml g<sup>-1</sup>.

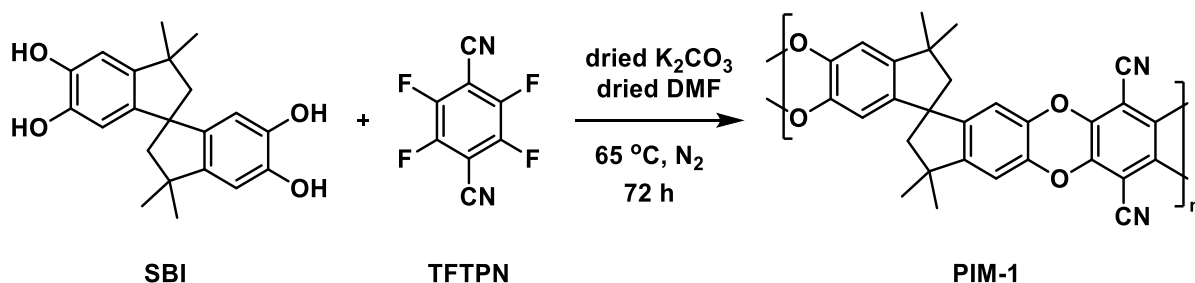


**Figure 1.8** Synthetic scheme of PIM-1.

In a theoretical study conducted by Hofmann *et al.*,<sup>94</sup> an atomistic packing model of PIM-1 was built to visualise the packing of PIM-1 chains in space (**Figure 1.9**). The simulation cell is composed of five PIM-1 chains, each consisting of 15 monomer units, demonstrating the amorphous nature of PIM-1. The study also presented the cross-sections of the simulated cell, further confirming the irregular packing of PIM-1 chains as each cross-section is unique in the way atoms are arranged. The cross-sections also highlight the intrinsic nature of the microporosity of PIM-1, where each slice displays significant presence of interconnected free volume within the polymeric structure.

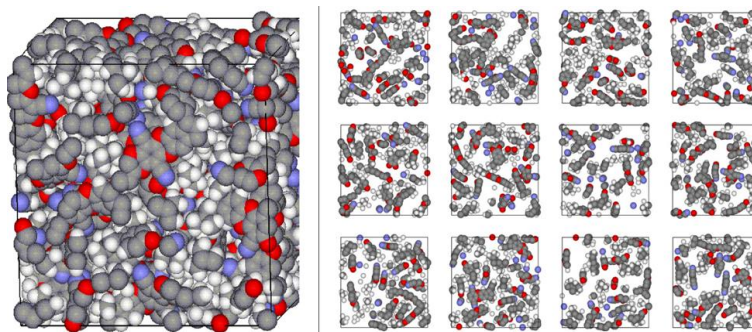


**Figure 1.9** Atomistic packing model of PIM-1 (left) and cross-sections of the packing model showing presence of free volumes (right).<sup>94</sup>

### 1.4.1 Current PIMs

Since the development of PIMs two decades ago, this class of microporous polymer has received considerable research interest, and continuing efforts has been put into expanding the family of novel PIMs. A PIM's structure comprises two essential components – a concaved structural unit to introduce sites of contortion into the polymer structure, and a linking group which joins the structural units together in an inflexible manner to restrict the rotation of the polymer chain (**Figure 1.10**).

Current reported methods of PIMs synthesis can be generalised into three main categories based on their structures – polydibenzodioxins, polyimides (PI) and Tröger's base (TB).

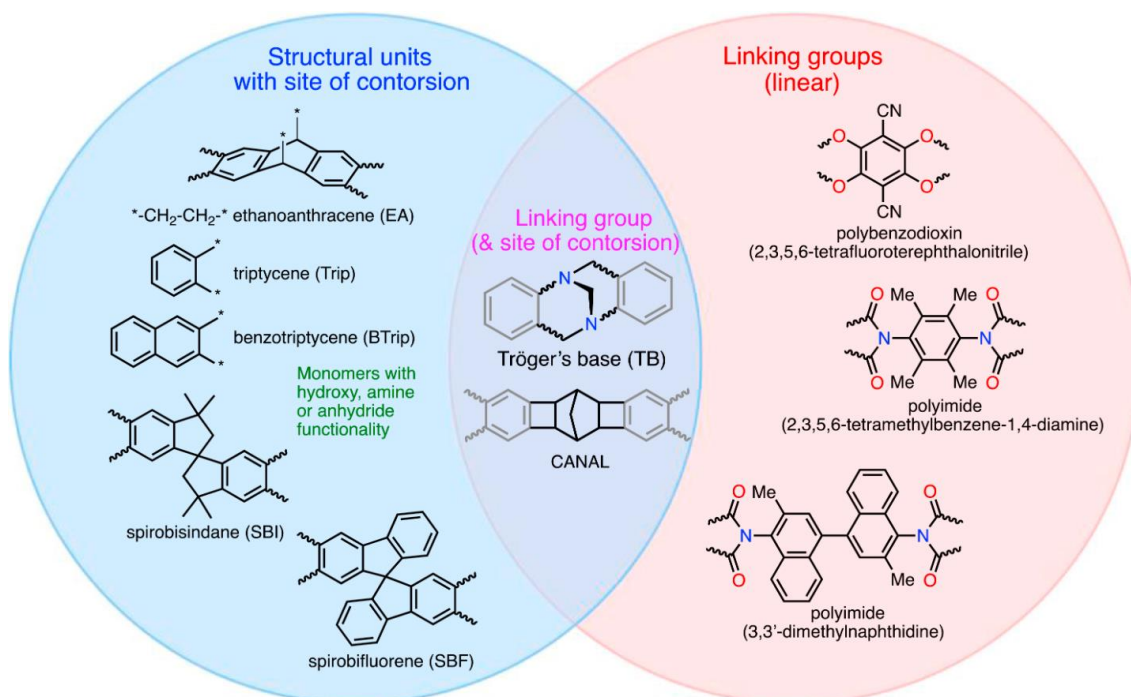


**Figure 1.10** PIMs are synthesised by joining contorted structural units using a linking group that can sufficiently inhibit the rotation of polymeric chains.<sup>91</sup>

The initial examples of PIMs was developed through the formation of dibenzodioxin linkages, notable examples include PIM-1,<sup>90</sup> and since then a library of dibenzodioxin-based PIMs has been intensively developed. Amongst the three types of linkages in PIMs, dibenzodioxin-based PIMs have received the most research attention.<sup>95</sup> Polybenzodioxin-PIMs, for example PIM-1, are synthesised using step-growth polymerisation, via a base-mediated double nucleophilic aromatic substitution reaction between a bisphenol and a tetrahalogenated (typically F or Cl) monomer as they are efficient leaving groups under  $S_NAr$  reaction in the presence of CN groups. The resulting dioxin ring creates a ladder-like structure, restricting rotation in the polymer chain, thus polybenzodioxin-PIMs can also be referred as ladder-PIMs.<sup>96</sup> Aside from the previously mentioned SBI units, other examples of structural units used for polybenzodioxin formation include spirobifluorenes (SBF)<sup>97,98</sup> and triptycenes (Trip).<sup>99,100</sup> A significant representation of this type of PIMs is PIM-TMN-Trip (**Figure 1.11**), which has a surface area of  $1050 \text{ m}^2 \text{ g}^{-1}$ , exceeding that of PIM-1 and exhibits ultra-permeability, especially towards  $\text{CO}_2$ .<sup>101</sup>

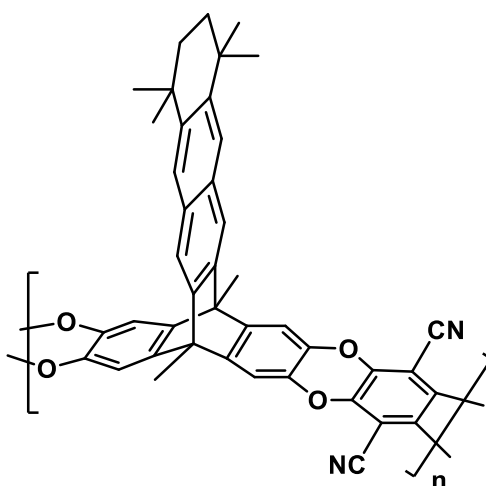


**Figure 1.11** Structural representation of PIM-TMN-Trip.

Subsequent to the development of the initial PIM examples, the incorporation of the unique rigid and contorted PIM characteristics into other traditional polymer types were explored. Polyimides (PIs) are a class of polymer commonly obtained from the reaction between a dianhydride and a diamine monomer. Commercial PIs such as Kapton® and Matrimid® (**Figure 1.12**) exhibit high thermal, mechanical and excellent electrical properties.<sup>102</sup> However, due to the linear and flexible nature of conventional PI structures, the polymer chains packed rather densely in space, resulting in limited performances in gas permeability,<sup>103,104</sup> especially compared to porous polymers such as PIM-1.

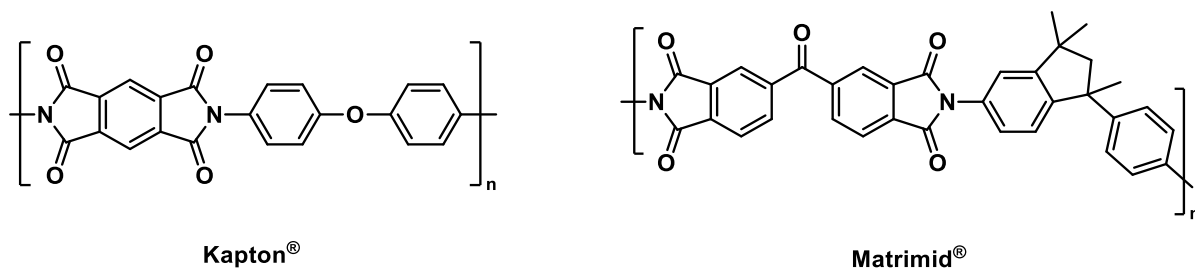


**Figure 1.12** Structures of Kapton® and Matrimid®

In 2009, a group of novel polyimide-based PIMs were reported as PIM-PIs by McKeown *et al.*<sup>105</sup> The study successfully combined characteristics of PIMs with PIs, by incorporating bulky and contorted monomers into the classical PI synthesis. The reported PIM-PIs, namely PIM-PI 1-8, from the study were prepared from the cyclodimerization between the dianhydride 8,8,9,9'-tetrahydro-9,9,9',9'-tetramethyl-7,7'-spirobi[7*H*-cyclopent[*g*]isobenzofuro[5,6-*b*][1,4]benzodioxin]-1,1',3,3'-tetrone (An-1) and various diamine monomers (**Figure 1.13**). The spiro-centre in An-1 allows sites of contortion to be introduced into the polymer backbone, while the substituents on the diamine monomers sufficiently limit the rotation within the polymeric chain. Gas adsorption analysis indicated that the PIM-PIs, especially PIM-PI-1 and PIM-PI-8, displayed high surface areas, high thermal stabilities and greatly improved gas permeabilities.<sup>102,105</sup>

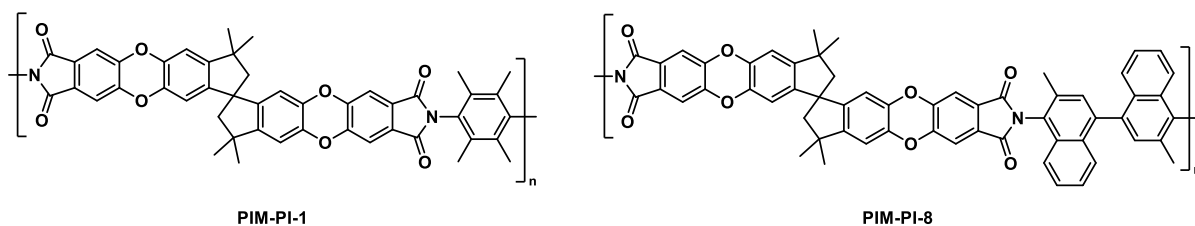


**Figure 1.13** Structure of PIM-PI-1 and PIM-PI-8.

Another notable development in the field of PIMs is the incorporation of the Tröger's base (TB) unit, a bridged bicyclic ring system, into PIMs structures, enhancing the rigidity of the polymer further compared to relatively flexible linking groups.<sup>91</sup> TB, fully named as 2,8-dimethyl-6*H*,12*H*-5,11-methanodibenzo[*b,f*][1,5]diazocine, was first synthesised by Julius Tröger in 1887. It is a chiral V-shaped molecule consisting of two aromatic rings fused onto a methanodiazocine unit (**Figure 1.14**); the unit is synthesised by the condensation between 4-methylaniline and formaldehyde in the presence of a strong acid.<sup>106</sup>



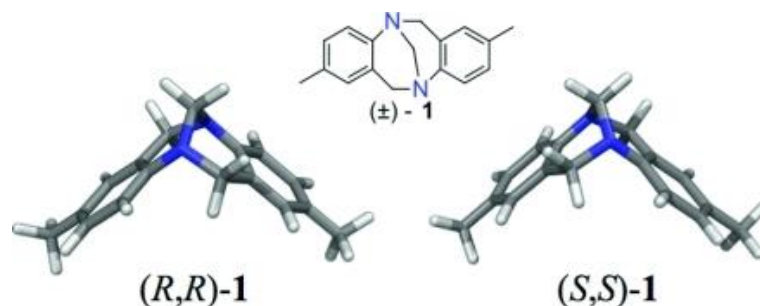


**Figure 1.14** Structure of TB and the crystal structure of its two enantiomers.<sup>106</sup>

In 2013, the McKeown group reported two novel TB-based polymers, prepared from monomers 5,5',6,(6)'-diamino-3,3,3',3'-tetramethyl-1,1'-spirobisindane, giving PIM-SBI-TB and 2,6(7)-diamino-9,10-dimethylethanoanthracene to yield PIM-EA-TB (**Figure 1.15**).<sup>107</sup> The resulting polymers both have high surface areas at 745 m<sup>2</sup> g<sup>-1</sup> and 1028 m<sup>2</sup> g<sup>-1</sup> respectively. The ethanoanthracene unit in PIM-EA-TB provides the polymer with additional rigidity and sites of contortion, which explains the higher surface area. Furthermore, PIM-EA-TB also excels in its gas permeability and gas selectivity performance compared to other PIMs. TB is a particular versatile unit that could also be included as a structural unit in PIMs structures such as PIM-PI.<sup>108,109</sup>

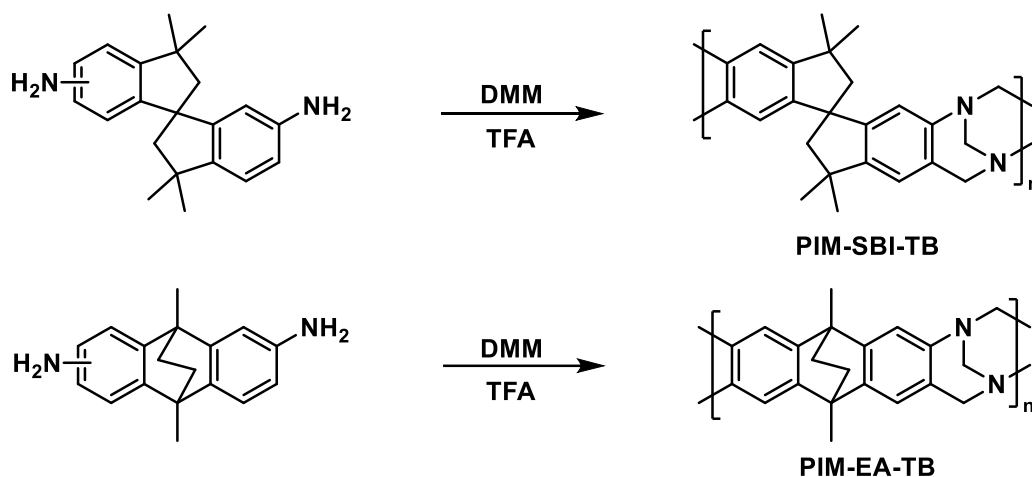


**Figure 1.15** Structures of PIM-SBI-TB and PIM-EA-TB from their respective monomers.

#### 1.4.2 Properties and Applications of PIMs

The unique structure of PIMs grants this class of polymers many useful properties that allowed them to be implemented in a wide range of applications. Unlike many other microporous materials such as MOFs, COFs and zeolites,<sup>110</sup> PIMs possess excellent solution-processability in common organic solvents, making them very versatile materials for membrane casting,<sup>111,112</sup> and electro-spun into fibrous materials.<sup>113</sup> The high solubility of PIMs makes them a versatile material to work with, and also easy to process on a large industrial scale. This property of PIMs arises from their contorted and inflexible backbone that keeps the polymeric chains sufficiently apart, with the result that they have weak



interchain attraction.<sup>114</sup> The aliphatic methyl groups on PIM-1 also contribute toward their good solubility.<sup>115</sup>

PIMs can also be structurally modified with the incorporation of functional groups to make targeted enhancement to their performance and change in specific properties.<sup>116,117</sup> For example, PIMs modified with nitrogen-containing functional groups has been shown to exhibit high affinity towards CO<sub>2</sub> molecules, thus attracting attention as potential materials to be used for CO<sub>2</sub> capture processes.<sup>118</sup> Furthermore, PIM-1 with amine and amidoxime groups has also been determined to be capable of removing anionic pollutants in aqueous conditions.<sup>116,119</sup> Some functional groups that have been successfully incorporated into PIM-1 are depicted in **Figure 1.16**.<sup>116</sup>

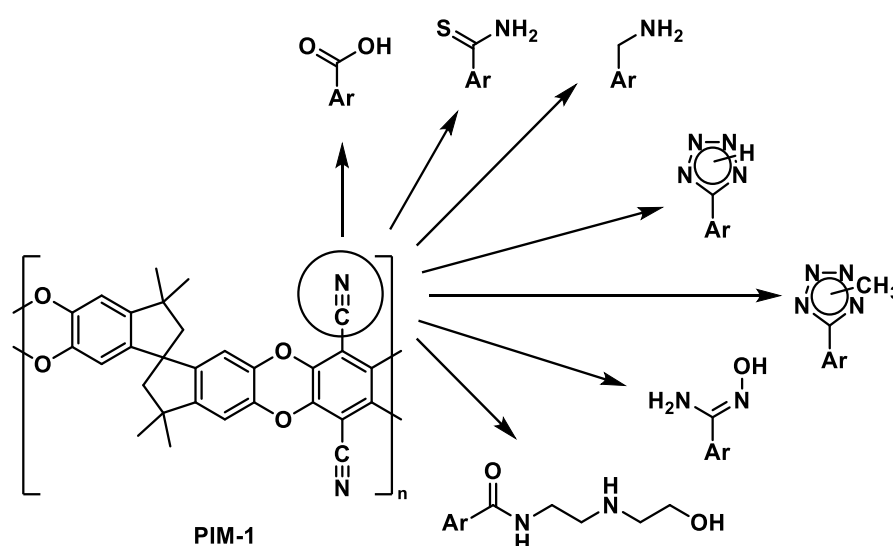


**Figure 1.16** Structural modification of PIM-1 with carboxylic acid, thioamide, amine, tetrazole, methyl tetrazole, amidoxime and hydroxyalkylaminoalkylamide.<sup>116</sup>

PIMs also exhibit good gas permeability and selectivity performances. The rigid backbone of PIMs ensure good gas selectivity performances<sup>120</sup> whilst the presence of bulky substituents, such as benzotriptycene units, push polymeric chains further away from each other resulting in less packing efficiency, thus ensuring excellent gas permeability of the polymers.<sup>121</sup> The above-mentioned features, combined with their large surface area, high thermal, chemical and oxidative stability makes PIMs eminent membrane materials for applications such as gas separation and nanofiltration materials.<sup>122,123</sup> Furthermore, the high surface area also grants PIMs high gas adsorption capability, making them promising materials for applications such as carbon capture, hydrogen storage, and sensing.<sup>124,125</sup>

## Chapter 2 Project Aims

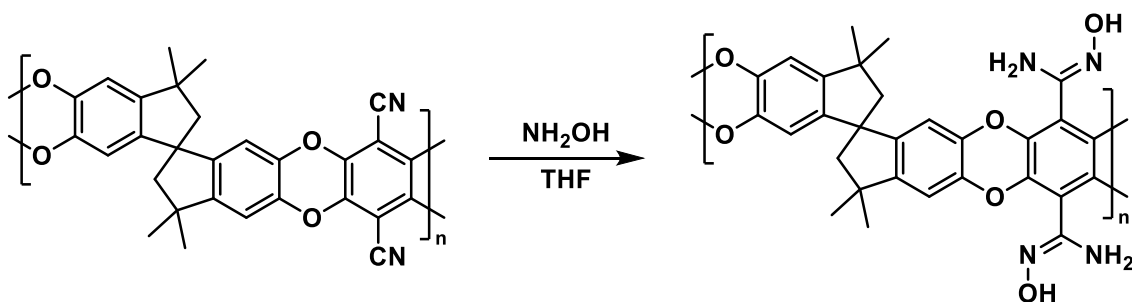
As noted, gas adsorption is an important technology used for many applications such as gas separation,<sup>126</sup> CO<sub>2</sub> capture,<sup>127</sup> and the removal of hazardous gases.<sup>128</sup> Microporous materials are often used as adsorbents owing to their high surface area and good pore accessibility. Considerable efforts have been made to develop new microporous materials with continuously enhanced gas adsorption properties. The overall aim of this project is to explore the synthesis of PIMs for gas adsorption purposes.

PIMs for gas adsorption applications need to possess several important features. The polymers must demonstrate a good selectivity towards the target gas molecules to avoid competitive adsorption of other gases and vapours present in the environment. One way to achieve this could be through incorporation of additional functional features to alter the polymer's interaction with different types of molecules. For example, it is well-established that the incorporation of basic functional groups such as amines and pyridines can lead to higher affinity for acidic gases such as CO<sub>2</sub>, through enhanced acid-base interactions. The same principle could also be applied for other vapours that are acidic in nature, such as organophosphate-based CWAs.<sup>121,122</sup> The polymers would also need to exhibit high adsorption capacity, which requires the materials to have high accessible porosity.<sup>129</sup> To achieve this, structural units that offer less rotational freedom and higher rigidity could be employed to increase the internal molecular free volume within the polymeric structure, thus offering improved porosity.

In this work, three different approaches were taken for the development of PIMs, each addressing a property mentioned above for gas or vapour adsorption. **1)** Functionalisation of PIMs using a basic pyridine unit and a super nucleophile, amidoxime, to increase the affinity of the polymers towards CO<sub>2</sub> gas. The reactivity of the amidoxime group towards some CWAs was also investigated. **2)** Highly bulky, rigid, and inflexible triptycene-like structural units were synthesised, and their corresponding PIMs formation was investigated. The porosity and gas uptake of PIMs containing the triptycene units were studied. Lastly, **3)** The attempted synthesis of fluorinated monomers for PIMs formation was explored, which could enhance the hydrophobicity of PIMs even further to reduce the competitive adsorption of water vapours. Incorporation of fluorine atoms onto PIMs could also lead to interesting solubility properties, which can be advantageous for commercialisation purposes.

## Chapter 3 Amidoxime Functionalised Polymers

The incorporation or modification of functional groups is often employed to enhance, alter, or introduce desired properties to a material. For PIMs, enhancement of the gas adsorption properties can also be achieved *via* this approach. Post-synthetic modification of PIMs can be easily carried out due to the presence of reactive nitrile groups on their polymeric backbones. Functionalisation of PIMs, especially that of PIM-1 has been widely explored.<sup>130–132</sup> The addition of basic functional groups, such as amines and pyridine units, has been shown to improve the affinity towards acidic molecules, such as CO<sub>2</sub>, through acid-base interactions.<sup>133,134</sup> However, it was discovered that the introduction of additional functional groups often results in a significant decrease in the porosity of PIMs. In 2012, Patel *et al.* overcame this issue via the so-called “non-invasive” post modification of PIMs with the introduction of amidoxime (AO) functional group onto PIM-1 (**Scheme 3.1**).<sup>135</sup> The modified polymer, AO-PIM-1, was reported to have a surface area of 482 m<sup>2</sup> g<sup>-1</sup>, which was a relatively small reduction compared to that observed for other modified versions of PIM-1. Furthermore, the addition of the AO group did not hinder the polymer’s solution processability, by enhancing solubility in polar aprotic solvents such as DMSO.



**Scheme 3.1** Amidoxime functionalisation of **PIM-1** to produce **AO-PIM-1**.

In addition to the above-mentioned features of the AO functional group, their incorporation onto PIMs could also introduce additional properties to the polymer. Since amidoxime functional groups demonstrate super-nucleophilicity due to the  $\alpha$ -effect,<sup>136</sup> caused by the presence of adjacent lone-pair containing nitrogen atom, the incorporation of AO groups onto microporous materials can lead to chemically active materials. Of particular interest is the potential hydrolytic activity towards toxic compounds such as chemical warfare agents (CWAs), in particular towards nerve agents in basic conditions.<sup>137</sup> The hydrolytic activity of **AO-PIM-1** towards organophosphorus nerve agents has been previously studied by Farha *et al.*, where the reactivity of PIM-1 modified with three different functional groups, amidoxime, carboxylic, and amide, towards dimethyl-4-nitrophenylphosphate (**DMNP**) was compared (**Figure 3.1**). Successful conversion of DMNP into the less toxic dimethyl phosphate (**DMP**) and methyl-4-nitrophenyl phosphate (**M4NP**) was achieved by all three of the

polymers in basic conditions, with AO-PIM-1 demonstrating by far the highest rate of conversion, which was ascribed to its super-nucleophilicity.<sup>138</sup>

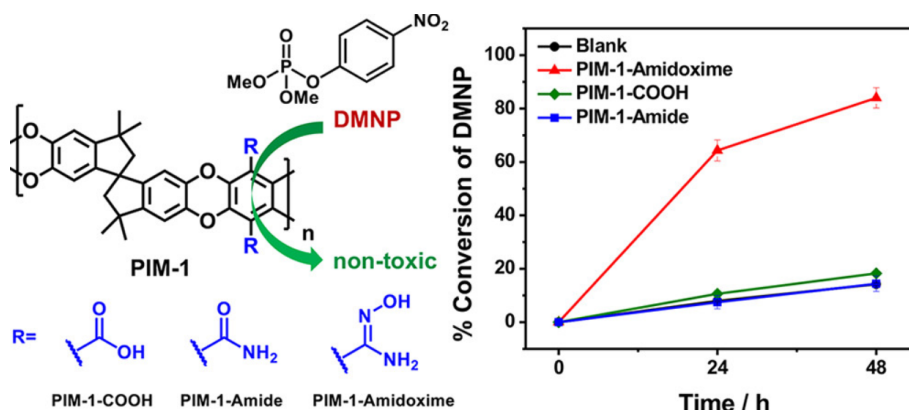


**Figure 3.1** DMNP conversion by PIM-1 modified with amidoxime, amide, and carboxylic group (left), and the % conversion of DMNP achieved by the polymers over time.<sup>138</sup>

AO-PIM-1 showed promising reactivity towards CWAs; however, the activation requirement of external basic reaction conditions hinders its applicability towards real-life scenarios. Therefore, for the present work, the reactivity of AO groups toward nerve agents with in-built basicity on the polymer structure was explored. The inclusion of a pyridine unit in the polymer backbone, derived from 2,3,5,6-tetrafluoro-4-pyridinecarbonitrile (TFPCN) to form **PIM-py** (Figure 3.2) was an obvious choice for the study,<sup>139</sup> as **PIM-py** has an otherwise very similar structure to that of **PIM-1**, making it the ideal candidate for comparison purposes. This chapter focuses on the results of comparing the novel **AO-PIM-py** with a selection of established polymers, namely **PIM-1**, **AO-PIM-1** and **PIM-py**, with respect to their physical properties and performances in areas such as gas separation, adsorption, and CWA decontamination.

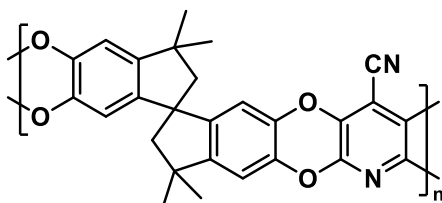
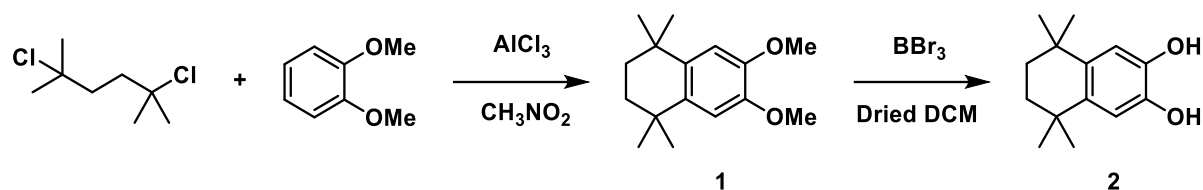


**Figure 3.2** Structure of **PIM-py**

### 3.1 Synthesis of Model Compounds

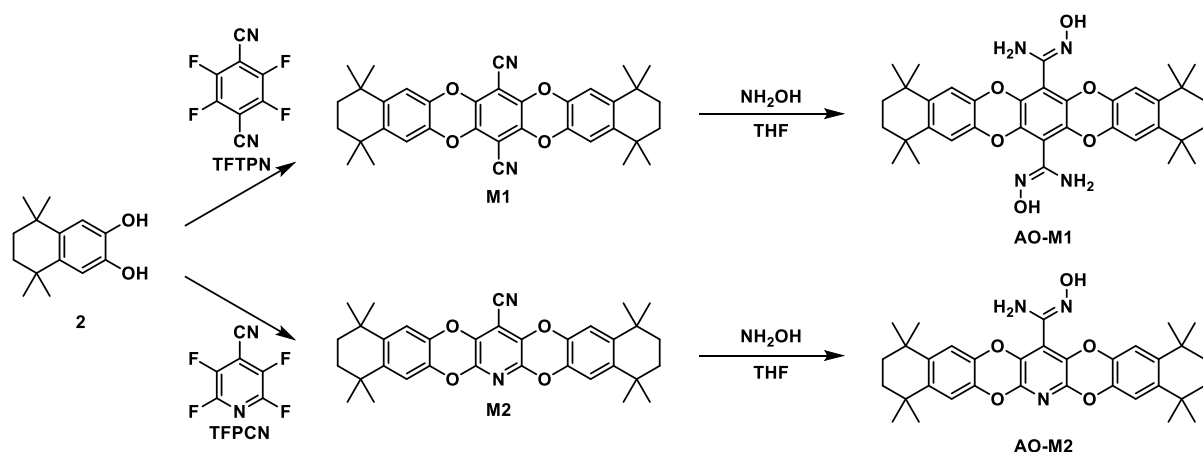
The chemistry involving the amidoxime group can be complex due to the functional group existing as its protonated, neutral, and deprotonated form depending on the pH of the environment.<sup>140</sup> All three forms of the AO group show reactivity towards toxic chemicals; however, the  $\alpha$ -effect appears to be the strongest when the functional group is in its deprotonated form.<sup>141</sup> Therefore, it was of interest to

determine the main form of AO group present on the polymer when additional basicity (pyridine unit) has been introduced to the system.



**Scheme 3.2** Synthesis of 6,7-dihydroxy-1,1,4,4-tetramethyl-2,3-dihydronaphthalene

For the synthesis of model compounds, a catechol resembling the fused ring system of 3,3,3',3'-tetramethyl-1,1'-spirobiindane-5,5'-6,6'-tetraol monomer, used for **PIM-1** synthesis was prepared (**Scheme 3.2**). Friedel-Crafts alkylation reaction between 2,5-dichloro-2,5-dimethylhexane and veratrole, based on literature procedure,<sup>142</sup> was carried out at room temperature, under N<sub>2</sub> atmosphere for 20 hours to give 6,7-dimethoxy-1,1,4,4-tetramethyl-2,3-dihydronaphthalene (**1**) as white crystals, with a yield of 38%. Demethylation reaction of compound **1** was performed following a modified literature procedure,<sup>100</sup> so that the catechol product 6,7-dihydroxy-1,1,4,4-tetramethyl-2,3-dihydronaphthalene (**2**) was obtained with 94% yield, using BBr<sub>3</sub>, under N<sub>2</sub> atmosphere for 3 hours. Successful conversion was confirmed by the appearance of OH groups located at 3259 cm<sup>-1</sup> on the FT-IR of compound **2**, as well as by <sup>1</sup>H NMR spectroscopy with the disappearance of the singlet at 3.86 ppm, corresponding to the OMe groups.



**Scheme 3.3** Synthesis of model compounds **M1**, **M2**, **AO-M1**, and **AO-M2**.

After successfully obtaining compound **2**, two nucleophilic aromatic substitution reactions were carried out using the catechol with TFTPn, and TFPCN. Following a modified procedure, the reaction was heated to 80 °C for 1 day, in the presence of K<sub>2</sub>CO<sub>3</sub> to obtain model compound **M1** and **M2**, in 92% and 91% yield, respectively. Their subsequent AO modifications were carried out using an excess of hydroxylamine 50wt. % in water, refluxed in THF for 1 day, following a modified literature

procedure.<sup>143</sup> **AO-M1** and **AO-M2** were obtained with a high conversion rate of 90% and 89% respectively (**Scheme 3.3**).

Successful AO transformation can be confirmed by comparing the IR and <sup>1</sup>H NMR spectra of the model compounds (**Figure 3.3**). **AO-M1** showed the appearance of primary amine peaks at 3460, 3364 cm<sup>-1</sup>, and hydroxyl peak at 3256 cm<sup>-1</sup> which belongs to the AO group. Similar amine peaks were observed at 3449, 3354 cm<sup>-1</sup> for **AO-M2**, but no strong broad OH peak was seen between 3300-3200 cm<sup>-1</sup>. This latter observation can be attributed to the pyridine unit introducing additional H-bonding to the system, hydroxyl groups under strong H-bonding interactions can often appear highly broadened.<sup>144</sup> In the case of **AO-M2**, the area near the 3449 cm<sup>-1</sup> peak appeared to have a slight bump, which could be its hydroxyl peak overlapping with the amine peak. Analysis of <sup>1</sup>H NMR further confirms the effect of the pyridine unit, as the peaks corresponding to NH and OH groups appeared slightly more downfield than in **AO-M1**.<sup>145</sup> The presence of the pyridine unit also led to the loss of symmetry in the molecule, resulting in the observation of two proton environments for the aromatic protons. For both **AO-M1** and **AO-M2**, the integration of their NH and OH peaks exhibited a 2:1 ratio, indicating that the AO groups exist in their neutral form, irrespective of the presence of the additional basic site.

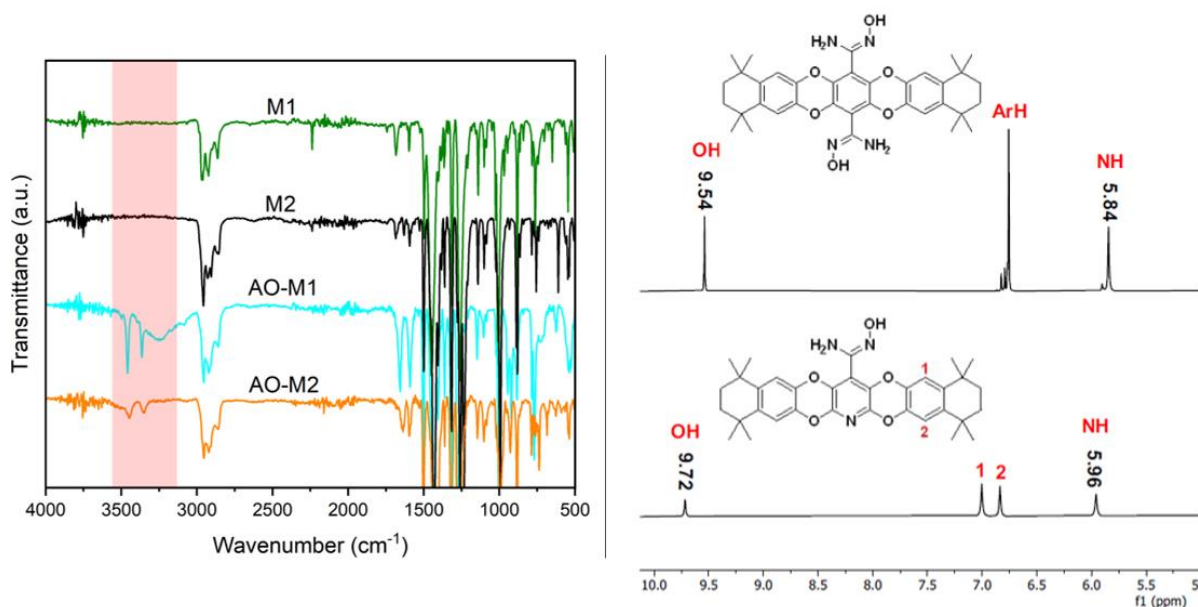
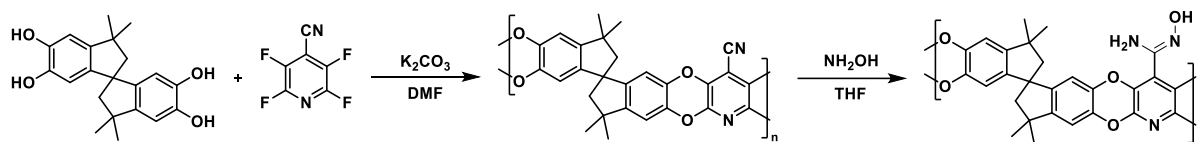


**Figure 3.3** FT-IR comparison of the model compounds before and after AO modification (left), and <sup>1</sup>H NMR comparison of AO groups on **AO-M1** and **AO-M2**.

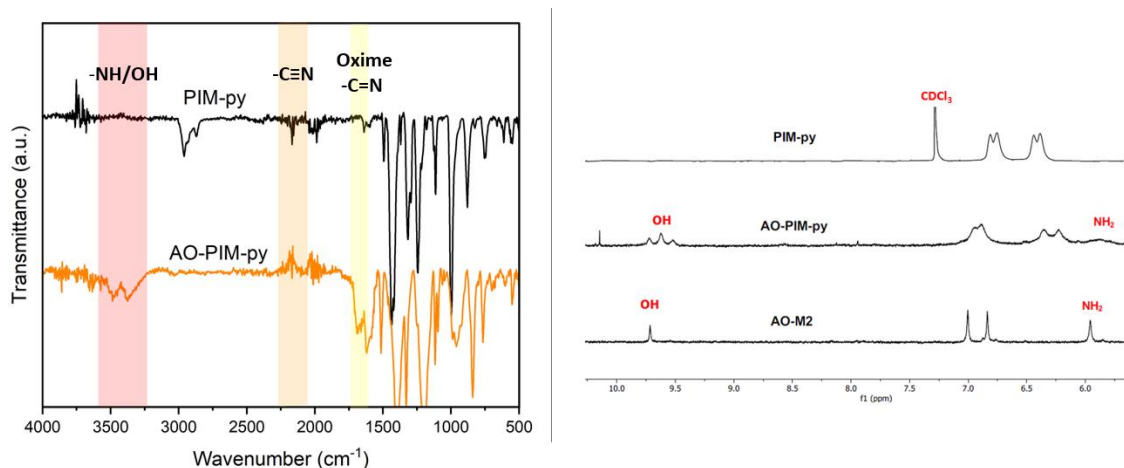
## 3.2 Polymer Synthesis



**Scheme 3.4** Polymerisation reaction of **PIM-py** and its AO modification.

**PIM-py** was successfully prepared from commercially available monomers 3,3,3'-tetramethyl-1,1'-spirobiindane-5,5'-6,6'-tetraol (**SBI**) and **TFPCN**, following a modified procedure from the literature (**Scheme 3.4**).<sup>101</sup> The polymerisation reaction was heated at 70 °C for 72 h under an inert atmosphere, in anhydrous DMF and in the presence of K<sub>2</sub>CO<sub>3</sub>. The target polymer was obtained as a yellow powder, with a high yield of 96%. The structure of the polymer was confirmed via FT-IR and NMR analysis, and compared against reported values in the literature.<sup>139</sup> AO modification on the obtained **PIM-py** was carried out using an excess of hydroxylamine 50 wt % in water, refluxed in THF for 1 day, following modified literature procedures.<sup>143</sup> The reaction yielded **AO-PIM-py** at 94%, and the colour of the polymer changed from yellow to an off-white colour.

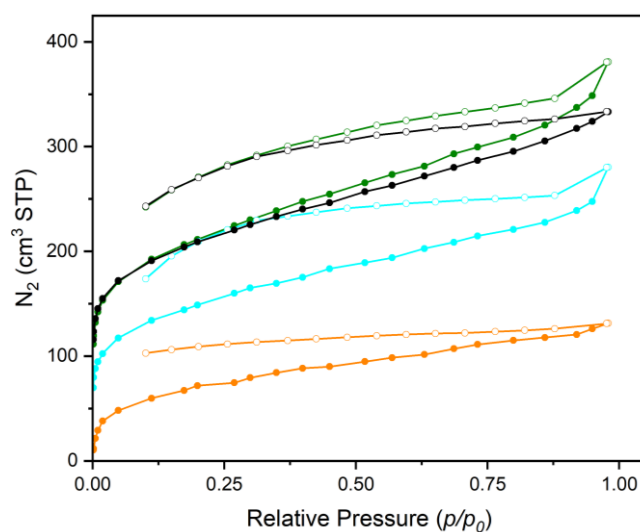
FT-IR analysis of the **AO-PIM-py** showed the appearance of peaks corresponding to the AO group at 3610-3230 cm<sup>-1</sup>, and C=N peaks at 1682 cm<sup>-1</sup>, confirming the successful modification. The disappearance of the nitrile peak at 2168 cm<sup>-1</sup> suggests a high percentage conversion was achieved (**Figure 3.4**). Comparison of <sup>1</sup>H NMR spectra also confirmed that **AO-PIM-py** was indeed obtained. Interestingly, the corresponding OH peak for the polymer was observed as a triplet as opposed to the singlet observed for the model compound. This is likely to be the result of the different types of intermolecular interactions it could have within the complex polymer structure.<sup>146</sup>



**Figure 3.4** a) FT-IR comparison of **PIM-py** and **AO-PIM-py**, b) a section of <sup>1</sup>H NMR for **PIM-py**, **AO-PIM-py**, and **AO-M2**.

### 3.3 Polymer Analysis

The adsorption and desorption isotherms were recorded for the synthesised polymers using nitrogen gas at 77 K (**Figure 3.6**). All polymers exhibited type I isotherm, suggesting the polymers are indeed microporous in nature.<sup>10</sup>

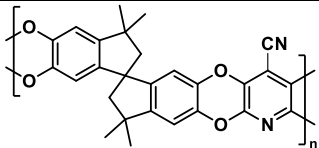
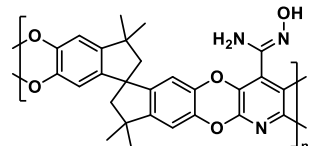
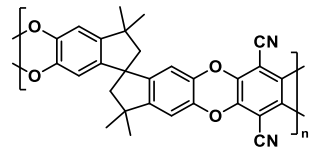
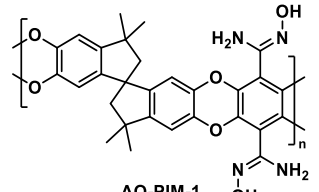


**Figure 3.6** N<sub>2</sub> adsorption (filled circle) and desorption (empty circle) isotherms of **PIM-1 (olive)**, **AO-PIM-1 (cyan)**, **PIM-py (black)**, and **AO-PIM-py (orange)**

From the obtained N<sub>2</sub> isotherms, BET surface area and total pore volume of the polymers were calculated (**Table 3.1**). Surface area calculation shows that for **PIM-py**, the incorporation of pyridine unit did not result in a decrease in the surface area compared to that of PIM-1, with an obtained value of 736 m<sup>2</sup> g<sup>-1</sup>. By comparing the values obtained for AO-polymers and the non-AO polymers, it is clear that the incorporation of AO group has a significant impact on the polymer surface area, with a much greater reduction in surface area for **AO-PIM-py** as compared to **AO-PIM-1**. This difference is likely due to hydrogen bonding between the AO and pyridine groups resulting in a denser packing arrangement of the polymer chains.



**Table 3.1** Gas adsorption properties of PIM-py, AO-PIM-py, PIM-1, and AO-PIM-1

| Polymer  | Solubility               | Surface area <sup>a</sup><br>(m <sup>2</sup> g <sup>-1</sup> ) | Total Pore<br>Volume <sup>b</sup> (ml g <sup>-1</sup> ) | CO <sub>2</sub> Uptake <sup>c</sup><br>(mmol g <sup>-1</sup> ) |
|--|--------------------------|--|---|--|
| <br>PIM-py    | protic organic solvents  | 736  | 0.517   | 2.26   |
| <br>AO-PIM-py | aprotic organic solvents | 254  | 0.204   | 1.96   |
| <br>PIM-1     | protic organic solvents  | 745  | 0.545   | 2.18   |
| <br>AO-PIM-1 | aprotic organic solvents | 544  | 0.435   | 2.29   |

<sup>a</sup>BET surface area was obtained from N<sub>2</sub> adsorption at 77 K, <sup>b</sup>total pore volume was calculated from N<sub>2</sub> uptake at  $P/P_0 = 0.98$ , and <sup>c</sup>CO<sub>2</sub> uptake was measured at 1 bar, 273 K.

The CO<sub>2</sub> adsorption isotherm for the polymers was also obtained, from which the CO<sub>2</sub> uptake at 1 bar, 273 K could be calculated (**Table 3.1**). The pore size distribution of the polymers was also calculated from this isotherm, using non-local density functional theory (NLDFT) (**Figure 3.7**). The polymers had very similar CO<sub>2</sub> adsorption performances. **PIM-1** and **PIM-py** demonstrated on par CO<sub>2</sub> uptake performances at 1 bar, 273 K, which was expected as the polymers share similar surface area and total pore volume. Despite a smaller surface area and the total pore volume compared to **PIM-1** and **PIM-py**, a better CO<sub>2</sub> uptake of 2.29 mmol g<sup>-1</sup> was observed with **AO-PIM-1** under the same testing conditions. This could be attributed to the addition of the CO<sub>2</sub>-philic functional group amidoxime.<sup>147</sup> Contrary to the observation made from **AO-PIM-1**, a reduction in CO<sub>2</sub> uptake was observed for **AO-PIM-py** compared to that of **PIM-py**. This observation is the result of the larger decrease in surface area caused by the AO modification of the pyridine-containing system, where the reduction in surface area and total pore volume has overcome the benefits brought about by AO group incorporation. The pore size distribution analysis has indicated that all polymers comprise a mixture of ultramicropores (pore diameter < 0.7 nm) and micropores (pore diameter < 2 nm), where the AO-modified polymers presented higher volume of ultramicropores with diameter less than 0.4 nm.

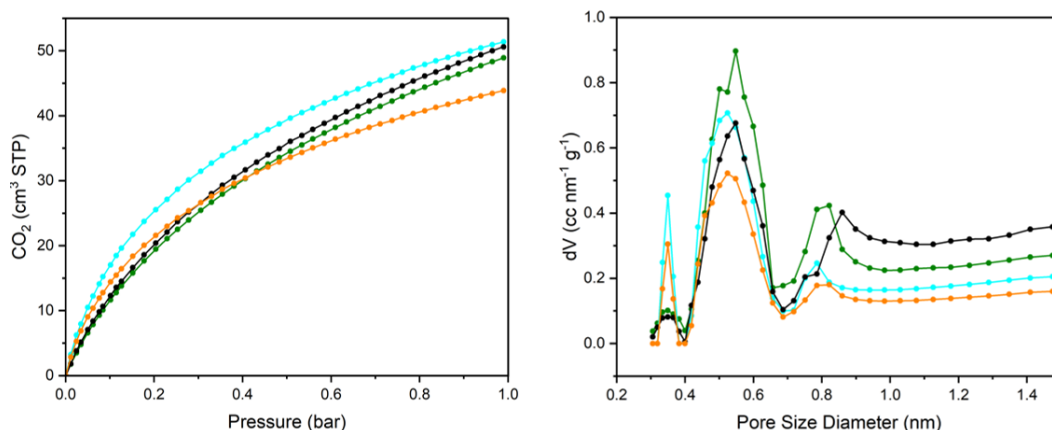


**Figure 3.7** CO<sub>2</sub> adsorption isotherm (left) and pore size distribution (right) of **PIM-1** (olive), **AO-PIM-1** (cyan), **PIM-py** (black), and **AO-PIM-py** (orange).

Thermogravimetric analysis was also performed on **PIM-py** and **AO-PIM-py** and compared against **PIM-1** and **AO-PIM-1** (Figure 3.8). Almost identical onset thermal decomposition temperature was obtained for **PIM-py** and **PIM-1**, due to their extremely similar structures. Both polymers showed apparent thermal stability up to nearly 500 °C. Conversely, the AO modified polymers presented two points of decomposition. The first onset of thermal decomposition, at approximately 270 °C, corresponds to the loss of the AO groups. As expected, a lower weight loss (4.6%) was observed for **AO-PIM-py** at its first onset decomposition temperature, compared to that of **AO-PIM-1** (6.5%). The second onset thermal decomposition temperature at around 470 °C, correlates to the decomposition of the main polymeric backbone. All polymers showed a char yield of near 60% or above, signifying the high aromatic content present in their polymeric structures.

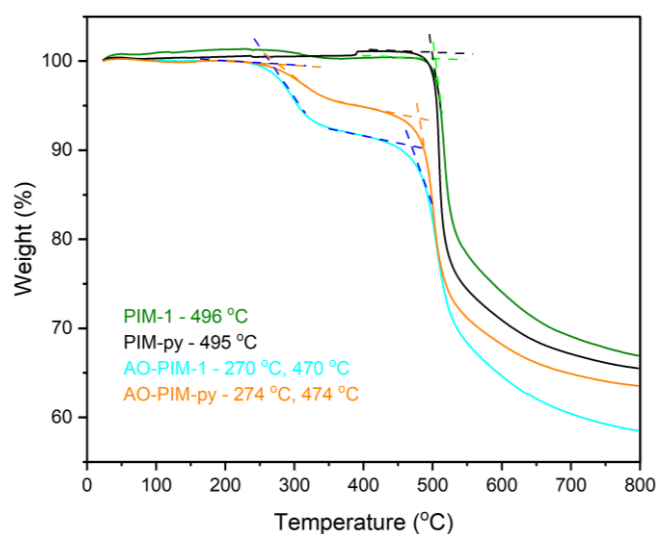


**Figure 3.8** TGA of **PIM-1** (olive), **AO-PIM-1** (cyan), **PIM-py** (black), and **AO-PIM-py** (orange), with their onset thermal decomposition temperatures identified.

The synthesised polymers were also sent to the Dr Gregory Peterson of the DEVCOM Chemical and Biological Division (part of the US army) for analysis of their ability to deactivate CWAs, namely Soman (GD), VX, and mustard gas (HD). The polymers were added to solutions containing a known concentration of each CWA. The mixtures were left at room temperature for 24 hours, and the change in concentration of the CWAs was observed using NMR spectroscopy. The percentage removal of CWAs was then calculated (**Figure 3.9**).

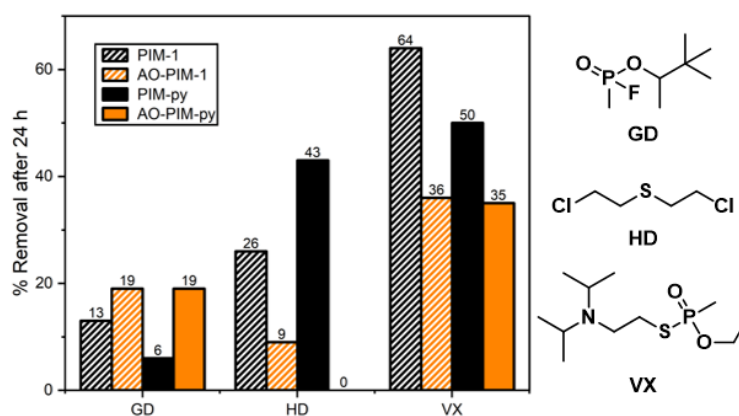


**Figure 3.9** Percentage of CWAs removed by contact with the PIMs in 24h (in a buffer at pH = 9).

No consistent trend could be concluded based on the results obtained. AO-modified polymers did appear to show a reduced performance in the removal of CWAs in general, perhaps due to the reduced surface area of polymers caused by AO modification, which suggests that the removal of the CWAs in the test is primarily based on adsorption. An exception was found in results obtained for GD removal, where AO modified polymers showed greater removal efficiency. This observation could be attributed to the smaller size of GD molecule, which has higher accessibility to the smaller ultramicropores of AO polymers. The better accessibility to ultramicropores, combined with the greater affinity towards AO group on the polymer, led to the higher adsorption of GD molecules. Overall, contrary to the initial hypothesis of the AO group contributing to CWA degradation, analysis suggests that CWA removal was still achieved through mainly adsorption with no strong evidence of enhanced hydrolysis.

### 3.4 Solution Processability

The solution processability of the synthesised **PIM-py** and **AO-PIM-py** was examined by solution casting the polymers into thin films suitable for testing as membranes. Films were successfully cast for both **PIM-py** and **AO-PIM-py**, using chloroform and DMSO respectively (**Figure 3.10**). The membranes obtained were then sent to the **Institute on Membrane Technology (ITM)**, for analysis of their gas selectivity and permeability properties, which will be discussed in more detail in the next section.

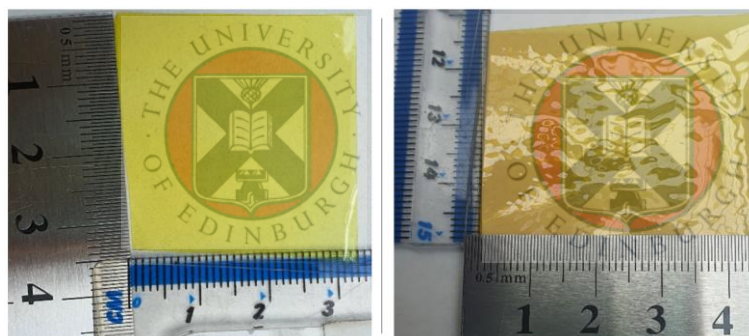


**Figure 3.10** Membranes casted from **PIM-py** (left) and **AO-PIM-py** (right)

In addition to membranes, electrospinning is another processing method that is used for making PIMs into nanofibers,<sup>113</sup> and is based on the use of a strong electric field applied to polymer solutions to generate very fine fibres.<sup>148</sup> The polymeric fibres produced this way are very versatile, as they are lightweight and have enhanced moldability, which allows them to be incorporated into various types of materials, such as clothing fabrics.<sup>149,150</sup> The technique works by loading a polymer solution into a syringe and applying an electric current to the syringe, where repulsion forces are created at the needle tip as it becomes charged. A charged jet of polymer solution is then ejected onto a collector plate, followed by the evaporation of the solution to obtain solid nanofibres (**Figure 3.11**).<sup>151</sup>

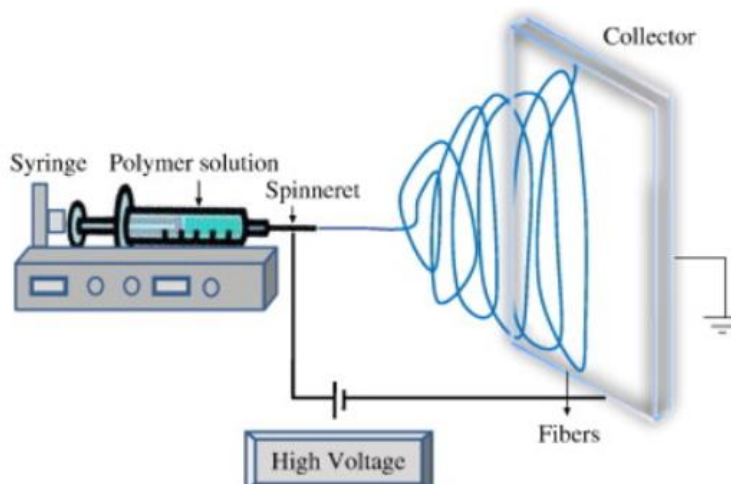


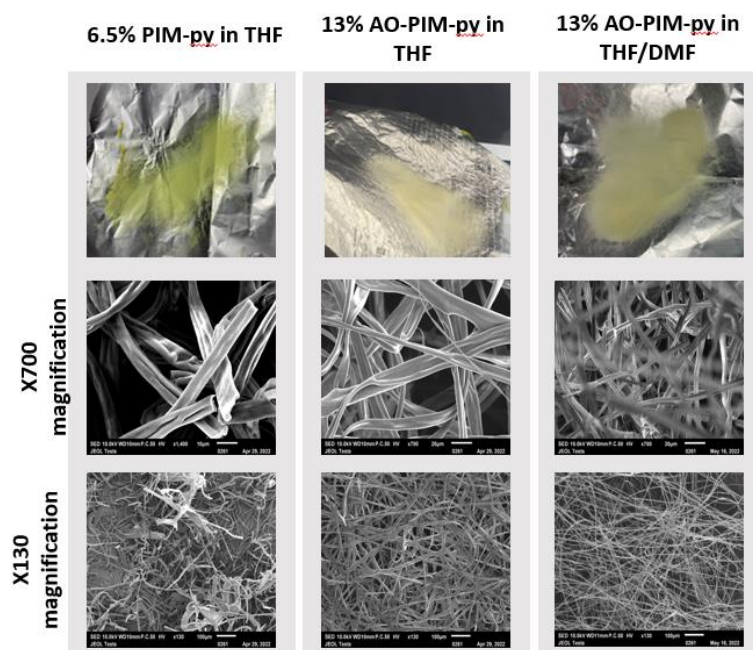
**Figure 3.11** Schematic illustration of an electrospinning equipment set up.<sup>148</sup>

Powdered samples of **PIM-py** and **AO-PIM-py** were sent to our collaborator, Prof. Maria-Chiara Ferrari in the School of Engineering, University of Edinburgh, for electrospinning studies to attempt to process fibrous materials. A series of solvent combinations and polymer concentrations were tested to identify the optimum electrospinning conditions (**Table 3.2**). The details of the fibrous films were observed by scanning electron microscopy (SEM). This technique involves scanning the surface of the fibrous mats with a beam of electrons, to generate micrographic images.

**Table 3.2** Electrospinning conditions for **PIM-py** and **AO-PIM-py**

| Solvents         | Concentration (%) | Observation             |
|------------------|-------------------|-------------------------|
| <b>PIM-py</b>    |                   |                         |
| THF              | 20                | No - Viscosity too high |
| THF              | 13                | No - Viscosity too high |
| THF              | 6.5               | Non-uniform fibres      |
| THF: DMF (9:1)   | 6.5               | No - Viscosity too low  |
| <b>AO-PIM-py</b> |                   |                         |
| DMF              | 30                | No - Viscosity too high |
| DMSO             | 20                | No - Viscosity too high |
| DMSO             | 13                | Agglomerated            |
| THF              | 20                | No - Viscosity too high |
| THF              | 13                | Non-uniform fibres      |
| THF: DMF (9:1)   | 13                | Non-uniform fibres      |

Results show that PIM-py and AO-PIM-py do indeed possess the ability to be electrospun into fibrous materials (**Figure 3.11**). A polymer solution containing 6.5% **PIM-py** in THF produced non-uniformly shaped nanofibres that appear bright yellow. For **AO-PIM-py**, polymer solutions using DMF and DMSO were found to be too viscous for electrospinning. THF was chosen as an alternative solvent, despite the polymer's poor solubility in this solvent. In pure THF at 13% concentration, the electrospun polymer produced off-white fibrous mats with non-uniformly shaped flat fibres but caused significant needle blockage due to its poor solubility. The addition of DMF to the polymer solution (10%) resulted in less blockage while producing similar quality nanofibres.

**Figure 3.11** Electrospun fibres obtained for PIM-py and AO-PIM-py under different conditions, with SEM images of the fibres at different magnitudes of magnification.

## 3.5 Gas Separation Measurements

### 3.5.1 Background of PIMs for Gas Separation Membranes

PIMs have excellent potential as membrane materials for gas separations due to their ultrapermeability. The effectiveness of PIM-based membranes is deduced by measuring gas selectivity and permeability of the material.

Gas separation in purely polymeric materials, such as PIM-based membranes, is widely believed to follow the solution-diffusion model, where the permeability ( $P$ ) of the gas molecules through a membrane is determined by the solubility ( $S$ ) – the volume of gas molecules adsorbed onto the polymer – and diffusivity ( $D$ ) – the rate at which the adsorbed molecules travel through the membrane. In a gas mixture containing two types of gases, X and Y, the membrane's selectivity ( $\alpha_{X/Y}$ ) toward gas A is determined by the difference in permeability between the gas pair.<sup>122</sup> Due to the unique structural characteristics of PIMs, with their rigid and contorted structure resulting in the formation of semi-permanent pores, gas separation using PIM-based membranes could also be achieved *via* a molecular sieving mechanism – allowing only gas molecules smaller than the pore diameter of the polymers to pass through whilst hindering the transport of larger gas molecules.<sup>152</sup>

All polymer membranes for gas separation exhibit a trade-off between permeability and selectivity, wherein highly selective membranes lack permeability, and vice versa. In 1991, Robeson compiled permeability data for six common gases, namely O<sub>2</sub>, N<sub>2</sub>, H<sub>2</sub>, H<sub>2</sub>, CO<sub>2</sub>, and CH<sub>4</sub>, using over 300 references.<sup>153</sup> The permeability/selectivity trade-off between pairs of these six gases was analysed, establishing an 'upper bound' for various common gas pairs describing the limits of selectivity at a given permeability value for existing membrane materials. The upper bound for permeability/selectivity has since been revisited.<sup>121,154,155</sup> Notably, PIMs have made key contributions to redefining upper bounds, with many polymers of this class demonstrating high selectivity while maintaining increased permeability performances. PIMs achieve this effect owing to their unique microstructure, which consists of a mixture of ultramicropores and high polymer chain rigidity for enhanced selectivity, and larger micropores for good permeability performances. TPIM-1, PIM-Trip-TB have set new limits for gas pairs O<sub>2</sub>/N<sub>2</sub>, H<sub>2</sub>/N<sub>2</sub> and H<sub>2</sub>/CH<sub>4</sub>,<sup>155</sup> while PIM-TMN-Trip has redefined limits for CO<sub>2</sub>/N<sub>2</sub> and CO<sub>2</sub>/CH<sub>4</sub> (**Figure 3.12**).<sup>121</sup>

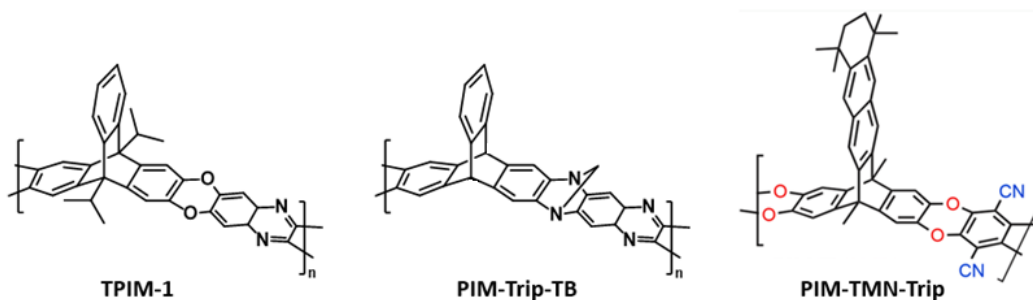


**Figure 3.12** Structures of PIMs that redefined the upper bound limits.

### 3.5.2 Analysis of Gas Permeability Data

Single gas permeabilities of the freshly methanol treated, solution cast films of **PIM-py** and **AO-PIM-py** membranes have been measured, and the results are compared against the equivalent figures for **PIM-1** and **AO-PIM-1**, provided by **ITM**. These data are summarised in **Table 3.2**.

**Table 3.2** Single gas permeabilities ( $P_X$ , *Barrer*) and ideal selectivities ( $\alpha_{X/Y}$ ) for **PIM-py**, **AO-PIM-py**, **PIM-1** and **AO-PIM-1** at 25 °C.

| Polymer   | $P_{N_2}$ | $P_{O_2}$ | $P_{CO_2}$ | $P_{CH_4}$ | $P_{H_2}$ | $P_{He}$ | $\alpha_{CO_2/CH_4}$ | $\alpha_{CO_2/N_2}$ | $\alpha_{O_2/N_2}$ | $\alpha_{H_2/CH_4}$ | $\alpha_{H_2/N_2}$ |
|-----------|-----------|-----------|------------|------------|-----------|----------|----------------------|---------------------|--------------------|---------------------|--------------------|
| PIM-py    | 766       | 2413      | 11692      | 1194       | 8489      | 4430     | 9.79                 | 15.27               | 0.73               | 7.11                | 11.09              |
| AO-PIM-py | 30.3      | 113       | 933        | 42.2       | 438       | 234      | 22.1                 | 30.81               | 3.87               | 10.38               | 14.48              |
| PIM-1     | 653       | 2072      | 12211      | 1153       | 4930      | 1938     | 10.59                | 18.71               | 0.4                | 4.28                | 7.55               |
| AO-PIM-1  | 33        | 147       | 1153       | 34         | 912       | 412      | 34                   | 33                  | 4.5                | 0.8                 | 27.6               |

\*PIM-py, AO-PIM-py and PIM-1 films were soaked in MeOH for 24 h prior to measurement.

All polymers showed a gas permeability order of  $CO_2 > H_2 > He > O_2 > CH_4 > N_2$ ; the gas permeability performances of **PIM-py** are similar to those of **PIM-1**, which is unsurprising due to its similarity in structure, BET surface areas, and pore size distributions. Interestingly, it was observed that **PIM-py** showed significant higher permeabilities for  $H_2$  and  $He$  compared to the other three polymers. One plausible explanation for this observation might stem from examining the structural differences of the polymers and the sizes of gas molecules (**Table 3.3**). The average bond length of a nitrile group attached to aromatic components is 1.138 Å.<sup>156</sup> **PIM-py** contains only one nitrile group on each of its repeating units, in contrast to **PIM-1**, which has two nitrile groups. While this difference may be negligible for larger gas molecules such as  $N_2$  and  $CH_4$ , it becomes substantial for smaller molecules such as  $H_2$  and  $He$ , as the absence of one of the nitrile groups may enhance ultramicroporosity. Therefore, this suggests that small gas molecules ( $He$ ,  $H_2$ ) might be able to pass through the membrane with less hindrance, while the difference in pore space is not significant enough to impact the permeabilities of larger gases.

**Table 3.3** The kinetic diameter (Å) of gas molecules in ascending order.<sup>157</sup>

| Gas Molecule         | He  | H <sub>2</sub> | CO <sub>2</sub> | O <sub>2</sub> | N <sub>2</sub> | CH <sub>4</sub> |
|----------------------|-----|----------------|-----------------|----------------|----------------|-----------------|
| Kinetic Diameter (Å) | 2.6 | 2.89           | 3.3             | 3.46           | 3.64           | 3.8             |

Both AO modified polymers showed the highest selectivity towards CO<sub>2</sub>, possibly due to the presence of H-bonding reducing the overall porosity, which will slow the transport of larger gases.<sup>133,134</sup> Overall, the incorporation of the pyridine group did not cause a notable impact in the gas separation performances of the polymers.

Observation of the diffusivity and solubility data obtained for the polymers (**Table 3.4**) further confirms that AO modification affects permeability performances mainly *via* reducing the speed of diffusion for gas molecules. A minor reduction in solubility post AO modification was also noted. This reduction could be due to the reduction in microporosity of the AO modified polymers, therefore reducing the volume of gas molecules that could dissolve into the polymer during testing.

**Table 3.4** Diffusivity ( $D_x$ , 10<sup>-12</sup> m<sup>2</sup> s<sup>-1</sup>) and solubility ( $S_x$ , cm<sup>3</sup><sub>STP</sub> cm<sup>-3</sup> bar<sup>-1</sup>) of PIM-py, AO-PIM-py, PIM-1 and AO-PIM-1 at 25 °C.

| Polymer   | $D_{N_2}$ | $D_{O_2}$ | $D_{CO_2}$ | $D_{CH_4}$ | $D_{H_2}$ | $D_{He}$ |
|-----------|-----------|-----------|------------|------------|-----------|----------|
| PIM-py    | 147       | 407       | 15.5       | 62.8       | 8512      | 14665    |
| AP-PIM-py | 8.8       | 29.3      | 11.8       | 2.7        | 715       | 1244     |
| PIM-1     | 144       | 397       | 172        | 63.9       | 5525      | 7175     |
| AO-PIM-1  | 9.9       | 40.6      | 24.6       | 2.6        | -         | -        |
| Polymer   | $S_{N_2}$ | $S_{O_2}$ | $S_{CO_2}$ | $S_{CH_4}$ | $S_{H_2}$ | $S_{He}$ |
| PIM-py    | 3.91      | 4.44      | 56.4       | 14.3       | 0.75      | 0.23     |
| AP-PIM-py | 2.59      | 2.9       | 59.1       | 11.6       | 0.46      | 0.14     |
| PIM-1     | 3.4       | 3.91      | 53.15      | 13.53      | 0.67      | 0.2      |
| AO-PIM-1  | 3.3       | 3.6       | 46.8       | 13         | -         | -        |

Physical aging of PIMs can occur, where the polymer becomes more dense over time, and a reduction in micropore volumes and size distribution occurs, which can significantly affect their gas separation performances.<sup>158</sup> The gas permeability and selectivity of the **PIM-py** membrane were measured again after 41 days, and compared against the results of its fresh membrane (**Table 3.5**). A general decrease in permeability of the aged sample is observed, with the exception of CO<sub>2</sub>. A small increase in the selectivity for the aged sample was observed, which could be attributed to the reduction in pore sizes, leading to a better molecular sieving effect.<sup>159</sup> The interesting enhanced selectivity for H<sub>2</sub> and He relative to **PIM-1** appears to decrease over time suggesting loss of ultramicroporosity.



**Table 3.5** Comparison of permeability ( $P_X$ , Barrer) and selectivity ( $\alpha_{X/Y}$ ) for fresh and 41 days aged PIM-py membrane.

| Polymer       | $P_{N_2}$ | $P_{O_2}$ | $P_{CO_2}$ | $P_{CH_4}$ | $P_{H_2}$ | $P_{He}$ | $\alpha_{CO_2/CH_4}$ | $\alpha_{CO_2/N_2}$ | $\alpha_{O_2/N_2}$ | $\alpha_{H_2/CH_4}$ | $\alpha_{H_2/N_2}$ |
|---------------|-----------|-----------|------------|------------|-----------|----------|----------------------|---------------------|--------------------|---------------------|--------------------|
| PIM-py        | 766       | 2413      | 11692      | 1194       | 8489      | 4430     | 9.79                 | 15.27               | 0.73               | 7.11                | 11.09              |
| PIM-py (41 d) | 686       | 2293      | 13310      | 1035       | 6141      | 2796     | 12.87                | 19.39               | 3.34               | 5.94                | 8.95               |

To gain a better grasp of the gas separation performance of **PIM-py** and **AO-PIM-py** in comparison to other polymers, their data were plotted onto Robeson plots to visualise their position relative to the upper bounds (**Figure 3.12**). The gas separation capabilities of fresh and 41 days aged **PIM-py** are generally similar to that of **PIM-1**, their performances generally lie close to the 2008 revised upper bound.<sup>154</sup> The **PIM-py** membrane demonstrated both good permeability and selectivity towards CO<sub>2</sub> over N<sub>2</sub> and CH<sub>4</sub> with their positions above the 2008 upper bounds but below the newest upper bounds set by McKeown *et al.* in 2019. **AO-PIM-py** also showed good permeability and selectivity performances towards CO<sub>2</sub>, with data placed near the 2008 upper bound for both CO<sub>2</sub>/CH<sub>4</sub> and CO<sub>2</sub>/N<sub>2</sub> gas pairs. However, their performances towards other gas pairs is comparatively modest, with data placed below the initial 1991 upper bounds, showing a modest combination of permeability and selectivity.

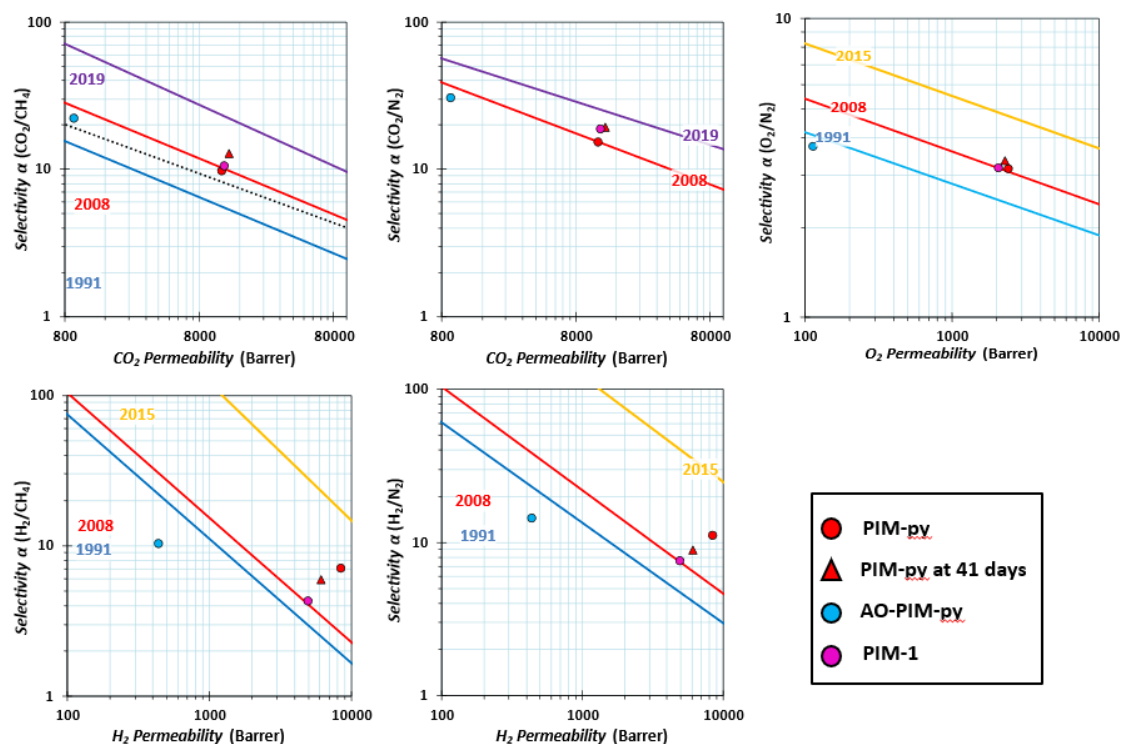


**Figure 3.12** Robeson plot for gas pairs CO<sub>2</sub>/CH<sub>4</sub>, CO<sub>2</sub>/N<sub>2</sub>, H<sub>2</sub>/CH<sub>4</sub>, H<sub>2</sub>/N<sub>2</sub>, and O<sub>2</sub>/N<sub>2</sub>, showing positions of **PIM-1**, fresh **PIM-py**, aged **PIM-py**, and **AO-PIM-1**. Initial upper bound (blue line), updated upper bound (red line), newest upper bounds for O<sub>2</sub>/N<sub>2</sub>, H<sub>2</sub>/N<sub>2</sub> and H<sub>2</sub>/CH<sub>4</sub> (yellow), and CO<sub>2</sub>/N<sub>2</sub> and CO<sub>2</sub>/CH<sub>4</sub> (purple) are shown on the plots.

To conclude, the introduction of pyridine sites onto a **PIM-1**-like polymer did not lead to notable changes in their characteristics such as surface area, as well as the size and volume of the pores. **PIM-py** showed comparable performances for gas adsorption ( $N_2$  and  $CO_2$ ), as well as similar gas permeability and separation performance. In contrast, the introduction of AO group onto **PIM-py** to give **AO-PIM-py** greatly affected the microporous characteristics of the polymers. The incorporation of the AO group generally reduced the permeability of the polymer and enhanced selectivity. The AO group also appeared to increase the affinity of the polymer towards  $CO_2$  relative to other gases perhaps due to greater polar-quadrupolar interactions.

## Chapter 4 Naphthopleiadene-Based Monomers

The adsorption capacity of microporous materials is dependent on their high porosity and large surface area.<sup>160</sup> Therefore, in order to improve the adsorption properties of PIMs, alternative structural units for polymerisation were investigated to increase their surface area.

The high surface area of PIMs relies on their rigid and contorted structure to pack inefficiently in space. To achieve the desired awkward packing effect of the polymer chains, structural units with high internal molecular free volume (IMFV) are highly preferred.<sup>161</sup> This concept is supported by computational studies conducted by Jiao *et al.*, on the relationship between the degree of deformation, represented by deformation parameter ( $p$ ) of an object, and their packing efficiency, evaluated by the density ( $\Phi$ ) where the fraction of space covered by the particles are measured.<sup>162</sup> In the study, Jiao *et al.* produced a representation depicting the degree of deformation of an object (**Figure 4.1a**). From a perfect sphere ( $p=1$ ), the shape of the object becomes convex when  $p > 1$  and concave when  $p < 1$ . The packing efficiency reaches maximum at  $p = 0.5$  and  $p = \infty$ , where the shape becomes a perfect square, and decreases as the degree of concavity increases ( $p \rightarrow 0$ ) (**Figure 4.1b**).<sup>163</sup>

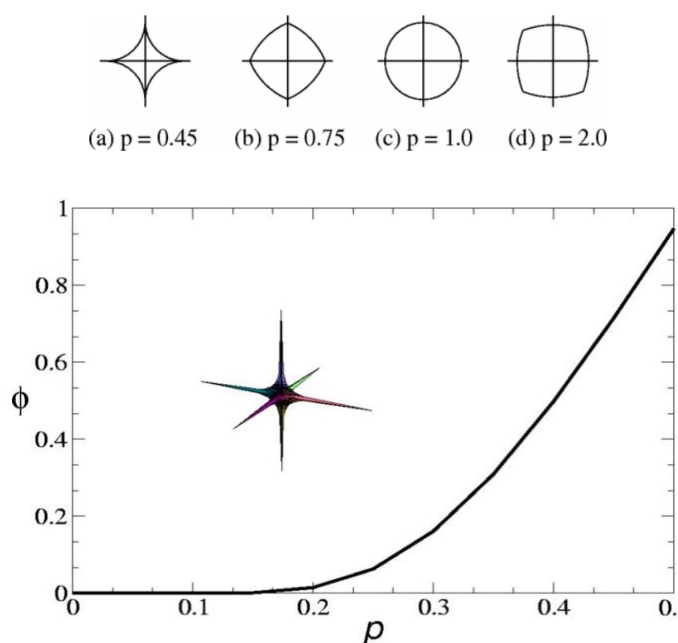


**Figure 4.1** (a) Illustration of shapes with different degrees of deformation  $p$ , deviating from a perfect sphere. (b) Relationship between density  $\Phi$  and the degree of deformation  $p$ .

In the past two decades, numerous analogues of PIMs composed of different structural units were reported,<sup>91</sup> with those containing units of triptycene derivatives achieving exceptionally high surface areas of up to  $1024 \text{ m}^2 \text{ g}^{-1}$ , due to the high IMFV associated with their structure (**Figure 4.2**).<sup>121,164</sup>

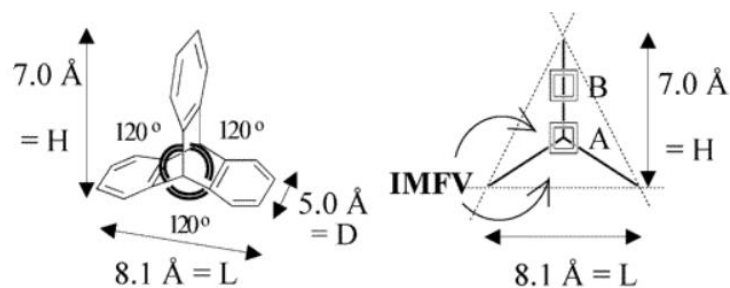


**Figure 4.2** Illustration of a basic triptycene molecule, highlighting its dimensions and IMFV.<sup>92</sup>

Despite the superior surface area and promising performances in properties such as gas permeability and selectivity offered by PIMs based on triptycene and structurally similar building blocks, a common drawback related to these types of structural units is their often complicated, multi-step synthesis required to obtain the target structure.<sup>99</sup>

Amin *et al.* from the McKeown group have recently reported a new group of compounds known as naphthopleiadenes (NPs).<sup>165</sup> These compounds feature a unique bridged bicyclic framework with in-built hydroxyl functionality. Their structures consist of two naphthalene units and a benzene ring, all connected by two bridging carbon atoms (**Figure 4.3**). NPs exhibit structural similarities to triptycenes, their planes are also at 120° relative to each other, offering a similarly high IMFV.<sup>165</sup> Unlike the typical complicated synthetic steps required for triptycene units, the reported NPs, bearing similar bulkiness and rigidity to the traditional triptycenes, can be prepared from a simple one-step synthesis from 2,7-dihydroxynaphthalene and phthalaldehyde in methanol with concentrated hydrochloric acid (HCl) as catalyst. Amin *et al.* reported that NP-based polymers can be prepared with outstanding average molecular mass ( $M_n = 140,000 \text{ g mol}^{-1}$ ) and demonstrate promising CO<sub>2</sub> uptake. To further explore the CO<sub>2</sub> uptake potential of naphthopleiadenes, and their general adsorption performance, this chapter investigates the synthesis of similar NP structures with in-built amine functionalities.

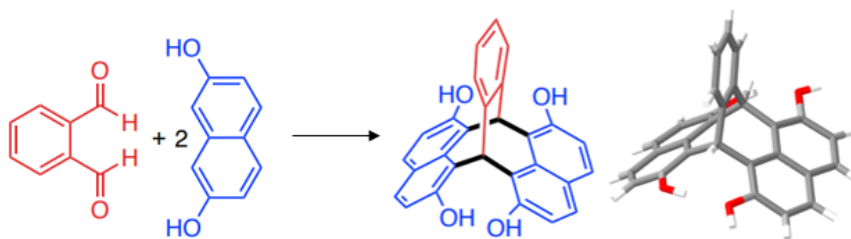
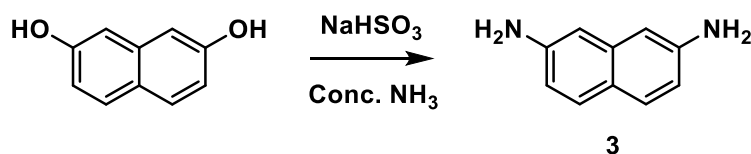


**Figure 4.3** One-step synthesis of tetra-hydroxyl naphthopleiadene (**NP1**) and its crystal structure.<sup>165</sup>

## 4.1 Monomer Synthesis

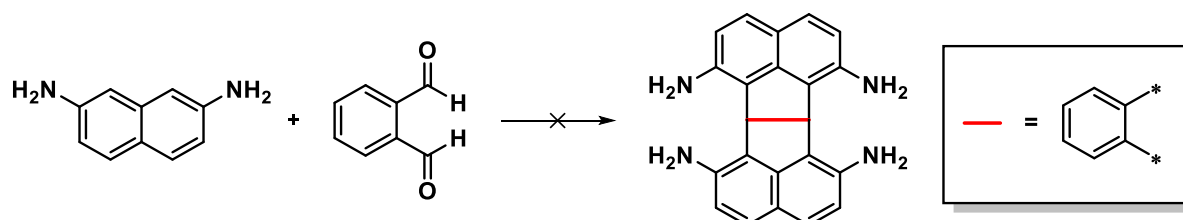
### 4.1.1 Synthesis of 2,7-diaminonaphthalene



**Scheme 4.1** Synthesis of 2,7-diaminonaphthalene

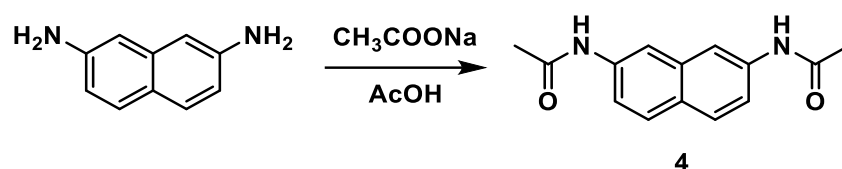
A classic Bucherer reaction was performed based on a modified procedure from the literature,<sup>166</sup> to convert 2,7-dihydroxynaphthalene into 2,7-diaminonaphthalene for the incorporation of amine functionality in naphthopleiadene compounds. The reaction was carried using sodium hydrogen sulfite ( $\text{NaHSO}_3$ ) and concentrated ammonia solution, heated to 170 °C in a pressurised vessel for 17 hours, and the diamine product was obtained with 96% yield.

The formation of NP from 2,7-diaminonaphthalene was attempted with phthalaldehyde in ethanol, with addition of conc. HCl. However, the characteristic bridgehead proton peaks of a NP compound could not be found on the  $^1\text{H}$  NMR spectrum, and the peaks obtained appeared to be broad and undefined, similar to those observed for PIM-like polymers. Therefore, it can be concluded that the target NP compound was not synthesised successfully (**Scheme 4.2**). The conditions used for the attempted synthesis of NP is similar to that used in Schiff base imine formation,<sup>167</sup> therefore it is likely that the Schiff base reaction has taken place instead of the intended NP formation. Given the reactive nature between primary amines and aldehydes, a series of protected derivatives of 2,7-diaminonaphthalene were then prepared to prevent the unwanted nucleophilic addition reaction between amine and aldehyde groups.



**Scheme 4.2** Targeted reaction between 2,7-diaminonaphthalene and phthalaldehyde.

#### 4.1.2 Protected 2,7-Diaminonaphthalene Derivatives



**Scheme 4.3** Synthesis of *N,N'*-2,7-naphthalenebis(acetamide)

As a common protecting group for amines, an acetamide group was the initial option for the protection of 2,7-diaminonaphthalene (**Scheme 4.3**). However, the protecting group's stability in acidic conditions was found to be problematic when the synthesised *N,N'*-2,7-naphthalenebis(acetamide) was reacted with phthalaldehyde in acidic reactions. Initially following the reaction condition reported by Amin *et al.*,<sup>165</sup> where the *N,N'*-2,7-naphthalenebis(acetamide) and phthalaldehyde were refluxed in a solution of conc. HCl acid in MeOH for 4 hours, *N,N'*-2,7-naphthalenebis(acetamide) showed no reactivity with phthalaldehyde. The reaction was then carried out using 0.2 and 0.5 mL of conc. HCl in 15 mL of MeOH respectively. At 0.2 mL of conc. HCl, no reaction had occurred, and the cleaving of the acetamide group was observed at 0.5 mL of conc. HCl which yielded a complex reaction mixture.

Following the unsuccessful outcome of using acetamide protection groups, several 2,7-diaminonaphthalene derivatives that are stable in acidic conditions were developed. Reactions of 2,7-diaminonaphthalene with methanesulfonyl chloride and 9-fluorenylmethyloxycarbonyl (**fmoc**) chloride as alternative protecting groups were performed, giving compound **5** and **6** with reasonably high yields at 67% and 61% respectively (**Table 4.1**).

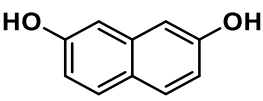
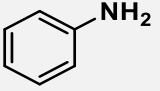
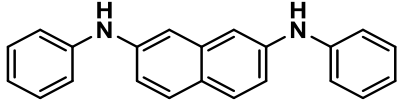
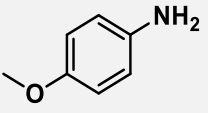
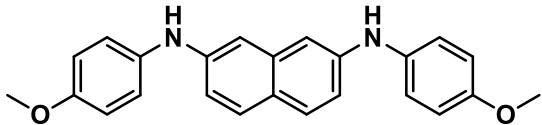
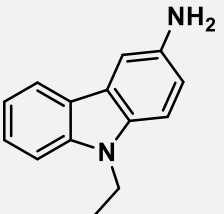
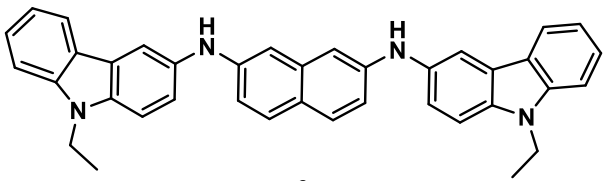
**Table 4.1** Protection of 2,7-diaminonaphthalene with methanesulfonyl chloride and fmoc.

| Reactant 1 | Reactant 2 | Product |
|------------|------------|---------|
|            |            |         |
|            |            |         |

Due to the inconvenience of 2,7-diaminonaphthalene production involving high pressure, alternative reactions to using the commercially available 2,7-dihydroxynaphthalene were also explored.

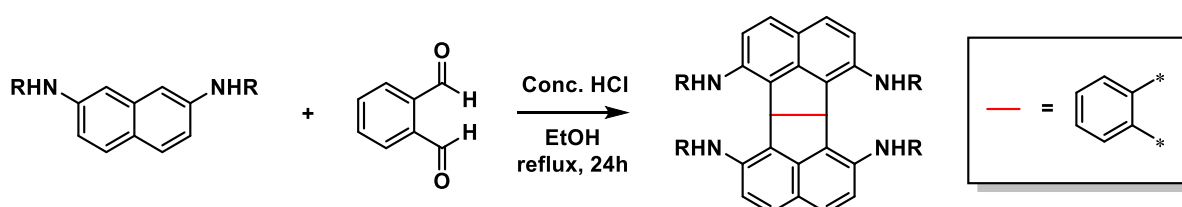
Compounds **7-9** were obtained *via* reaction between 2,7-dihydroxynaphthalene and their respective precursors (**Table 4.2**). The synthesis of compound **7** based on a literature method<sup>168</sup> was carried out at 145 °C in a microwave reactor for 3 hours in the presence of aniline chloride, giving 98% conversion. The synthesis of compounds **8** and **9** based on a modified literature method<sup>169</sup> were both carried out in the presence of a catalytic amount of I<sub>2</sub>. Compounds **8** and **9** were produced in 33% and 40% yield respectively.

**Table 4.2** Reaction between 2,7-dihydroxynaphthalene and primary amines.

| Reactant 1  | Reactant 2   | Product  |
|---|--|--|
|  |   | <br>7  |
|   |   | <br>8  |
|   |  | <br>9 |

#### 4.1.3 Amine-Containing Naphthopleiadenes

After the successful synthesis of amine-based naphthalenes (compounds **5-9**), their subsequent reactions with phthalaldehyde were performed in an attempt to obtain their respective naphthopleiadene (NP) structures (**Scheme 4.4**).



**Scheme 4.4** General reaction scheme between amine-based naphthalenes and phthalaldehyde in ethanol with conc. HCl.

Initial attempts between the amine-based naphthalenes **5-9** and phthalaldehyde were carried out following the procedure described by Amin *et al.* using 0.1 mL of conc. HCl in 15 ml of alcohol solution. However, no reaction was observed with any of the amine-based naphthalenes. The reactions

were attempted repeatedly with increasing amount of conc. HCl present. It was found that all protecting groups proved to be stable in the increasingly acidic conditions. However, compounds **5**, showed negligible reactivity towards phthalaldehyde, possibly due to the electron withdrawing effect of the mesylate group deactivating the ring system.<sup>170</sup> Similarly, compounds **6** and **9** also showed no reaction even in a large excess of conc. HCl, which is believed to be the result of the incorporation of extremely bulky protecting groups, blocking the access to the reaction sites.

Amine-containing NPs (**NNPs**) were successfully obtained from naphthalene **7** and **8** in strongly acidic conditions with a large excess of conc. HCl. Reaction of phthalaldehyde with *N,N'*-bis(phenyl)-2,7-naphthalelediamine (**5**) resulted in a 61% conversion to **NNP1**. The obtained product was analysed by <sup>1</sup>H NMR spectroscopy, where the presence of characteristic bridgehead protons at 6.52 ppm strongly indicates the formation of the NP structure (**Figure 4.4**).

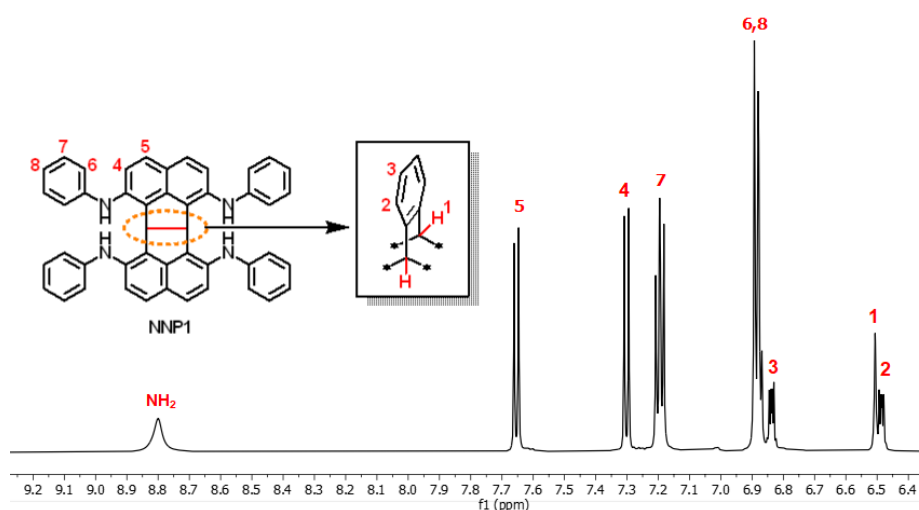
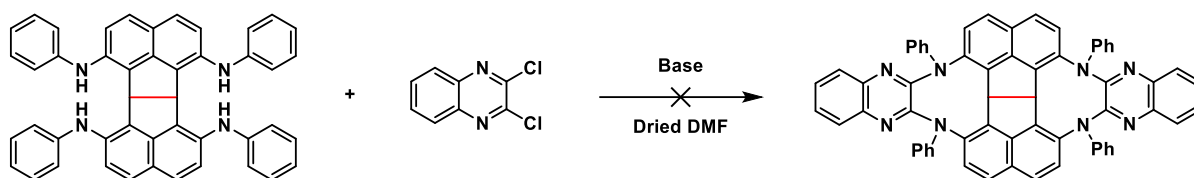


**Figure 4.4** Structure of **NNP1** with its <sup>1</sup>H NMR assignments.

After successfully obtaining **NNP1**, its reaction with 2,3-dichloroquinoxaline to form a derivative *via* a PIM forming reaction was investigated. **NNP1** and 2,3-dichloroquinoxaline in 1:2 ratio were reacted together in dried DMF at 65 °C, in the presence of K<sub>2</sub>CO<sub>3</sub> (**Scheme 4.5**). A small aliquot of the reaction mixture was worked up after 1 day. The <sup>1</sup>H NMR showed no reaction thus the reaction was allowed to react for 2 more days at an elevated temperature of 80 °C, but still no reactivity was observed. Finally, the reaction was attempted again at 120 °C with 8 eq. NaOH but the outcome was still without success. The due cause for this inactivity likely arises from the bulky aniline substituents, being crowded due to the structure of the NP unit making the nitrogen atoms inaccessible to 2,3-dichloroquinoxaline.





**Scheme 4.5** Reaction between **NNP1** and 2,3-dichloroquinoxaline in basic conditions

Reaction between 2,7-dihydroxynaphthalene and *N,N'*-bis(4-methoxyphenyl)-2,7-naphthalenediamine (**6**) yielded **NNP2** with 68% conversion and, a demethylation reaction was performed following a modified method described in the literature,<sup>100</sup> to obtain its tetrahydroxy-derivative **NNP3** in 93% yield (**Figure 4.5**). Bridgehead protons for **NNP2** and **NNP3** were found at 6.35-6.29 ppm and 6.23 ppm respectively, confirming the successful formation of NP structures. The successful conversion from **NNP2** to **NNP3** can be confirmed by the disappearance of methyl peaks in its <sup>1</sup>H NMR spectrum, as well as the appearance of peak corresponding to the OH group at 3223 cm<sup>-1</sup> in the IR spectrum.

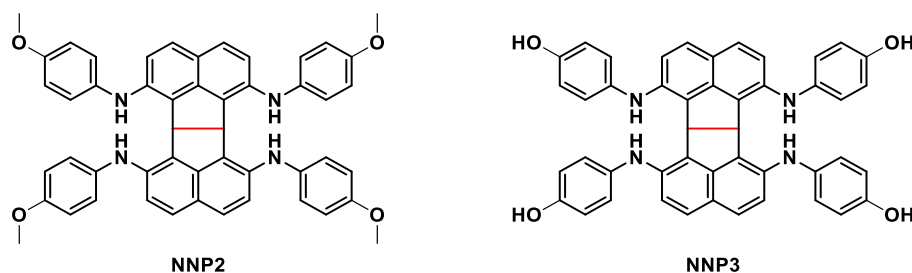
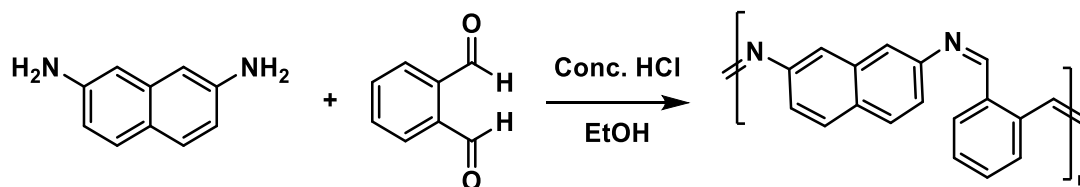


**Figure 4.5** Structure of **NNP2** and **NNP3**

## 4.2 Polymer Synthesis

As discussed previously in section 5.1, the reaction between 2,7-diaminonaphthalene and phthalaldehyde, refluxed in ethanol with the addition of 0.5 ml conc. HCl, yielded an unexpected product with a yield of 96%. Based on the similar reaction conditions involved,<sup>167</sup> imine formation via a Schiff base reaction is suspected to have occurred, instead of the targeted NP formation. **Scheme 4.6** shows the assumed structure of the polymer product **CP1** of the Schiff base reaction.



**Scheme 4.6** Ideal outcome of the Schiff based reaction between 2,7-diaminonaphthalene and phthalaldehyde.

The <sup>1</sup>H NMR showed very broad peaks, all merging together in the region between 9.0-4.9 ppm, suggesting the product is likely to be polymeric in nature. IR analysis of the product showed the

appearance of a C=N peak at  $1650\text{ cm}^{-1}$ , and the missing primary amine peaks at  $3385$ ,  $3296$ , and  $3196\text{ cm}^{-1}$ , further confirming the formation of an imine bond. Presence of a weak but noticeable C=O peak at  $1728\text{ cm}^{-1}$  points to the possibility of the product possibly being oligomeric rather than a polymer (**Figure 4.6**). The solubility of **CP1** was tested, and the polymer was found to have limited solubility in hot DMSO.

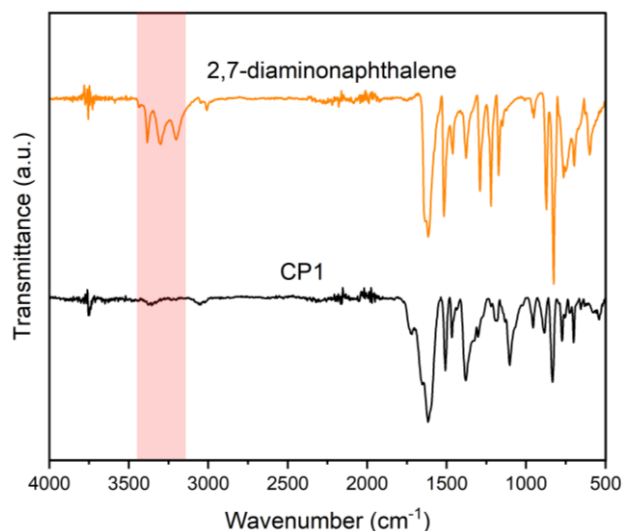
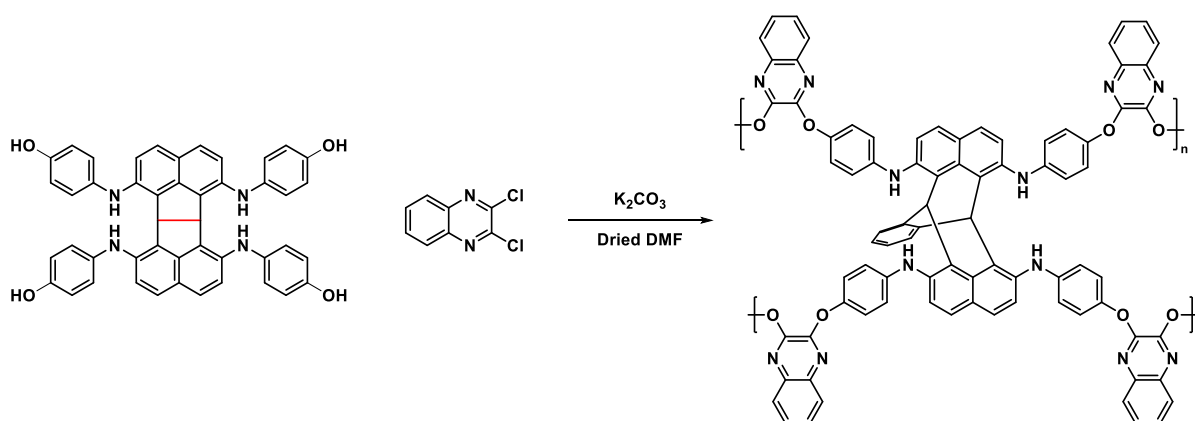


**Figure 4.6** Comparison between the IR spectra of 2,7-diaminonaphthalene and **CP1**

In addition to the preparation of **CP1**, the reaction between **NNP3** and 2,3-dichloroquinoxaline was performed to obtain a network polymer **CP2**. The reaction was carried out following similar reaction conditions to those used for making **PIM-1**, where the reactants were heated at  $65\text{ }^{\circ}\text{C}$  in dried DMF for 3 days, in the presence of  $\text{K}_2\text{CO}_3$ . The reaction yielded the polymer with 92% yield (**Scheme 4.7**).



**Scheme 4.7** Polymerisation reaction between **NNP3** and 2,3-dichloroquinoxaline.

The polymer remained insoluble in all common organic solvents, which suggests a high degree of crosslinking. Due to its insolubility, only  $^{13}\text{C}$  solid state NMR could be performed. Limited information

could be deduced from the spectra. A standalone peak was found at 44.79 ppm which corresponds to the bridgehead carbons, while all other peaks merged in the aromatic region between 160-104 ppm, as expected due to the polymer being comprised of predominantly aromatic rings. Successful polymerisation could be confirmed through comparison of IR spectra of **NNP3** and **CP2**, where the lack of an OH peak in the 3200-3100  $\text{cm}^{-1}$  region suggests that all hydroxyl groups had reacted (**Figure 4.7**).

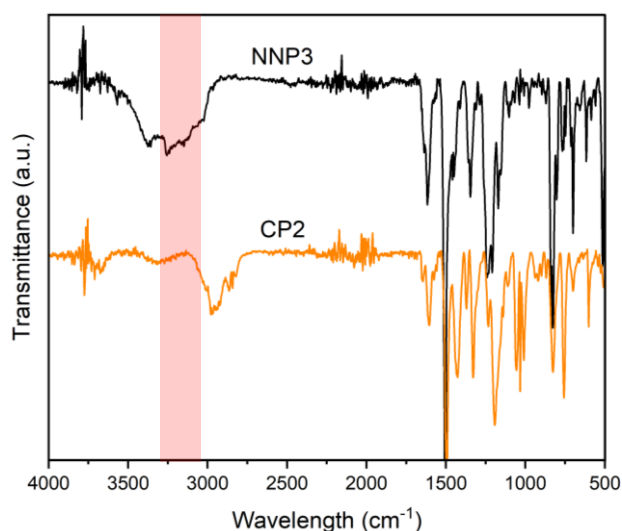
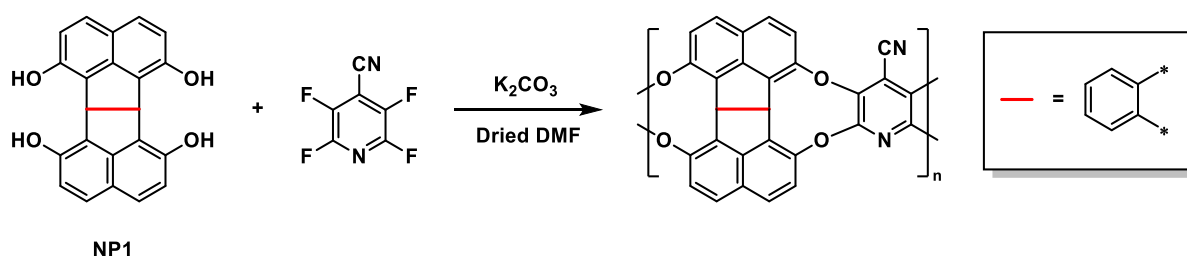


**Figure 4.7** Comparison of IR spectra between **NNP3** and **CP2**

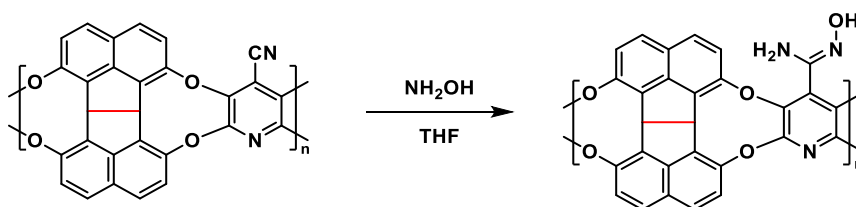
The failure of amine-containing NPs to form PIMs could be blamed on the steric confinement of the amine groups. However, based on the work reported by Amin *et al.*,<sup>165</sup> polymerisation was successfully performed between the initial hydroxy-containing **NP1** and tetrafluoroterephthalonitrile (TFTPN), to obtain **PIM-NP** with a high BET surface area of 635  $\text{m}^2 \text{g}^{-1}$ .<sup>165</sup> Inspired by this work along with the promising  $\text{CO}_2$  permeability property of reported pyridine-containing PIMs,<sup>171,172</sup> synthesis of **PIM-NP-py** from TFPCN and **NP1** unit was carried out (**Scheme 4.8**).



**Scheme 4.8** Synthesis of **PIM-NP-py** from **NP1** and TFPCN

The product obtained was found to be soluble in only hot quinoline. The occurrence of polymerisation could be confirmed due to this decrease in solubility from its relatively soluble monomers, and *via* the comparison of IR spectra between the product and **NP1** monomer, where the disappearance of the OH peak at 3177  $\text{cm}^{-1}$  was noted. However, the confirmation of the structure was

challenging as conventional analysis methods such as GPC and solution-state NMR could not be performed. A  $^{13}\text{C}$  solid state NMR of the product was obtained, but similar to that of **CP2**, limited structural information could be deduced from the spectra. However, a standalone peak could be observed at 39 ppm, corresponding to the bridgehead carbons, and broad, semi-merging peaks located at 151, 139, 128, and 120 ppm which correlate to the aromatic carbons.



**Scheme 4.9** Formation of **AO-PIM-NP-py**

The AO modification of PIM-NP-py was carried out using an excess of hydroxylamine 50wt. % in water, refluxed in THF for 1 day. The resulting polymer **AO-PIM-NP-py** was obtained as a pale-yellow powder at 96%. Successful conversion was determined by IR analysis, where the appearance of NH and OH peaks at  $3477\text{ cm}^{-1}$  and  $3369\text{ cm}^{-1}$  respectively signify the presence of the amidoxime group (**Figure 4.8**). The incorporation of the AO group did not lead to an improvement in solubility, likely due to the extensive hydrogen bonding between the AO group and the pyridine unit.

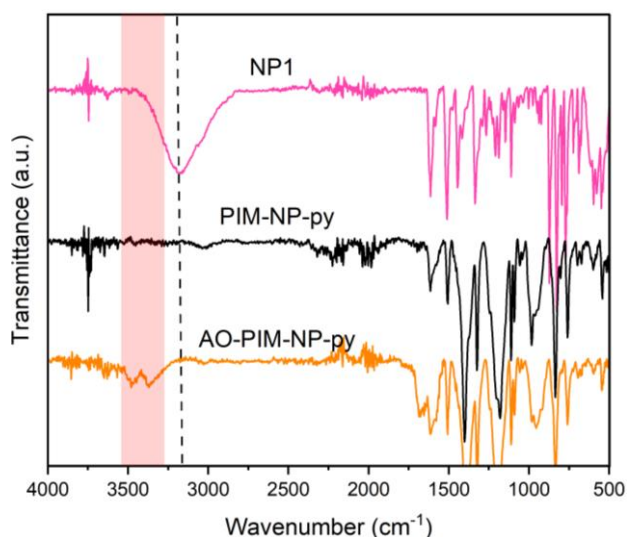


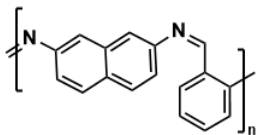
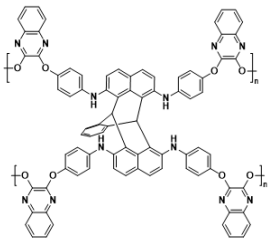
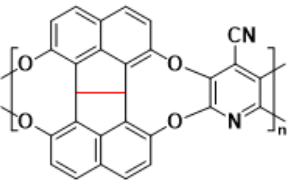
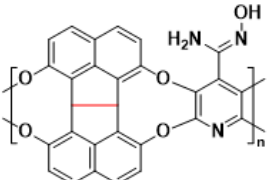
**Figure 4.8** IR comparison between the monomer **NP1**, polymers **PIM-NP-py** and **AO-PIM-NP-py**, noting the disappearance of OH peak (dotted line), and the appearance of amidoxime group (red highlight).

### 4.3 Polymer Analysis

Polymer **CP1** was found to be soluble in hot DMSO, and **PIM-NP-py** was soluble in hot quinoline, while **CP2** and **AO-PIM-NP-py** were found to be insoluble in all common organic solvents. The bad solubility

of the naphthalene-based polymer **CP1** is presumed to be the result of crosslinking between polymeric chains, while that for the NP-based **AO-PIM-NP-py** is believed to be due to the extensive hydrogen-bonding present between the polymeric chains caused by the additional nitrogen sites present. Due to the bad solubility of all those polymers, film formation was not attempted, and electrospinning could not be carried out for potential microfibre formation.

**Table 4.1** Gas adsorption properties of naphthalene/NP-based polymers

| Polymer  | Solubility    | Surface Area*<br>(m <sup>2</sup> g <sup>-1</sup> ) | Total Pore Volume*<br>(ml g <sup>-1</sup> ) | CO <sub>2</sub> Uptake*<br>(mmol g <sup>-1</sup> ) |
|--|---------------|--|---|--|
|  <p><b>CP1</b></p>            | Hot DMSO      | 12.0   | 0.0374                                      | 0.597  |
|  <p><b>CP2</b></p>           | Insoluble     | 0  | 0.00372                                     | 0.736  |
|  <p><b>PIM-NP-py</b></p>    | Hot Quinoline | 514  | 0.0582                                      | 2.32   |
|  <p><b>AO-PIM-NP-py</b></p> | Insoluble     | 1  | 0.00293                                     | 1.39   |

\*BET surface area was obtained from N<sub>2</sub> adsorption at 77 K, total pore volume was calculated from N<sub>2</sub> uptake at  $P/P_0 = 0.98$ , and CO<sub>2</sub> uptake was measured at 1 bar, 273 K.

The adsorption and desorption of nitrogen gas at 77 K were recorded for the synthesised polymers (**Figure 4.9**), from which the BET surface area and total pore volume of the polymers were calculated (**Table 4.1**). The N<sub>2</sub> uptake for **CP1** and **CP2** were very low, indicating their non-porous nature. The  $S_{A_{BET}}$  of the cross-linked polymers were also very low, which was expected due to the high rotational freedom of their polymeric chains. The N<sub>2</sub> adsorption isotherm for **PIM-NP-py** resembles

that of a Type I isotherm, indicating the polymer is indeed microporous.<sup>10</sup> A high surface area of 514 m<sup>2</sup> g<sup>-1</sup> was obtained for **PIM-NP-py**, showing significant improvement **CP1** and **CP2**. However, comparing to **PIM-py** and **PIM-1**, where the surface area of the polymers exceeded 700 m<sup>2</sup> g<sup>-1</sup>, the bulky NP structural unit did not appear to have any beneficial effect for surface area enhancement. Incorporation of AO has caused severe reduction in surface area, presumably due to the extensive H-bonding network introduced by the AO group.<sup>173</sup>

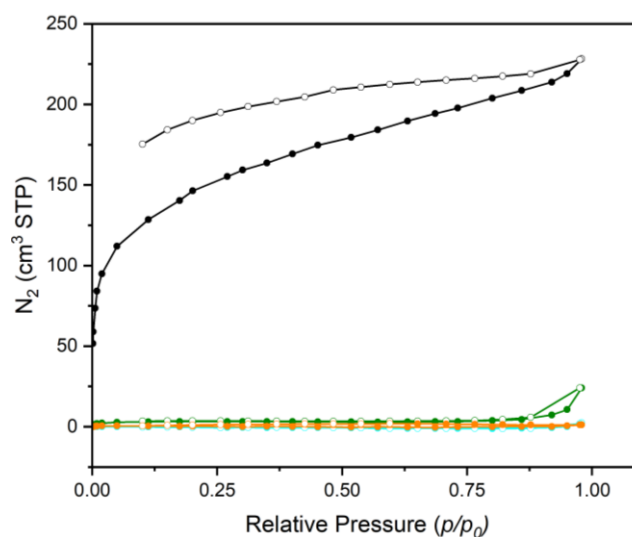


**Figure 4.9** N<sub>2</sub> adsorption (filled circle) and desorption (empty circle) isotherms of **CP1** (olive), **CP2** (cyan), **PIM-NP-py** (black), and **AO-PIM-NP-py** (orange).

The CO<sub>2</sub> adsorption characteristics for the polymers were recorded at 273 K (**Figure 4.10a**), from which their CO<sub>2</sub> uptake at 1 bar were determined, and the pore size distribution of the polymers were calculated using the density functional theory (DFT) model. Despite their non-porous structures from N<sub>2</sub> adsorption, **CP1** and **CP2** still exhibited CO<sub>2</sub> adsorption capacities. This difference could be attributed to the greater attractive surface interactions between the polymers and CO<sub>2</sub>,<sup>174</sup> and the temperature dependency of the rate of diffusion for gas molecules, where CO<sub>2</sub> adsorption was recorded at a much higher temperature (273 K) compared to the 77 K used for N<sub>2</sub> adsorption.<sup>175</sup> As expected, **PIM-NP-py**, which has the greatest surface area amongst the 4 polymers showed the highest CO<sub>2</sub> adsorption capacity, with an CO<sub>2</sub> uptake of 2.32 mmol g<sup>-1</sup> at 1 bar, 273 K. The functionalised **AO-PIM-NP-py** showed a reduced CO<sub>2</sub> uptake of 1.39 mmol g<sup>-1</sup> at 1 bar, due to its lower surface area. From the DFT model, all polymers were shown to consist of a mixture of ultramicropores (pore diameter < 0.7 nm) and micropores (pore diameter < 2 nm) (**Figure 4.10b**). **PIM-NP-py** comprises of mainly ultramicropores in its structure, which could also attribute to its higher CO<sub>2</sub> adsorption performance.<sup>176,177</sup> Contrary to the observation made with AO incorporation into a PIM-1 like structure in the previous chapter, where AO introduction resulted in a small increase in the number of smaller

ultramicropores (<0.4 nm), it was noticed that the introduction of AO groups into the NP-based polymer led to an apparent increase in the proportion of larger micropores present.

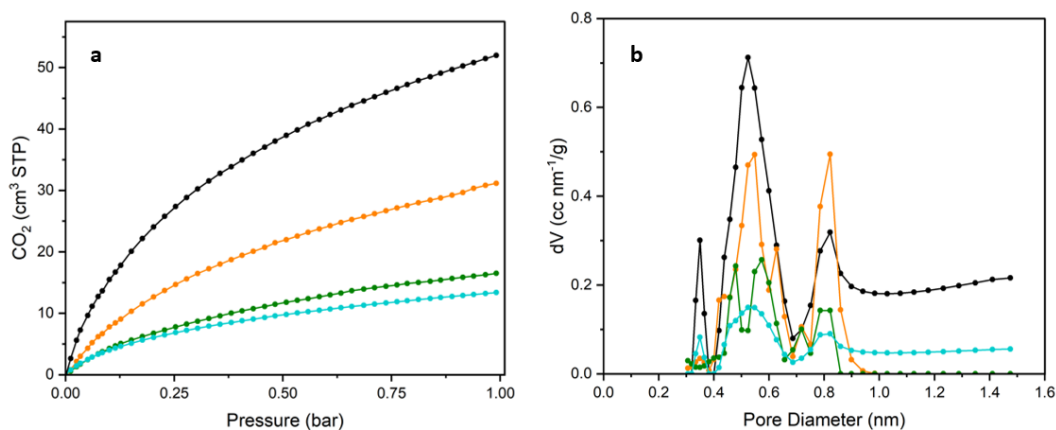


**Figure 4.10** a) CO<sub>2</sub> adsorption isotherms at 273 K, and b) pore size distributions for **CP1 (cyan)**, **CP2 (olive)**, **PIM-NP-py (black)** and **AO-PIM-NP-py (orange)**.

Thermogravimetric analysis (TGA) was also carried out on the synthesised polymers (**Figure 4.11**). All polymers exhibited good thermal stability, with **CP2**, and **PIM-NP-py** showing onset thermal decomposition at over 350 °C. **CP1** showed a slightly lower onset thermal decomposition temperature, which could be attributed to its more oligomeric structure.

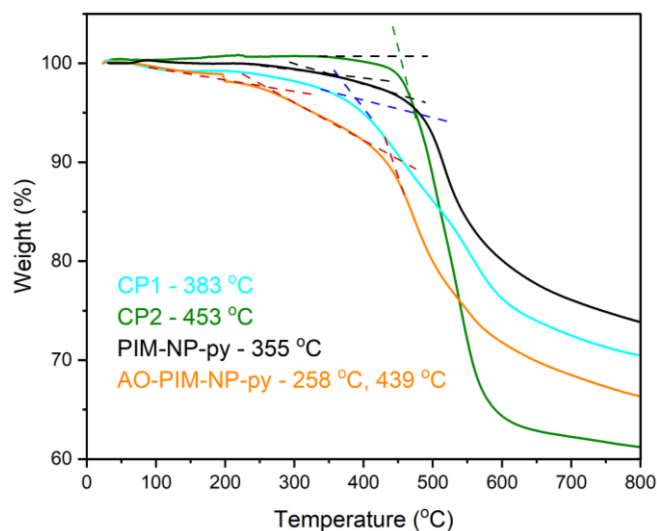


**Figure 4.11** TGA of **CP1 (cyan)**, **CP2 (olive)**, **PIM-NP-py (black)** and **AO-PIM-NP-py (orange)**, with their onset thermal decomposition temperature identified.

Film formation of **PIM-NP-py** was attempted from solutions made from 0.5 g of the polymer dissolved in 10 mL of quinoline, with the mixture subjected to heating and sonification to ensure the complete dissolution of the polymer. However, a membrane was unable to be obtained from the polymer (**Figure 4.12**). Possible reasons for this failure of film formation could be due to the extremely

rigid structure of the NP monomer unit, or that this polymer sample does not have sufficient molecular weight.



**Figure 4.12** Attempted film formation using **PIM-NP-py**.

Overall, the synthesis of amine-containing NP structural units was challenging. Protection groups were needed to prevent unwanted Schiff base side reactions between primary amine functionalities and phthalaldehyde. Steric hindrance played a key role at hindering the formation of NNP structural units, as well as the subsequent PIM synthesis. A PIM structure was obtained using a hydroxyl functionalised NP structural unit reported in the literature,<sup>165</sup> but the highly rigid and bulky NP structural unit did not make any notable improvements on the properties of the polymer. Introduction of AO groups significantly reduced the microporous characteristics of the polymer. Finally, incorporation of the NP structural unit appeared to greatly reduce the solubility of the polymers.



## Chapter 5 Synthesis of Fluorinated PIM Precursors

Competitive adsorption of water vapours is a persisting challenge faced by microporous materials for gas adsorption and separation.<sup>178–180</sup> PIMs in general are considered hydrophobic and therefore demonstrate a decent level of resistance to water vapours, however the performance of PIMs (e.g. **PIM-1**) are still impacted by its exposure to water vapours.<sup>181</sup> Moreover, the presence of adsorbed water vapour can induce plasticisation of PIMs, which can greatly alter the structure and adsorption properties of the polymers.<sup>182</sup> Therefore in this chapter, ways to increase the water repellent characteristic of PIMs further in order to minimise the impact of water vapours are explored.

Fluorinated polymers constitute a unique class of material that offer a set of distinctive commercially attractive properties, including chemical and thermal stability, as well as low surface energies.<sup>183,184</sup> These polymers are known for their hydrophobicity, stemming from the ability of fluorine atoms to minimise interactions, such as van der Waals and hydrogen bonding, between the polymer and molecules such as water.<sup>184,185</sup> Additionally, fluorinated polymers have demonstrated the capability to increase CO<sub>2</sub> uptake due to reduced inter-chain cohesion allowing greater interaction with CO<sub>2</sub>.<sup>186–188</sup> Moreover, the reduced intermolecular interactions between the polymeric chains due to the incorporation of fluorine can also alter the solubility of the polymer.

One common strategy for introducing fluorine is through the addition of trifluoromethyl (-CF<sub>3</sub>) groups.<sup>189</sup> These are similar in size to that of isopropyl groups, and in addition to the previously mentioned properties that fluorine atoms can bring, the incorporation of -CF<sub>3</sub> groups could also lead to a small increase in the internal molecular free volume of the molecule.<sup>190</sup> The functional group also exhibits similar electronegativity to that of Cl atoms,<sup>190</sup> which can lead to an enhancement of adsorption for polar gas molecules, such as CO<sub>2</sub>.<sup>191</sup> Furthermore, the incorporation of -CF<sub>3</sub> groups has been reported to increase a polymer's solubility in numerous cases,<sup>192–194</sup> owing to their ability to reduce interchain interactions while still leaving sufficient C-H bonds on the polymer to interact with organic solvents. This is a highly desirable property, considering that in previous chapters it was established that the solubility of polymers is greatly affected by the introduction of AO groups. The possibility of overcoming this disadvantage *via* the addition of -CF<sub>3</sub> groups was an attractive objective. This chapter explores the attempted synthesis of a series of -CF<sub>3</sub> containing monomers for utilisation in the preparation of PIMs.

## 5.1 Synthesis of Tetra(trifluoromethyl) Spirobisindane Monomers

In order to analyse the effect that  $-CF_3$  groups have on PIMs, the initial target was to prepare the fluorinated derivative of PIM-1, by replacing the  $-CH_3$  groups on spiro bisindane (SBI) units with  $-CF_3$  groups (**Figure 5.1**). A strapped SBI monomer with  $-CF_3$  was also designed with the aim to limit the rotational freedom of the spiro centre on the TTSBI molecule (**Figure 5.1**), hence increasing the rigidity and surface area further.

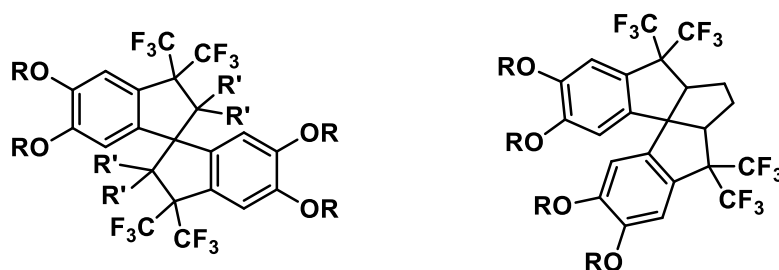
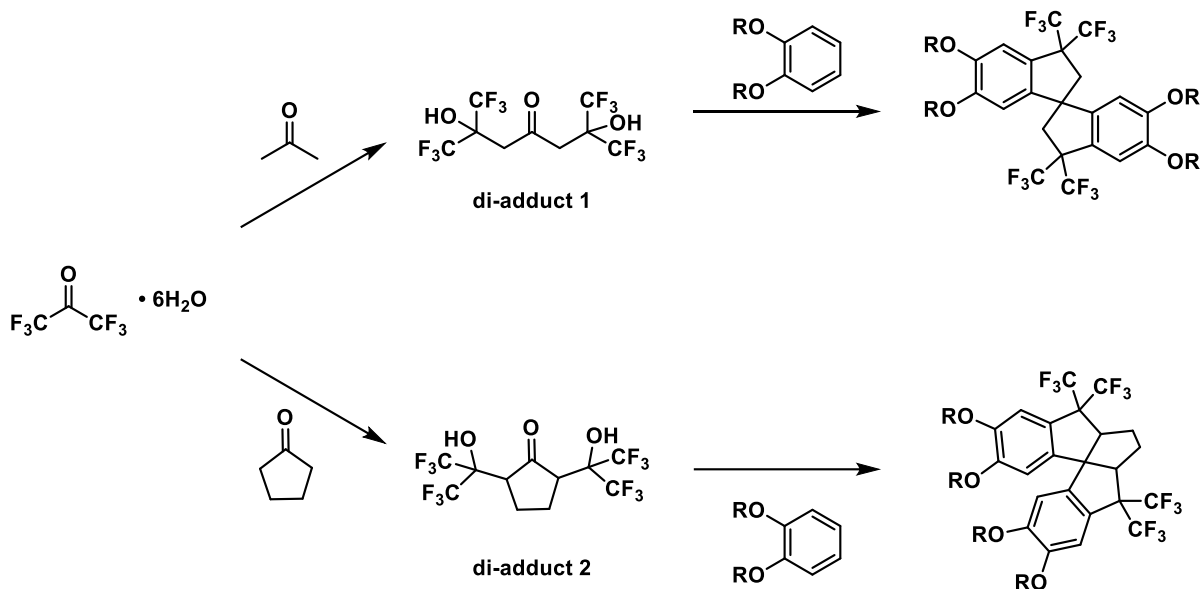


**Figure 5.1** SBI unit with  $-CF_3$  groups (left) and strapped SBI with  $-CF_3$  groups (right), with  $R = H$  or methyl groups, and  $R' = H$  or  $F$  atoms.

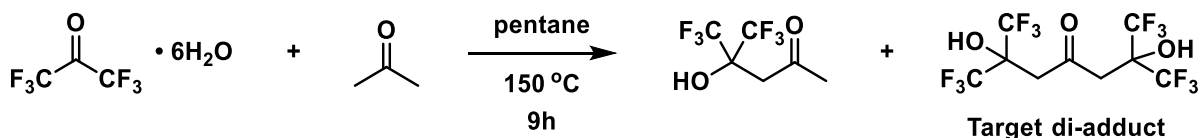
Following a procedure described in a series of patents from Jilin University China,<sup>195–197</sup> the first attempt at synthesising the fluorinated SBI monomer was made using similar reaction conditions used for TTSBI synthesis. Perfluoroacetone sesquihydrate and catechol was reacted using conc. HI acid, refluxed in acetic acid for 24 h. No reaction was observed, likely due to the superior stability of the fluorinated starting material arising from the presence of strong C-F bonds, causing difficulties for the initiation of the aldol condensation reaction between the perfluoroacetone molecules.

Instead, multi-step synthetic routes were designed to reach the targeted monomers (**Scheme 5.1**), which allows more appropriate conditions to be applied for the initial aldol reactions. Furthermore, to increase the reactivity, instead of carrying out aldol reaction between perfluoroacetone molecules, cross-aldol reaction between acetone (or cyclopentanone) and perfluoroacetone molecules were proposed.



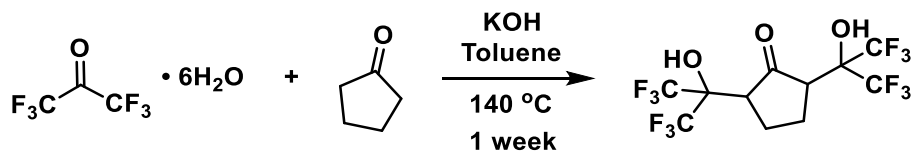
**Scheme 5.1** Proposed reaction route to obtain fluorinated SBI monomers.

### 5.1.1 Synthesis of tetra(trifluoromethyl) precursors



**Scheme 5.2** Reaction between perfluoroacetone sesquihydrate and acetone, producing a mixture of mono-adduct and the target **di-adduct 1**.

Following a literature procedure,<sup>198</sup> perfluoroacetone sesquihydrate and acetone were added to a pressure reactor vessel in the ratio of 2:1, the system was sealed under N<sub>2</sub> atmosphere and 30 ml of pentane was added to introduce pressure into the system. The reaction was heated to 150 °C for 9 hours, and a mixture of the mono-adduct and di-adduct was produced. The mono- and di-adduct was separated through vacuum distillation. The mono-adduct was collected with a yield of 73%, as a colourless liquid, and the target **di-adduct 1** was collected with a yield of 20%, as a white solid. The identity of the products was confirmed by NMR spectroscopy, which agreed with literature values.



**Scheme 5.3** Synthesis of **di-adduct 2**.

The novel **di-adduct 2** was successfully synthesised by heating perfluoroacetone sesquihydrate and cyclopentanone in toluene at 140 °C for 1 week (**Scheme 5.3**), using an excess of KOH. The reaction was carried out using a dean-stark apparatus, and toluene was used to form an azeotrope with water

molecules in order to remove water. Toluene was frequently added to the reaction mixture in small aliquots until no more water was collected. **Di-adduct 2** was obtained as a white solid, in 46% yield. The structure of the di-adduct was confirmed through NMR spectroscopy (**Figure 5.2**).

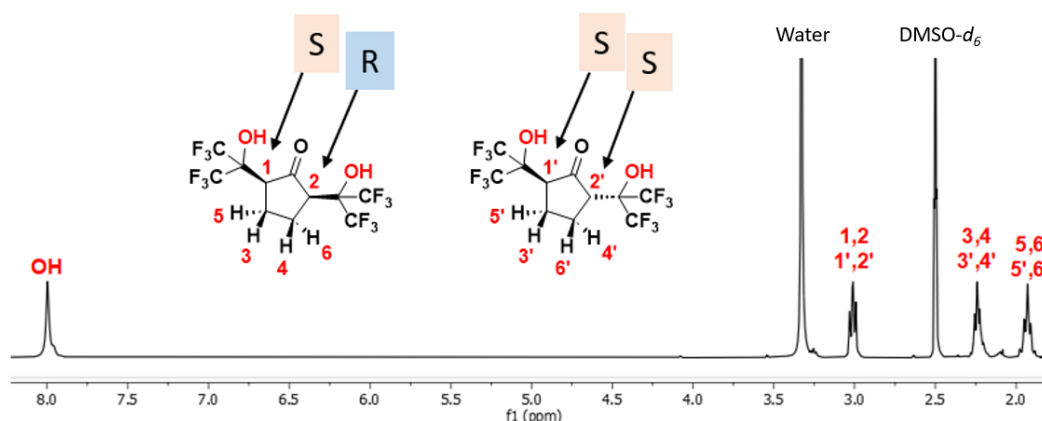
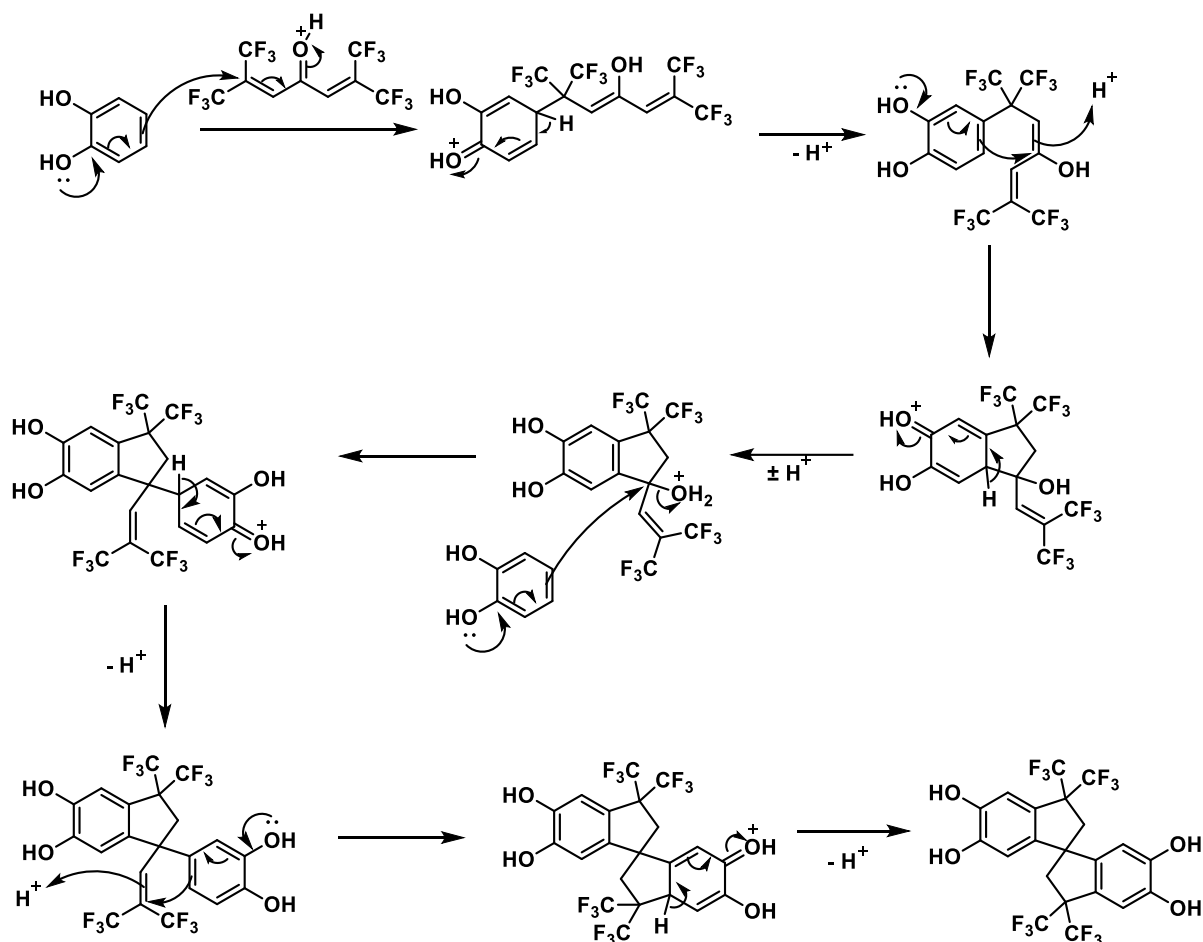


**Figure 5.2**  $^1\text{H}$  NMR of **di-adduct 2** isomers, with their assigned stereocentre.

As **di-adduct 2** contains two chiral centres, it was predicted that the reaction will result in a mixture of (S,R)- and (S,S)-isomers that are diastereomers of each other. However, the  $^1\text{H}$  NMR spectrum is relatively simple suggesting that only one isomer is formed giving three multiplets with an integration of 2 each in the alkyl proton region. The multiplet corresponding to -CH is the most downfield due to their close proximity to the highly electron withdrawing  $-\text{CF}_3$  and  $-\text{OH}$  groups. The most upfield multiplet at 1.93 ppm was assigned to those hydrogens out-of-phase in relation to the  $-\text{CF}_3$  and  $-\text{OH}$  groups, as they are furthest and least affected by the electron withdrawing groups.

### 5.1.2 Attempted Synthesis of Target Monomers

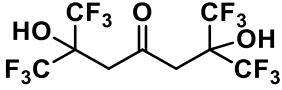
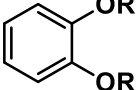
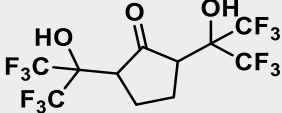
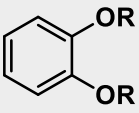
After successfully obtaining **di-adduct 1** and **2**, the synthesis of the targeted monomers was attempted from their acid mediated reactions with catechol or veratrole. A possible reaction pathway from the starting materials to the monomer was proposed, where the initial reaction involves in an *in-situ* alkene formation of the di-adducts in acidic conditions, followed by an electrophilic substitution reaction between catechol/veratrole and the tetra(trifluoromethyl) alkene (**Figure 5.3**).



**Figure 5.3** Proposed mechanism for tetra(trifluoromethyl) SBI monomer formation, between catechol and the dehydrated **di-adduct 1**.

The reactivity between catechol and **di-adduct 1** was initially tested using conc. HCl, and conc. H<sub>2</sub>SO<sub>4</sub> separately, the reaction mixture was refluxed in the concentrated acid for 24 h, after which the reaction was quenched with water, and the product extracted using organic solvent. Both starting materials were retrieved, indicating no reaction had occurred. Consequently, the reagents conventionally used for TTSBI monomer synthesis were employed.<sup>199</sup> Initial reactions were carried out between **di-adduct 1** and catechol, using 1.5, 3, or 8 equivalents of conc. HI acid, and refluxed in acetic acid for 24 h, but no reaction was observed under these conditions. A range of reaction conditions (temperature, time, *etc.*) were then investigated between the di-adducts and catechol/veratrole, using 8 equivalents of conc. HI acid. The results are recorded in **Table 5.1**.

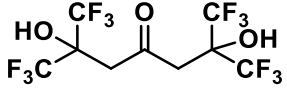
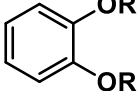
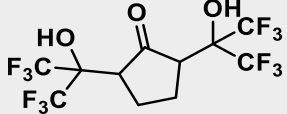
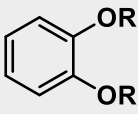
**Table 5.1** Reactions conditions and outcome for the reaction between di-adducts (**1** and **2**) and catechol/veratrole (where R = H or methyl), in conc. HI acid and acetic acid.

| Reactant A  | Reactant B  | Reaction conditions  | Outcome     |
|---|---|--|-------------|
|  |  | Reflux, 24h  | No reaction |
|   |   | Reflux, 48h  | No reaction |
|   |   | Microwave, 120 °C, 4h  | No reaction |
|   |   | Microwave*, 120 °C, 4h   | No product  |
|   |   | Microwave*, 120 °C, 9h   | No product  |
|   |   | Hydrothermal Autoclave*,<br>120 °C, 5h<br>(with hydrazine hydrate) | No product  |
|  |  | Reflux, 48h  | No reaction |
|   |   | Microwave, 120 °C, 4h  | No reaction |
|   |   | Microwave*, 120 °C, 4h,  | No reaction |
|   |   | Microwave*, 120 °C, 9h   | No reaction |

\*Pentane was added to the reaction mixture to generate pressure under heat.

Under standard refluxing conditions, both the catechol/veratrole and di-adducts starting materials were recovered, indicating the absence of any reaction. For reactions conducted in a microwave reactor, there was still no reactivity observed between **di-adduct 2** and the catechol/veratrole starting materials. In the case of **di-adduct 1**, when pressure was applied to the system through pentane addition, although most catechol/veratrole was recovered, negligible amounts of **di-adduct 1** were detected in the  $^1\text{H}$  NMR, while complex  $^{19}\text{F}$  NMR spectra were obtained. One possible explanation for this observation could be attributed to the occurrence of a retro-aldol reaction. Deviating from the reagents used for classic TTSBI formation, a set of other reagents and reaction conditions were also explored for **di-adduct 1** and **2**. All reactions listed below were carried out using anhydrous DCM as solvent, unless stated otherwise.

**Table 5.2** Alternative reaction conditions for target monomer synthesis from di-adduct 1 and 2, and catechol/veratrole.

| Reactant A  | Reactant B  | Reagents                                      | Conditions                     | Observation |
|---|---|---|--------------------------------|-------------|
|    |    | MsOH <sup>a</sup>                             | r.t, 4 h<br>reflux, 4, 9, 24 h | No product  |
|   |   | MsOH <sup>b</sup>                             | Reflux, 24 h                   | No product  |
|   |   | MsOH <sup>c</sup>                             | 120 °C, 24 h                   | No product  |
|   |   | Eaton's reagent (2 equiv)                     | r.t, 24 h                      | No product  |
|   |   | Triflic                                       | r.t, 4 h                       | No reaction |
|   |   | Triflic                                       | Reflux, 24 h                   | No product  |
|  |  | Eaton's reagent (2 equiv)                     | 45 °C, 2 days                  | No product  |
|   |   | POCl <sub>3</sub>                             | Reflux, 1, 2, 3 days           | No product  |
|   |   | mercaptopropionic acid/triflic                | 160 °C, 24 h                   | No product  |
|   |   | BF <sub>3</sub> .OEt <sub>2</sub> (1.5 equiv) | r.t, reflux, 24 h              | No reaction |
|   |   | DBU   | r.t, 48 h                      | No reaction |

<sup>a</sup>Reactions were carried using 2 and 5 equivalent of MsOH acid, <sup>b</sup>reaction was carried out using MsOH as solvent, <sup>c</sup>melted catechol/veratrole was used as the solvent.

The reaction between **di-adduct 1** and catechol/veratrole using methanesulfonic acid (MsOH), was carried out following a modified literature procedure.<sup>200</sup> No reaction was observed when the reaction was carried out at room temperature for 4 hours. However, under refluxing conditions for 4 hours, the NMR analysis revealed the absence of di-adduct 1, and new multiplets were observed between 7-8 ppm. Increasing the reaction temperature and time yielded much more complex NMR spectra. Initially thought to be due to the decomposition of catechol, the same multiplets were seen using veratrole as well, despite being more stable towards oxidation. A simple control experiment of refluxing **di-adduct 1** in in MsOH/anhydrous DCM confirmed that its decomposition products were responsible for the observed multiplets in the NMR. The formation of fully dehydrated **di-adduct 1** was

speculated, as protons on the C=C bond with two -CF<sub>3</sub> groups attached have been previously reported to appear as multiplets in the same region.<sup>201</sup> However, this control reaction produced a chaotic <sup>13</sup>C spectrum, and the <sup>19</sup>F NMR spectrum also showed the presence of more than one fluorine environment, suggesting the production of other by-products. As an alternative superacid to MsOH, monomer synthesis was also attempted using Eaton's reagents, which contains phosphorus pentoxide, and POCl<sub>3</sub>, both of which are strong dehydrating agents. Reactions using Eaton's reagent gave similar results in the case of **di-adduct 1**, but for **di-adduct 2** some of the starting material was recovered.

For most of the reactions attempted, large amounts of the catechol/veratrole starting materials were recovered, suggesting the unsuccessful outcome can be mainly attributed to the low reactivity of the fluorinated di-adducts. This is likely due to the presence of strongly electron withdrawing -CF<sub>3</sub> groups strengthening the C-O bond, making it harder to initiate the required carbocation formation.<sup>202,203</sup> A dehydration reaction using **di-adduct 2** was attempted following a modified literature procedure,<sup>204</sup> using methanesulfonyl chloride and pyridine. The reaction was expected to proceed first by converting the -OH groups to -OMs groups, which is a much better leaving group, followed by its removal using pyridine (**Figure 5.4**). However, the <sup>1</sup>H NMR of the crude product only showed a negligible amount of alkene formation, with no peak observed at 3-4 ppm which correspond to the mesylate (Ms) group, suggesting also minimal formation of the mesylate intermediate. Further investigation on the attempted conversion from hydroxyl to trimethylsilyl (TMS) groups were also unsuccessful, once again demonstrating the poor reactivity of the hydroxyl groups within the di-adducts.

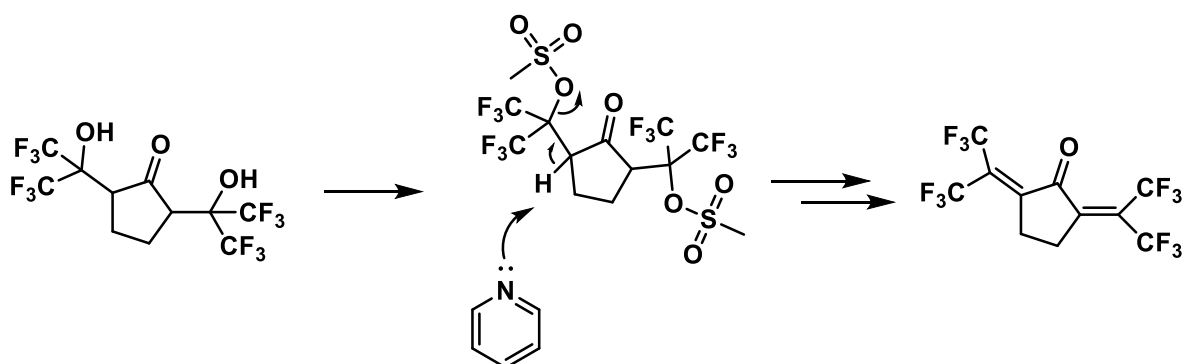


**Figure 5.4** Anticipated outcome of the dehydration of di-adduct 2, using methanesulfonyl chloride and pyridine.

## 5.2 Alternative Routes to Tetra(trifluoromethyl) Incorporation

Due to the challenges encountered whilst exploring the reactivities of the perfluoroacetone-derived di-adducts, including their relatively inconvenient synthetic routes, and issues with the stocks of the



chemical at the time of study, alternative ways to obtain the desired CF<sub>3</sub>-containing monomers were explored.

Trifluoromethyltrimethylsilane (TMSCF<sub>3</sub>) is a nucleophilic reagent commonly used as a source of -CF<sub>3</sub> in organic synthesis. Some advantages of this reagent include being easy to handle, stable and cost-effective.<sup>205</sup> TMSCF<sub>3</sub> exhibits good reactivity towards carbonyl groups such as ketones and aldehydes, in the presence of fluoride ions as an initiator (**Figure 5.4**).<sup>205</sup> Successful mono- and bis-trifluoromethylation can be achieved on other types of carbonyl compounds including activated esters and carboxylic acids.<sup>206,207</sup>

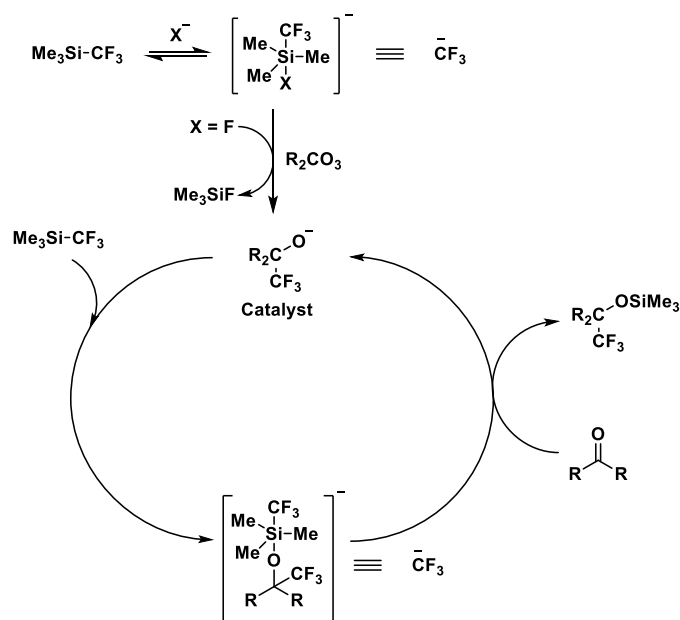
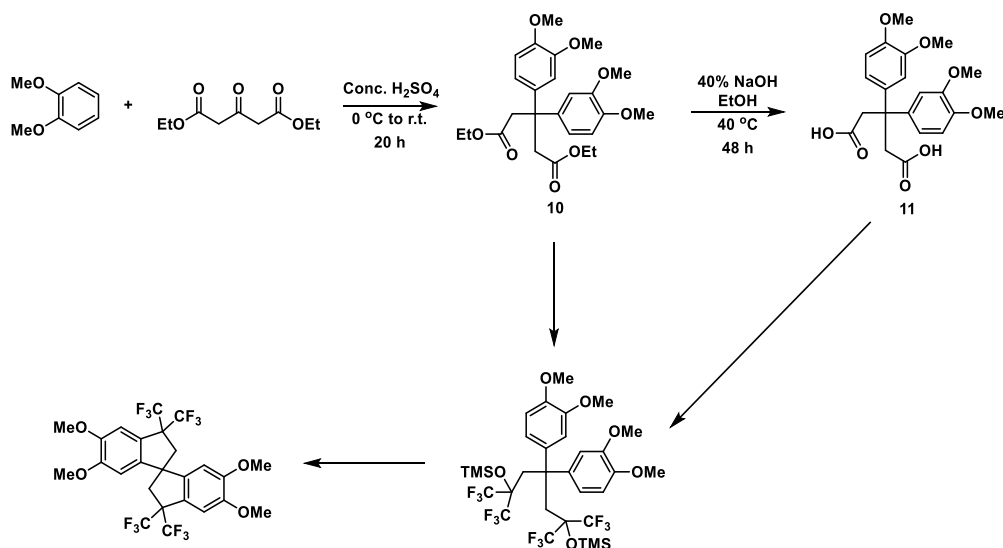


**Figure 5.4** TMSCF<sub>3</sub> act as -CF<sub>3</sub> source for carbonyl compounds.<sup>205</sup>

### 5.2.1 Synthesis of Carbonyl-Containing Precursors for Trifluoromethylation



**Scheme 5.4** Proposed synthesis route to obtain targeted tetra(trifluoromethyl) monomer.

A multi-step synthetic route to obtain the desired CF<sub>3</sub>-containing monomer utilising TMSCF<sub>3</sub> reagent was designed (**Scheme 5.4**). Following literature procedures,<sup>115</sup> compounds **10** and **11** were prepared. Initially, electrophilic aromatic substitution reaction between veratrole and diethyl-1,3-acetone dicarboxylate were carried out in acidic conditions, and diester compound **10** was obtained as a white powder with an 88% yield. A saponification reaction was carried out on **10** using NaOH, resulting in the dicarboxylic acid product **11** which was collected as a pale-yellow precipitate in 54% yield. The formation of the products was confirmed through NMR spectroscopy and compared against values reported in the literature.<sup>115</sup>

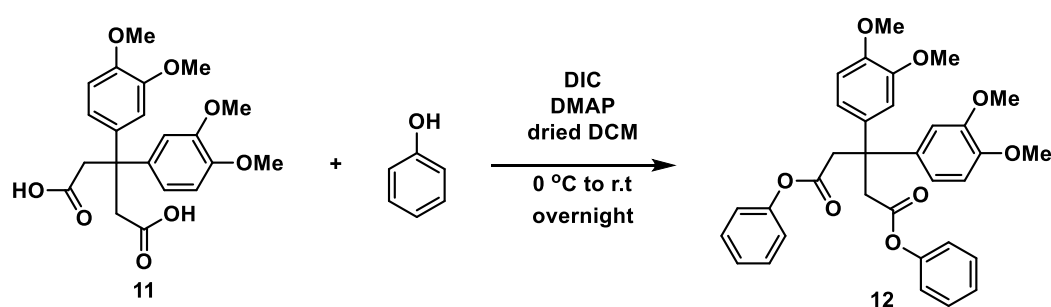


**Figure 5.5** Synthesis of 3,3-bis(3,4-dimethoxyphenyl) diphenylester.

Due to ethyl chains being poor leaving groups, for the -CF<sub>3</sub> group their addition on compound **10** was anticipated to be challenging. Therefore, the diphenol ester (**12**) was prepared from the dicarboxylic acid **11**, following a modified literature procedure (**Scheme 5.5**).<sup>208</sup> The esterification between compound **11**, and phenol were performed under N<sub>2</sub> atmosphere, using 1 equivalent of N,N'-diisopropylcarbodiimide (DIC) as a coupling reagent, 4-dimethylaminopyridine (DMAP) as catalyst, and anhydrous DCM as solvent. The target compound **12** was collected as a white powder, with a yield of 25%. The structure of the product was confirmed via <sup>1</sup>H NMR analysis (**Figure 5.5**).

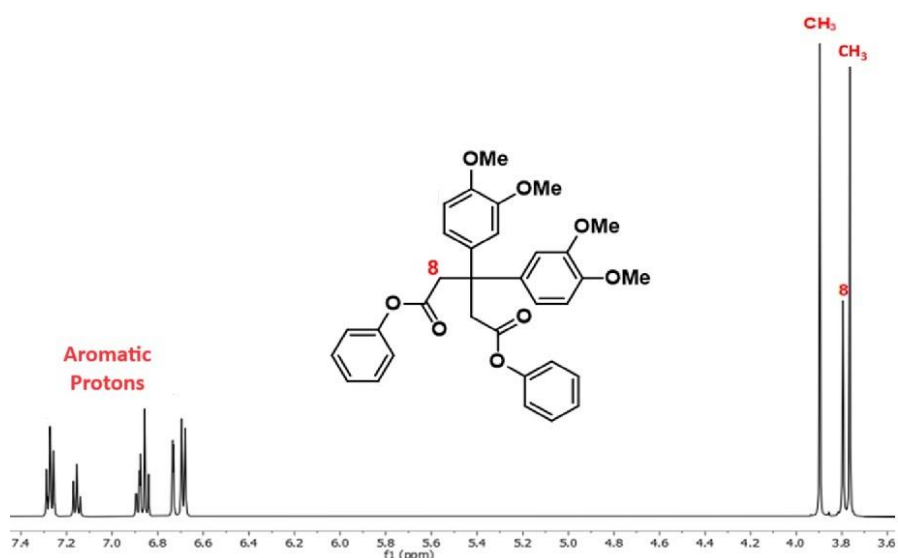


**Figure 5.5** <sup>1</sup>H NMR of compound **12**, with its proposed proton assignments.

## 5.2.2 Attempted Trifluoromethyl Incorporation with TMSCF<sub>3</sub>

Upon the successful synthesis of the non-fluorinated precursors **10-12**, the trifluoromethylation of these compounds using TMSCF<sub>3</sub> was explored using a range of fluoride ion sources and reaction conditions. The results are reported below in **Table 5.3**.

**Table 5.3** A summary of reaction conditions attempted for the addition of tetra(trifluoromethyl) to compounds **10-12**, using 12 equiv. TMSCF<sub>3</sub>.

| Reactant  | Reagents/Solvents  | Reaction conditions     | Observations |
|-----------|--|-------------------------|--------------|
| <b>10</b> | K <sub>2</sub> CO <sub>3</sub> /anhydrous DMF <sup>209</sup> | r.t, 48 h, reflux, 48 h | No reaction  |
|           | CsF/1,4-dioxane <sup>206</sup>                               | r.t, 24 h, reflux, 48 h | No reaction  |
|           | MgCl <sub>2</sub> /anhydrous DMF <sup>210</sup>              | r.t, 24 h, reflux, 24 h | No reaction  |
| <b>11</b> | K <sub>2</sub> CO <sub>3</sub> /anhydrous DMF                | r.t, 48 h, reflux, 48 h | No reaction  |
|           | CsF/1,4-dioxane  | r.t 24 h, reflux, 24 h  | No reaction  |
|           | MgCl <sub>2</sub> /anhydrous DMF                             | r.t, 24 h, reflux, 24 h | No reaction  |
|           | TFTPN, NEt <sub>3</sub> /Acetonitrile                        | r.t, 3h, 60 °C, 3-24h   | No product   |
|           | 1,2-Benzenedicarbonitrile                                    | 60 °C, 3-24h            | No product   |
|           | TBAF/THF <sup>211</sup>                                      | r.t, 3h                 | No product   |
| <b>12</b> | K <sub>2</sub> CO <sub>3</sub> /anhydrous DMF                | reflux, 48 h            | No reaction  |
|           | CsF/1,4-dioxane  | reflux, 48 h            | No reaction  |
|           | MgCl <sub>2</sub> /anhydrous DMF                             | reflux, 48 h            | No reaction  |
|           | [Bu <sub>4</sub> N]F/anhydrous DMF <sup>212</sup>            | -50 °C to r.t, 24 h     | No product   |
|           | TBAF/THF   | r.t, 1 h, 3 h, 5 h      | No product   |

For the addition of tetra(trifluoromethyl) groups on to compound **10**, no reaction was observed between the precursor with any reaction conditions, likely due to ethyl chains being relatively bad leaving groups. Therefore, more focus has been put onto the more reactive compounds **11** and **12**, however, neither compound **11** nor **12** demonstrated any reactivity towards TMSCF<sub>3</sub> when K<sub>2</sub>CO<sub>3</sub>, CsF, MgCl<sub>2</sub> were used as the basic reagents.

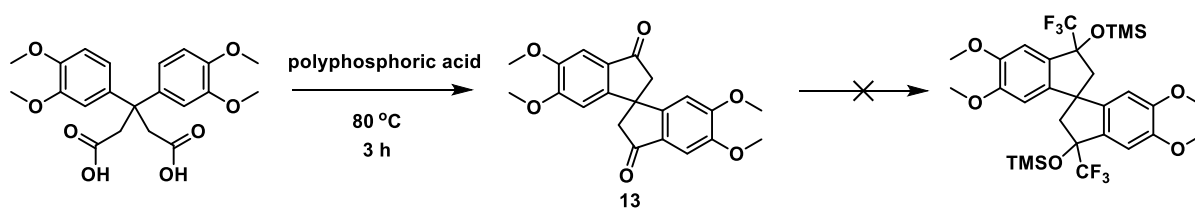
For reactions of compound **11** carried out using TFTPN/1,2-Benzenedicarbonitrile, the precursor remained mostly unreactive, a mixture of by-products could be observed on the TLC plate, and purification using column was difficult. Only negligible amount of TMS group could be observed using <sup>1</sup>H NMR for the by-products, therefore these reactions were deemed unsuccessful. A much stronger catalyst, TBAF was tried on compound **11**, which could have caused too much reactivity, with more than 5 spots observed by TLC, all with similar polarity. Therefore, purification of the reaction

was not attempted. Another possible explanation to the inactivity of compound **11** under these reaction conditions was only realised at a later time – since the synthesis of compound **11** was carried out in basic conditions using NaOH, it is more likely to result in its carboxylate salt being isolated rather than the carboxylic acid itself, which will lead to a reduced reactivity. The FT-IR obtained on compound **11** seem to be in agreement with this proposal, as there was no visible -OH peak present.

The phenoxy ester precursor **12** also demonstrated surprising inactivity, with no reactions observed for most attempted reactions. Similar to compound **11**, when TBAF was used as the catalyst, a mixture of by-products was observed by TLC. The reaction was attempted over short durations, but similar outcomes were observed. Similar to TBAF, reactions attempted using [Bu<sub>4</sub>N]F also resulted in a mixture of by-products which could not be purified.

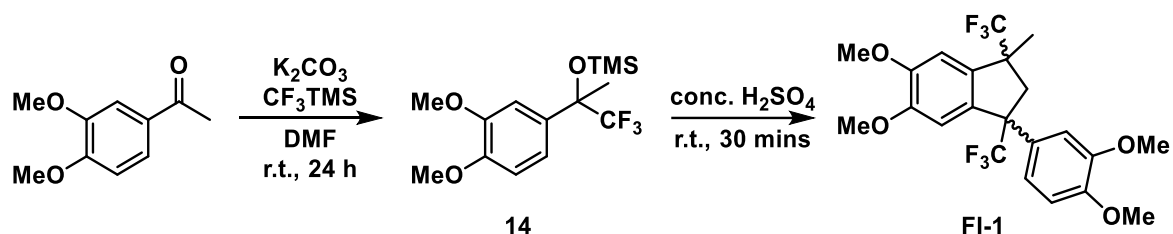
#### 5.4 Synthesis of Bis(trifluoromethyl) Monomer

After the disappointing results obtained for the attempted synthesis of the desired tetra(trifluoromethyl) monomers, the formation of a bis(trifluoromethyl) indane monomer was attempted. Initially, using the already synthesised compound **11**, its cyclisation reaction in polyphosphoric acid was carried out following literature procedure (**Scheme 5.6**).<sup>115</sup> Subsequent addition of trifluoromethyl groups was attempted following a modified literature procedure,<sup>209</sup> using K<sub>2</sub>CO<sub>3</sub> in DMF, which is an effective method for the addition of -CF<sub>3</sub> to ketones employed by other members of the McKeown group.



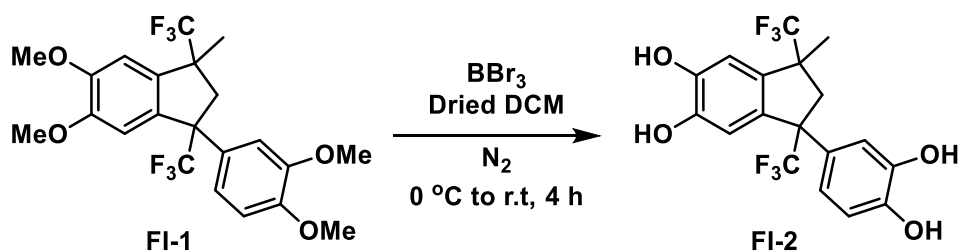
**Scheme 5.6** Synthesis of 5,6,5',6'-tetramethoxy-1,1'-spirobisindane-3,3'-dione (**13**) and the target bis(trifluoromethyl) monomer.

After several attempts using various amounts of K<sub>2</sub>CO<sub>3</sub>, TMSCF<sub>3</sub> and reaction durations, the desired product was not obtained. According to research conducted by Ms. Anli Ji and Dr. John Tobin in the McKeown group, the reactivity of diketones is significantly decreased with methoxy groups present on adjacent aromatic rings, presumably due to their electron donating effect making the ketones less electrophilic. It was therefore decided to not carry on with the synthesis of this monomer.



**Scheme 5.7** Synthesis of FI-1 from 3,4-dimethoxyacetophenone.

Instead, the synthesis of **FI-1** was carried out from 3,4-dimethoxyacetophenone (**Scheme 5.7**). A recent literature procedure<sup>213</sup> was followed for both the synthesis of compound **14** and monomer **FI-1**. An excess of  $\text{TMSCF}_3$  was added to a solution containing compound **13** and  $\text{K}_2\text{CO}_3$  in DMF, cooled to  $0\text{ }^\circ\text{C}$ . The mixture was then stirred at room temperature for 1 day to obtain compound **14** as orange oil, with a yield of 68%. Compound **14** was collected as a mixture of enantiomers, and the successful addition of  $-\text{CF}_3$  and TMS groups was confirmed by the appearance of a singlet at 0.13 ppm on the  $^1\text{H}$  NMR spectrum, corresponding to the TMS group, and  $-\text{CF}_3$  peak at  $-81.83$  ppm on the  $^{19}\text{F}$  NMR spectrum. To obtain **FI-1**, compound **14** was then stirred in conc.  $\text{H}_2\text{SO}_4$  at room temperature for 30 minutes. The indane monomer was collected as a colourless oil with a yield of 40%. The successful conversion was confirmed by observing the disappearance of the TMS group in the  $^1\text{H}$  NMR, as well as the presence of multiple peaks corresponding to different fluorine environments on the  $^{19}\text{F}$  spectrum. NMR spectra also confirmed that **FI-1** was collected as a mixture of diastereomers. Separation of the isomers was not attempted, as polymer formation using a mixture of isomers can result in a higher structural irregularity, which can be beneficial for PIMs as this can lead to greater solubility and a more disordered packing of its polymeric chains.



**Scheme 5.8** Demethylation of FI-1.

The demethylation reaction of **FI-1** was carried out using  $\text{BBr}_3$  in anhydrous DCM (**Scheme 5.8**). The crude product was obtained as a dark coloured viscous oil. After repeated attempts at recrystallisation or reprecipitation, pure bis-catechol product **FI-2** by NMR was collected as beige solid with a 70% yield. The successful demethylation was confirmed by the disappearance of  $-\text{OMe}$  peaks on the  $^1\text{H}$  NMR at 3.77-3.97 ppm, as well as the appearance of a strong  $-\text{OH}$  peak at  $3360\text{ cm}^{-1}$  on the FT-IR spectrum (**Figure 6.6**). Polymerisation was then carried using this synthesised bis-catechol.

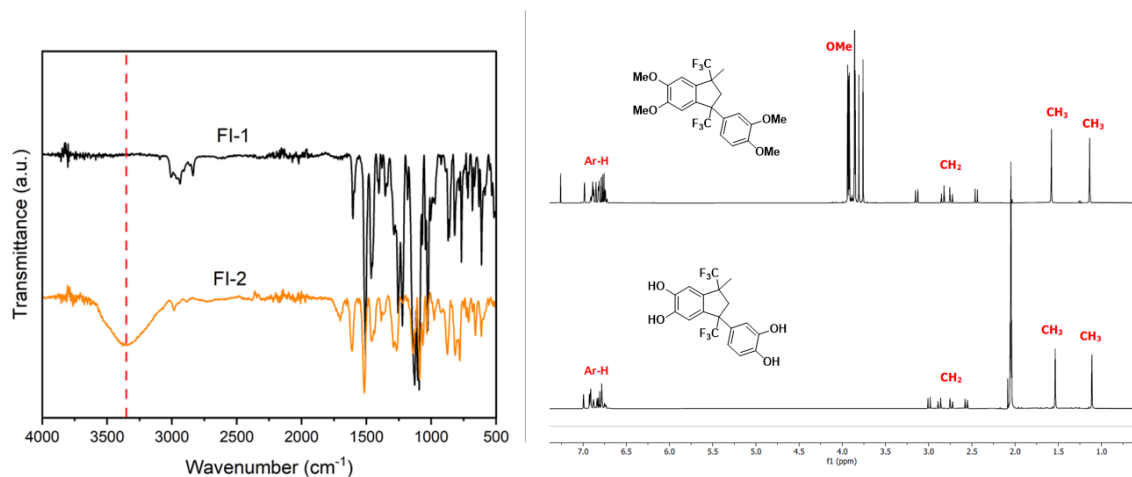
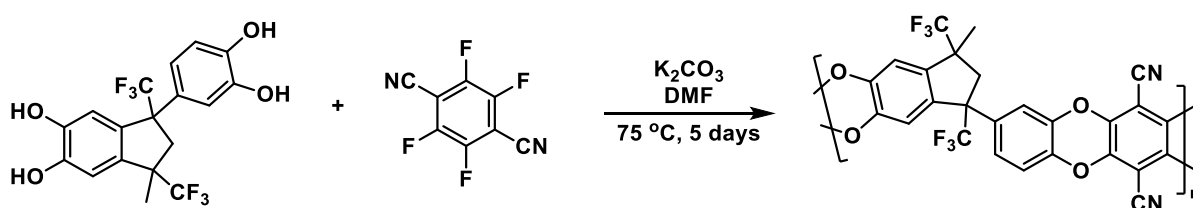


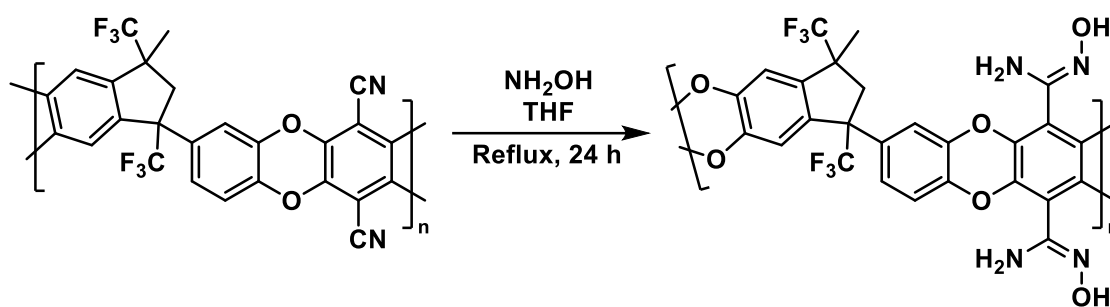
**Figure 5.6** FT-IR (left) and  $^1\text{H}$  NMR (right) comparison of **FI-1** and **FI-2**, highlighting the appearance of OH peak at  $3360\text{ cm}^{-1}$  and removal of  $-\text{OMe}$  groups at  $3.77\text{--}3.97\text{ ppm}$ .

## 5.5 Polymer Synthesis



**Scheme 5.9** Synthesis of **PIM-FI** from **FI-2** and TFTP.

The polymerisation reaction was carried out using **FI-2** and TFTP, following a modified literature procedure (**Scheme 5.9**).<sup>101</sup> The polymerisation reaction was heated at  $75\text{ }^\circ\text{C}$  for 5 days under an inert atmosphere, in anhydrous DMF and in the presence of  $\text{K}_2\text{CO}_3$ . **PIM-FI** was collected as a dark yellow powder, with a yield of 78%. The comparatively low yield obtained from the reaction was likely due the polymerisation not being fully complete, and the remaining oligomers were washed away by methanol during reaction work-up. Interestingly, **PIM-FI** was demonstrated to be readily soluble in acetone, which is an unusual trait for PIMs. A likely explanation for this observation could be due to a combination of the presence of  $-\text{CF}_3$  groups reducing the interchain interactions within the polymer structure, as well as the higher rotational freedom present in the polymeric backbone compared to conventional PIM structures. Successful synthesis was confirmed through NMR spectroscopy and the disappearance of the  $-\text{OH}$  peak on the FT-IR spectrum.



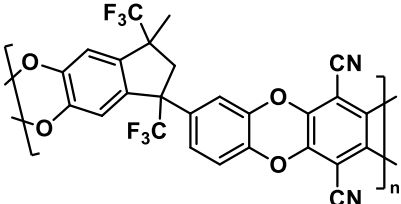
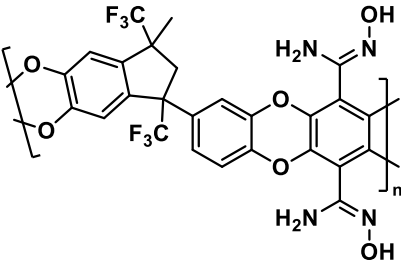
**Scheme 5.10** AO-modification of **PIM-FI**

AO modification on the synthesised PIM-FI was performed using an excess of hydroxylamine 50wt. % in water, refluxed in THF for 1 day (**Scheme 5.10**). **AO-PIM-FI** was obtained as a dark brown solid, with a yield of 94%. Successful conversion can be confirmed by FT-IR analysis, where the appearance of NH/OH peaks at  $3608\text{-}3074\text{ cm}^{-1}$  signifies the presence of the amidoxime group. As observed with AO modified polymers from the previous chapters, the introduction of AO to **PIM-FI** did also impact on solubility such that the polymer is no longer soluble in acetone. Surprisingly, the polymer exhibited solubility in methanol with heating and sonication. The unexpected solubility of **PIM-FI** and **AO-PIM-FI** could arise from the incorporation of  $-\text{CF}_3$  atoms and the chain flexibility, but a likely contributor could also be that only relatively low molecular weight polymers were obtained. Determination of the molecular weight of the polymers would be a helpful indicator to determine which of the proposed explanations is more reliable, however Gel Permeation Chromatography (GPC), commonly used for a polymer's molecular weight analysis, was not available to use at the time of polymer synthesis.

## 5.5 Polymer Analysis

The adsorption and desorption of nitrogen gas at 77 K were recorded for the synthesised polymers, from which the BET surface area and total pore volume of the polymers were calculated (**Table 5.4**).

**Table 5.4** Gas adsorption properties of trifluoromethyl-containing polymers.

| Polymer  | Solubility                                    | Surface Area*<br>(m <sup>2</sup> g <sup>-1</sup> ) | Total Pore Volume*<br>(ml g <sup>-1</sup> ) | CO <sub>2</sub> Uptake*<br>(mmol g <sup>-1</sup> ) |
|--|---|--|---|--|
|   | Soluble in acetone, but not CHCl <sub>3</sub> | 436  | 0.313                                       | 1.97   |
|  | Soluble in MeOH, but not acetone              | 0  | 0.005                                       | 1.52   |

\*BET surface area was obtained from N<sub>2</sub> adsorption at 77 K, total pore volume was calculated from N<sub>2</sub> uptake at  $P/P_0 = 0.98$ , and CO<sub>2</sub> uptake was measured at 1 bar, 273 K.

Despite the flexibility in its polymeric backbone, **PIM-FI** exhibited a reasonably high BET surface area of 436 m<sup>2</sup> g<sup>-1</sup>. Its measured N<sub>2</sub> adsorption isotherm (**Figure 5.9**) also demonstrated a type I isotherm, typical of that obtained for a PIM, confirming the microporous nature of the polymer. **AO-PIM-FI** was found to have a surface area of 0 m<sup>2</sup> g<sup>-1</sup> with a flat isotherm, indicating that the incorporation of AO groups has greatly impacted on the polymer's porosity. The same trend was observed for the previously prepared polymers described in this thesis, where AO functional group incorporation generally led to a reduction of over 300 m<sup>2</sup> g<sup>-1</sup> in the surface area of the polymers, due to AO groups introducing additional H-bonding into the polymer system. In the case of **AO-PIM-FI**, the inclusion of fluorine atoms on the polymer did not interfere with the AO-induced H-bonding interaction.



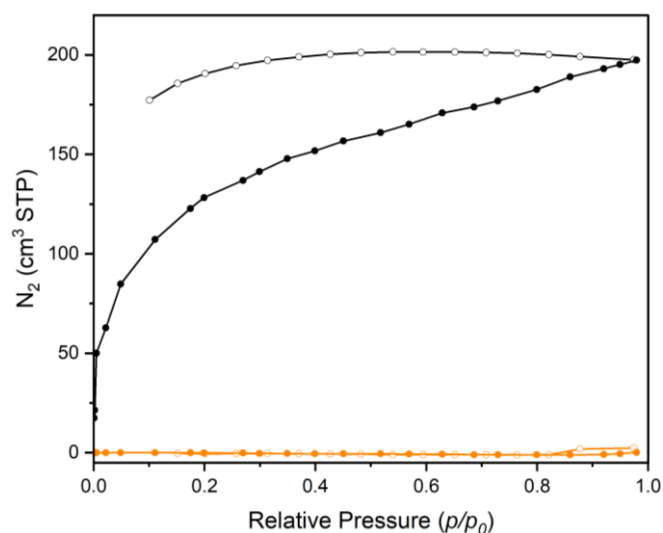


**Figure 5.9**  $N_2$  adsorption (filled circle) and desorption (empty circle) isotherms of **PIM-FI (black)** and **AO-PIM-FI (orange)**.

The  $CO_2$  adsorption properties for the polymers were recorded at 273 K (**Figure 5.10a**), from which their  $CO_2$  uptake at 1 bar were determined, and the pore size distribution (**Figure 5.10b**) of the polymers were calculated using the density functional theory (DFT) model. Similar to that observed for the AO-modified polymer in Chapter 5, **AO-PIM-FI** showed a reasonable  $CO_2$  uptake despite being non-porous towards nitrogen. Again, attractive interactions between AO groups on the polymer surface and  $CO_2$  is a likely contributor to this observation, as well as the temperature dependency of the rate of diffusion for gas molecules, where  $CO_2$  adsorption was recorded at a much higher temperature (273 K) compared to the 77 K used for  $N_2$  adsorption.<sup>175</sup> A good  $CO_2$  uptake for **PIM-FI** was obtained, which was expected, as the polymer demonstrated useful surface area, and the high electronegativity of the  $-CF_3$  groups. The pore size distribution of the polymers showed that both **PIM-FI** and **AO-PIM-FI** contain a mixture of ultramicropores and micropores, which are beneficial for the gas separation performances as membranes. The introduction of AO groups onto **PIM-FI** have decreased the proportion of larger micropores present in the structure, likely due to H-bonding between AO groups pulling polymeric chains closer together, and thus creating smaller pores.

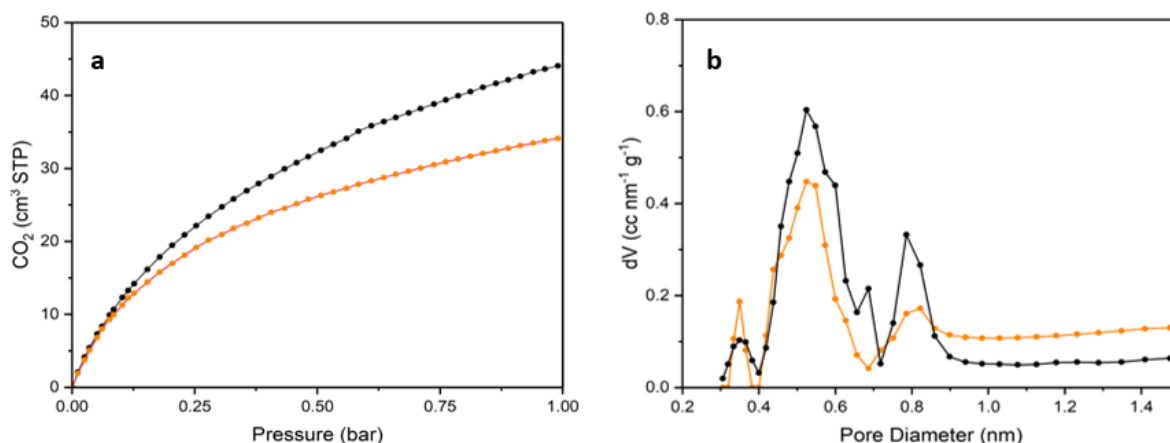


**Figure 5.10** a) CO<sub>2</sub> adsorption isotherm and b) pore size distribution of **PIM-FI** and **AO-PIM-FI**.

TGA analyses were also carried out on the fluorinated polymers (**Figure 5.11**). Both polymers demonstrate good thermal stability as expected, with **PIM-FI** showing an onset decomposition temperature at over 450 °C, and **AO-PIM-FI** losing its AO-group at around 250 °C, followed by a second decomposition temperature at over 400 °C.

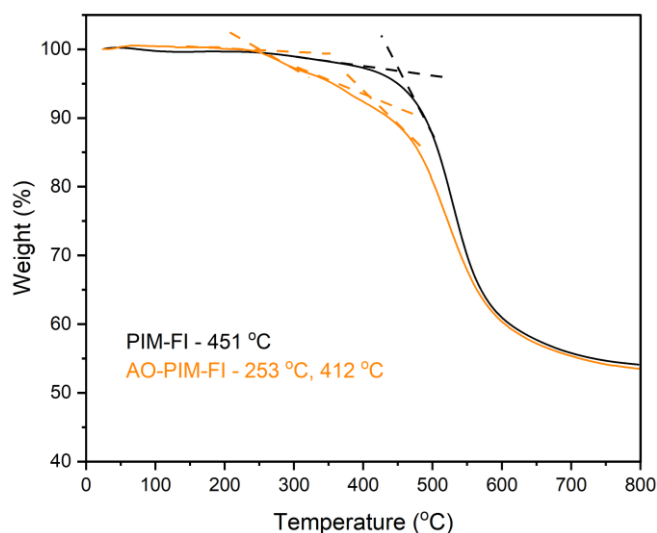


**Figure 5.11** TGA analysis of **PIM-FI** and **AO-PIM-FI**.

Film formation of **PIM-FI** was attempted from solutions made from 0.5 g of the polymer dissolved in 10 ml of acetone, with the mixture subjected to quick sonication to ensure the complete dissolution of the polymer. A film was successfully cast but was highly brittle (**Figure 5.12**) and fractured during transportation. The brittleness of the film could be due to multiple factors, such as the polymer being low molecular weight, or the film formation condition not being optimised. Therefore, no gas separation analysis was performed using this film. An attempt to cast **AO-PIM-FI** from DMSO solution was not successful, likely due to the casting conditions not being optimised.

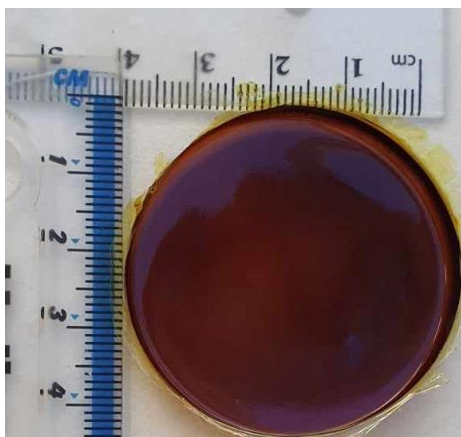


**Figure 5.12** Film cast from **PIM-FI**.

To conclude, various synthetic routes to the formation of tetra(trifluoromethyl)-containing monomers were designed and attempted, but the incorporation of four  $-CF_3$  groups onto one monomer proved to be too challenging. Instead, the formation of a bis(trifluoromethyl)-containing monomer was successful. Polymerisation using the synthesised monomer was carried out to obtain **PIM-FI**, as well as the AO modification of the polymer to obtain the **AO-PIM-FI**. The incorporation of  $-CF_3$  did indeed alter the solubility of PIMs, with **PIM-FI** being soluble in acetone, and its AO-modified version being soluble in methanol. However, the presence of  $-CF_3$  groups were not able to prevent the interchain H-bonding caused by AO groups, thus incorporation of AO still drastically reduced the surface area of the polymer.

## Chapter 6 Future Work

### 6.1 Amine-containing structural units

To build from the idea of Chapter 5, the incorporation of amine functionalities onto rigid and restricted-NP structural units could be further explored. Crystal growth of **NNP1-3** monomers could be attempted to obtain crystal structures for further structural elucidation, although given their poor solubility, some structural modification might be needed (e.g. addition of acetyl groups). Alternatively, new analogues of NNP compounds could be designed to exhibit better solubility in volatile organic solvents, for example, the inclusion of more methyl groups (**Figure 7.1**)

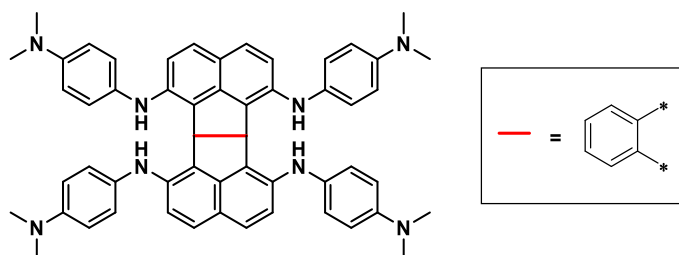


**Figure 7.1** An example of an interesting novel NNP structure to prepare.

Since the synthesis of the NP structure with primary amines from 2,7-diaminonaphthalene was met with challenges, the classic Bucherer reaction could be carried out on the hydroxyl-functionalised NP monomer for direct amination of the NP monomer to avoid the need of protecting the primary amine groups (**Figure 7.2**).

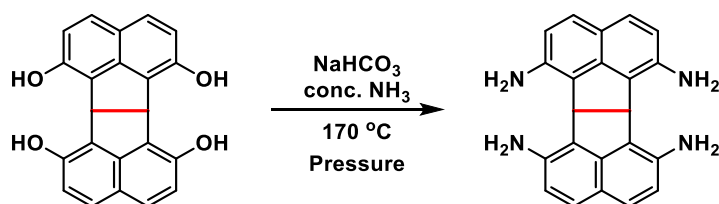


**Figure 7.2** Proposed reaction for the direct amination of NP monomer.

Furthermore, alternative amine-containing structural units with restricted rotation could be explored. The synthesis of two tetracyclic, nitrogen-containing catechols that resemble the structure of Troger's base are already in progress (**Figure 7.3**).

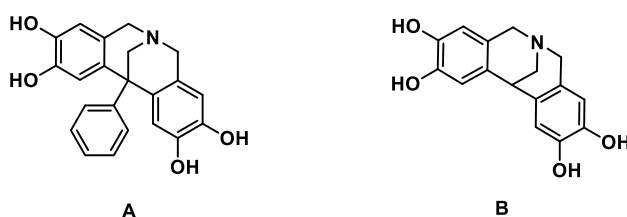


**Figure 7.3** Targeted tetracyclic catechol monomers.

The monomers are expected to provide a high degree of rigidity due to their fused-multi cyclic system, and with the presence of both oxygen and nitrogen, the monomers are also expected to exhibit high affinity towards CO<sub>2</sub> gas. The synthesis of **monomer A** was continued from work carried out by a previous MSc student from the McKeown group, with the current progress of this monomer synthesis demonstrated in **Figure 7.4**. Compounds **15** and **16** were synthesised based on modified literature procedures,<sup>214,215</sup> with yield of 65% and 23% respectively. The crude product of the methoxy-derivative **monomer A** was successfully obtained, with its purification presenting some challenges.

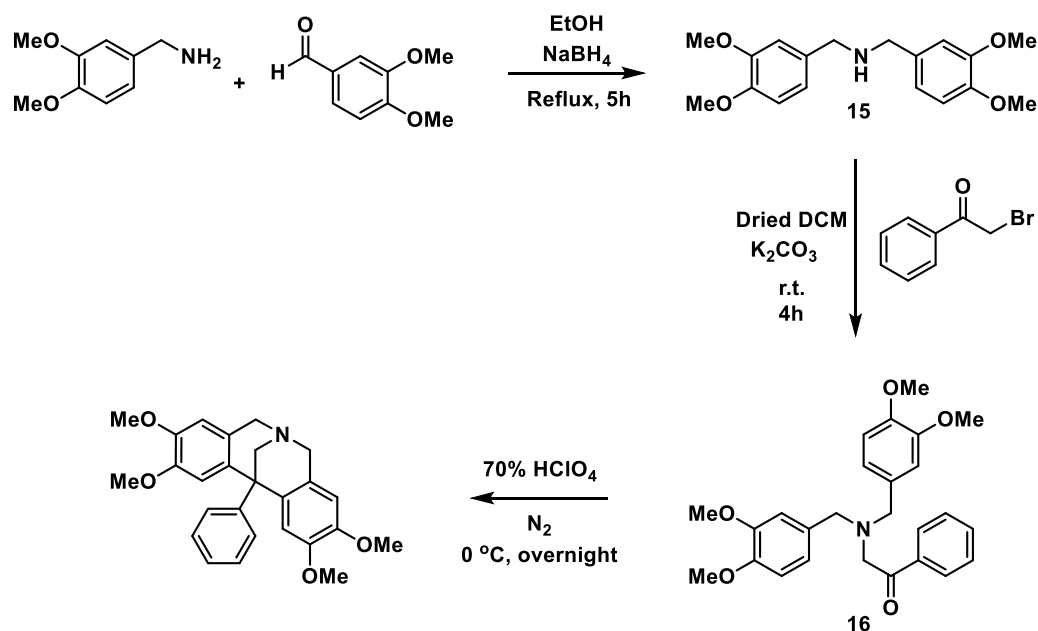


**Figure 7.4** Current progress for the synthesis of **monomer A**.

The synthesis of **monomer B** was also conducted in parallel to that of **monomer A** (**Figure 7.5**), and modified literature procedures were followed. Compound **17** was successfully obtained with a yield of 61%, and the crude product for the methoxy monomer was obtained, with its purification also presenting some challenges.

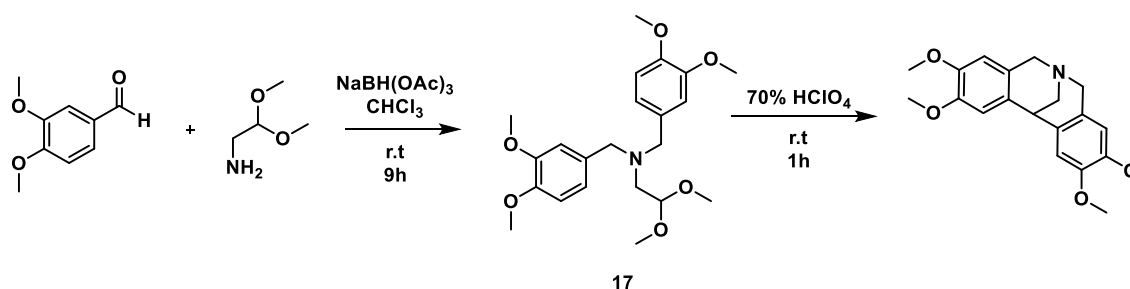


**Figure 7.5** Current progress for the synthesis of **monomer B**.

## 7.2 Continuation of fluorinated monomer and polymer synthesis

As an extension to work carried out in Chapter 6, reaction conditions for the synthesis of **PIM-FI** should be optimised to ensure a polymer with high molecular weight is obtained. The polymerisation reaction between the synthesised **FI-2** monomer and TFPCN monomer could be carried out, with its subsequent AO modification reaction in order to study the effect that  $-CF_3$  groups have on a polymer structure with extensive H-bonding present (**Figure 7.6**), *via* analysis methods such as BET and TGA.

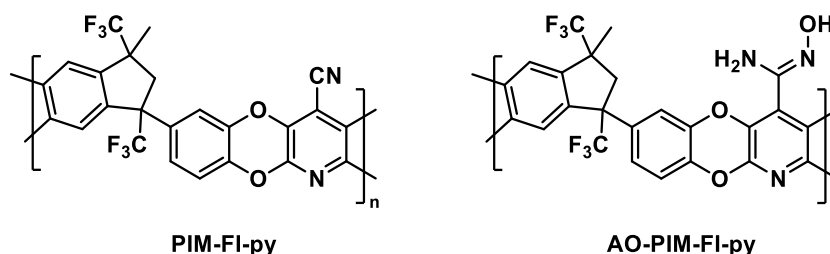


**Figure 7.6** Proposed polymers from the reaction between **FI-2** and TFPCN monomer, and its subsequent AO modification.

In addition to the monomers **FI-1** and **FI-2**, the synthesis of another bis(trifluoromethyl) monomer is currently in progress (**Figure 7.7**). The synthesis of compound **18** was carried out following a modified literature procedure,<sup>216</sup> progress of the reaction was monitored via TLC, with addition of small aliquots of acetone added through out the reaction duration. The product was purified by vacuum distillation, and was obtained as a white solid with a yield of 29%.

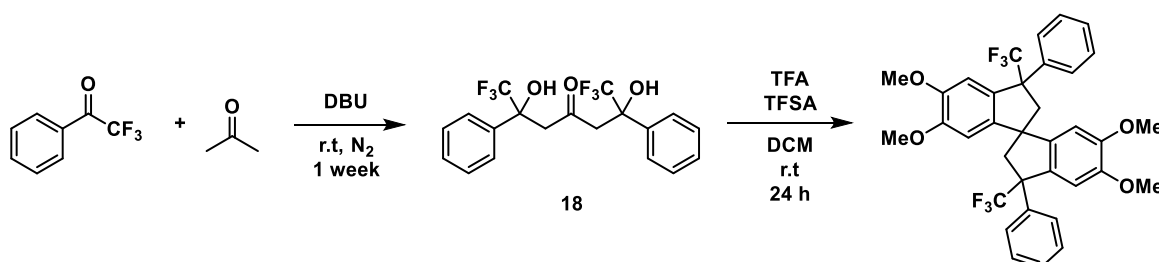


**Figure 7.7** Synthesis of bis(trifluoromethyl) monomer **FI-3**.

The subsequent bis(indane) formation was carried out following a method provided by another PhD student from the McKeown group, Anli Ji, and the product was collected as a white powder, with a yield of 23%. For future work, the demethylation of **FI-3** needs to be carried out, and its polymerisation reaction with TFTPn and TFPCN should be attempted, followed by the AO modification of the polymers.

## Chapter 7 Conclusion

Chapter 4 described the synthesis of a pyridine containing polymer, **PIM-py** that has otherwise a very similar structure to that of **PIM-1**, making it the ideal candidate for comparison purposes. The pyridine-containing polymer exhibited a surface area of  $736 \text{ m}^2 \text{ g}^{-1}$ , a total pore volume of  $0.517 \text{ ml g}^{-1}$ , and a  $\text{CO}_2$  uptake of  $2.26 \text{ mmol g}^{-1}$  at 1 bar, 273 K. Following its subsequent AO modification, a novel polymer **AO-PIM-py** was obtained, with a surface area of  $254 \text{ m}^2 \text{ g}^{-1}$ , total pore volume of  $0.204 \text{ ml g}^{-1}$ , and a  $\text{CO}_2$  uptake of  $1.96 \text{ mmol g}^{-1}$ . The introduction of the AO group led to a large reduction in the surface area of the polymer. It can be deduced that the presence of pyridine sites on the polymer resulted in a more significant decrease in the surface area, compared to that observed for the AO modification of **PIM-1**, and can be attributed to the additional H-bonding network caused by the presence of both AO groups and the pyridine sites. However, despite the large reduction in the nitrogen adsorption, there was only a small decrease in the  $\text{CO}_2$  uptake observed for the AO-modified polymer, which was believed to be due to the additional H-bonding acid-base interaction brought by the functional sites. The ability of these synthesised polymers to deactivate chemical warfare agents Soman, VX, and mustard gas, appeared to be primarily based on adsorption from solution. The processability of **PIM-py** and **AO-PIM-py** was confirmed, and films were successfully cast from both polymers, and both showed potential to be processed into nanofibers *via* electrospinning. Lastly, the gas separation properties of the polymers were measured. **PIM-py** generally showed similar gas permeability performances to that of **PIM-1**, but with a significant increase in the permeabilities of  $\text{H}_2$  and He gases. The incorporation of AO groups was found to result in a noticeable enhancement of  $\text{CO}_2$  selectivity over  $\text{N}_2$  and  $\text{CH}_4$ . Overall, the incorporation of pyridine units did not affect the gas separation properties of the polymer greatly.

In Chapter 5, the synthesis of highly bulky and rigid naphthopiperidine (NP) units were explored using 2,7-hydroxynaphthalene as the primary starting material. Initially, the direct amination of 2,7-dihydroxynaphthalene was carried out to yield 2,7-diaminonaphthalene, followed by its subsequent attempted NP formation using phthalaldehyde, the primary amine functionalities were too reactive and a Schiff base reaction appeared to take place instead, to obtain an imine-based polymer **CP1**. The polymer was found to have a surface area of  $12 \text{ m}^2 \text{ g}^{-1}$ , total pore volume of  $0.0374 \text{ ml g}^{-1}$ , and a  $\text{CO}_2$  uptake of  $0.6 \text{ mmol g}^{-1}$  at 1 bar, 273 K. A series of naphthalene precursors containing secondary amine functionalities was synthesised, and their potential to form NP monomers was investigated. Two NP monomers, **NNP1** and **NNP2** were successfully obtained from the precursors, *N,N'*-bis(Phenyl)-2,7-naphthalenediamine (**7**) and *N,N'*-bis(4-methoxyphenyl)-2,7-naphthalenediamine (**8**) respectively. However, the polymerisation attempts using these monomers were unsuccessful.

Demethylation reaction of **NNP2** was carried out to yield monomer **NNP3**, which was reacted with 2,3-dichloroquinoxaline to yield a non-porous crosslinked polymer **CP2**, with a CO<sub>2</sub> uptake of 0.74 mmol g<sup>-1</sup> at 1 bar, 273 K. A successful PIM synthesis was achieved between the hydroxy-containing monomer **NP1**, reported by Amin *et al.*,<sup>165</sup> with TFPCN to yield the novel polymer **PIM-NP-py**, with a surface area of 514 m<sup>2</sup> g<sup>-1</sup>, total pore volume of 0.058 ml g<sup>-1</sup>, and a CO<sub>2</sub> uptake of 2.32 mmol g<sup>-1</sup> at 1 bar, 273 K. AO modification of this polymer gave **AO-PIM-NP-py** which demonstrated a surface area of only 1 m<sup>2</sup> g<sup>-1</sup>, but a CO<sub>2</sub> uptake of 1.39 mmol g<sup>-1</sup> due to the interaction between AO groups and CO<sub>2</sub>. Contrary to the initial predictions, incorporation of bulky NP units in PIMs did not lead to any enhancement on the porosity of PIMs.

In Chapter 6, the incorporation of trifluoromethyl (-CF<sub>3</sub>) functional groups onto PIMs was attempted due to their potential to alter the solubility of PIMs by reducing interactions between polymeric chains, and to enhance the hydrophobicity of PIMs. Initially, two target tetra(trifluoromethyl) spirobisindane monomers were designed. Their tetra(trifluoromethyl) precursors **di-adduct 1** and **2** were synthesised, and the subsequent spirobisindane monomer formation was attempted in a large range of acids and reactions conditions. However, due to the difficult dehydration step associated with the di-adducts, the targeted tetra(trifluoromethyl) monomers were not obtained. An alternative reaction route was then devised, starting from the synthesis of a diethyl ester, dicarboxylic acid, and diphenyl ester compound. The -CF<sub>3</sub> incorporation on the precursors was attempted using CF<sub>3</sub>TMS as the fluorinating reagent, with no success. Synthesis of bis(trifluoromethyl)-spirobisindane monomer was then attempted by first obtaining the 5,5',6,6'-tetramethoxy-1,1'-spirobisindane-3,3'-dione (**13**) precursor, but the -CF<sub>3</sub> addition was again unsuccessful probably because the ketones were made less electrophilic by the additional electron donating effect induced by the methoxy groups. A bis(trifluoromethyl) indane monomer **FI-1** was successfully obtained from its precursor 3,4-dimethoxyacetophenone, followed by its demethylation to collect a tetrahydroxy-containing **FI-2** monomer. Upon the polymerisation reaction using **TFTPN**, the polymer **PIM-FI**, with a surface area of 436 m<sup>2</sup> g<sup>-1</sup>, total pore volume of 0.31 ml g<sup>-1</sup> and a CO<sub>2</sub> uptake of 1.97 mmol g<sup>-1</sup> was obtained. AO modification was conducted on the polymer to obtain **AO-PIM-FI**. The presence of trifluoromethyl groups was not able to reduce the H-bonding introduced by AO group addition, therefore a large reduction in surface area was still observed. However, this polymer still showed a noticeable amount of CO<sub>2</sub> uptake, with 1.52 mmol g<sup>-1</sup> at 1 bar, 273 K. The gas separation performance was not obtained for these fluorinated polymers, due to lack of film formation, thus their ability to prevent competitive water vapour adsorption could not be measured.



## Chapter 8: Experimental

### 8.1 Techniques

Commercially available chemicals were used without further purification, unless stated otherwise. Anhydrous dichloromethane and tetrahydrofuran were acquired from the Solvent Purification System. Anhydrous DMF was purchased from Sigma-Aldrich. All reactions requiring inert conditions were performed under nitrogen atmosphere using apparatus pre-dried in an oven. Thin-layer chromatography were performed using Merck Kieselgel 60 GF<sub>254</sub> coated aluminium-back plates. Column chromatography was performed using silica gel 60 Å (40-63 µm) chromatography grade from Fischer Scientific. High pressure reactions were carried out using High Pressure Reactor Model PressureSyn MKII 125 mL, under nitrogen atmosphere.

#### **Melting points (Mp)**

Melting points were measured using Stuart Digital Melting Point Apparatus with a temperature upper limit of 300 °C. The measurements were uncorrected.

#### **Infrared Spectroscopy (IR)**

IR measurements were taken using Shimadzu IR Affinity-1S FTIR spectrometer, in the region between 4000-500 cm<sup>-1</sup>.

#### **Nuclear Magnetic Resonance (NMR)**

<sup>1</sup>H NMR spectra were recorded using Avance Bruker AVA400, AVA500, PRO500, or AVA600, at 400, 500 or 600 MHz respectively. <sup>13</sup>C NMR spectra were recorded using the same NMR instruments at 100 MHz, 125MHz or 126 MHz; <sup>19</sup>F NMR spectra were recorded using PRO500 or AVA400 with 471 or 376 MHz respectively. Solid state <sup>13</sup>C NMR spectra were recorded using Bruker Ultrashield™ 300 WB spectrometer at 76 MHz.

#### **Mass Spectrometry (MS)**

HRMS (high resolution mass spectrometry) was performed using Fisonsn VG platform II quadruple instrument plus Thermos Finnigan MAT 900 XP, electron ionisation sector MS in electron impact (EI).

#### **Thermo-Gravimetric Analysis (TGA)**

TGA were performed using Thermal Analysis SDTQ600 system with heating rate of 10 °C min<sup>-1</sup> up to 800 °C under nitrogen atmosphere.

## Gas adsorption analysis

Quantachrome Quadrasorb automated surface area analyser was used to acquire measurements for N<sub>2</sub> and CO<sub>2</sub> adsorption/desorption isotherms, at temperature 77 K and 273 K respectively. Samples were de-gassed at 100 °C for 12 hours under high vacuum and weighed precisely before measurement.

## 9.2 General Procedures

### General Procedure 1 (GP 1) for demethylation reaction<sup>100</sup>

To a solution of the tetra-methoxy precursor in anhydrous dichloromethane, cooled to 0 °C under inert atmosphere, boron tribromide was added dropwise. The mixture was left stirring at 0 °C for 1 hour, allowed to warm to room temperature, and left to react overnight. The reaction mixture was poured into ice water, stirred under inert atmosphere until dichloromethane was evaporated and extracted with ethyl acetate. The crude product was then precipitated from *n*-hexane.

### General Procedure 2 (GP 2) for the synthesis of 2,7-diaminonaphthlene derivatives<sup>169</sup>

2,7-Dihydroxynaphthalene and the corresponding aniline were dissolved in xylene followed by the addition of iodine. The mixture was refluxed overnight, then poured into water after cooling to 90 °C. Precipitates were collected by filtration and purified according to individual compounds.

### General Procedure 3 (GP 3) for the synthesis of amine-containing NP monomers<sup>165</sup>

To a stirred solution of the required 2,7-diaminonaphthaene derivative, phthalaldehyde (0.50 eq.) in ethanol at reflux temperature, an excess of concentrated hydrochloric acid was added dropwise. The mixture was left to reflux overnight. The mixture was then cooled to room temperature, poured into water and neutralised with aqueous sodium hydroxide solution (2M). The crude product was filtered and purified accordingly.

### General procedure 4 (GP 4) for PIMs synthesis<sup>101</sup>

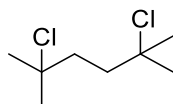
The appropriate biscatechol (1.00 eq.) and tetrafluoroterephthalonitrile (1.00 eq.) were fully dissolved in anhydrous DMF. Anhydrous potassium carbonate (8.00 eq.) was then added to the mixture, and the temperature slowly raised to 65 °C and allowed to react for 72 hours. The reaction mixture was then poured into water and acidified with concentrated hydrochloric acid. The precipitates were filtered, washed with water, acetone and methanol consecutively and dried. For polymers synthesis, the precipitates were then dissolved in suitable solvent and reprecipitated in acetone to remove oligomers. The final precipitates were refluxed in methanol and dried in vacuum oven.

### General Procedure 5 (GP 5) for amidoxime functionalisation<sup>143</sup>

Excess hydroxylamine 50 wt. % H<sub>2</sub>O were added to a solution of the target molecule in THF, then heated to reflux and left to react for 24 hours. The reaction mixture was then poured into ethanol, filtered and washed again with ethanol.

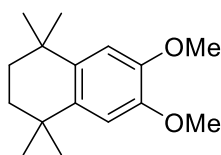
### 9.3 Amidoxime-functionalised polymers

#### 2,5-Dichloro-2,5-dimethylhexane<sup>217</sup>



2,5-Dimethyl-2,5-hexanediol (80.0 g, 0.547 mol) was dissolved in 37% Conc. HCl (600 mL) and stirred for 24 hours at room temperature. Precipitates were filtered under vacuum and washed with water until no longer acidic. The precipitate was dissolved in DCM and washed with water 2 more times and the solvent removed under vacuum. The collected solid was purified by recrystallization using methanol to give 2,5-dichloro-2,5-dimethylhexane (83.5 g, 83%) as white needle-like crystals. Mp: 66 °C (Lit: 68 °C<sup>217</sup>);  $\nu_{max}$  (cm<sup>-1</sup>): 2980.02, 2922.16, 1438.90, 1371.39; <sup>1</sup>H NMR (500 MHz, CDCl<sub>3</sub>-d)  $\delta$  1.95 (s, 4H, CH<sub>2</sub>), 1.60 (s, 12H, CH<sub>3</sub>) ppm; <sup>13</sup>C NMR (126 MHz, CDCl<sub>3</sub>-d)  $\delta$  70.02, 40.94, 32.30 ppm.

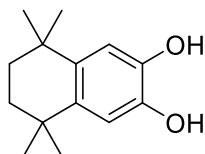
#### 6,7-Dimethoxy-1,1,4,4-tetramethyl-2,3-dihydronaphthalene<sup>142</sup>



1

AlCl<sub>3</sub> (42.9 g, 0.323 mol) was dissolved in anhydrous nitromethane (70 mL). This mixture was added dropwise to a solution of veratrole (11.1 g, 80.5 mmol) and 2,5-dichloro-2,5-dimethylhexane **1** (29.5 g, 161 mmol) in anhydrous nitromethane (70 mL). The mixture was stirred for 20 hours at room temperature, poured into ice water and washed twice with water and brine. The organic layer was dried over anhydrous magnesium sulphate and the solvent removed using a rotary evaporator to give a dark brown solid. The solid was purified by repeated recrystallization in ethanol. White crystals (7.50 g, 38%) were obtained. Mp: 60 °C (Lit: 60-62 °C<sup>142</sup>);  $\nu_{max}$  (cm<sup>-1</sup>): 2922.16, 1608.63, 1512.19, 1450.47, 1361.74, 1255.66, 1217.08; <sup>1</sup>H NMR (500 MHz, CDCl<sub>3</sub>-d)  $\delta$  6.77 (s, 2H, Ar H), 3.86 (s, 6H, OCH<sub>3</sub>), 1.67 (s, 4H, CH<sub>2</sub>), 1.27 (s, 12H, CH<sub>3</sub>) ppm; <sup>13</sup>C NMR (126 MHz, CDCl<sub>3</sub>-d)  $\delta$  147.09, 137.26, 109.50, 56.01, 35.42, 34.18, 32.02 ppm.

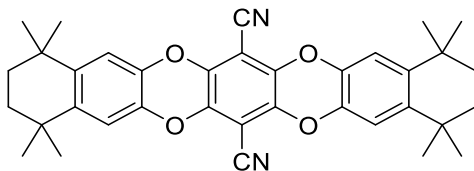
## 6,7-Dihydroxy-1,1,4,4-tetramethyl-2,3-dihydronaphthalene <sup>142</sup>



**2**

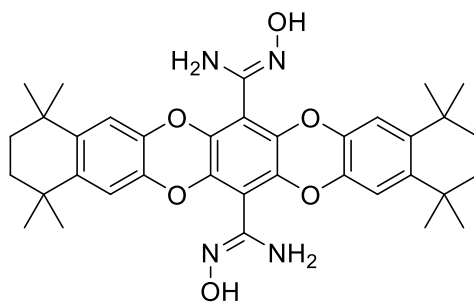
GP 1 was followed with 6,7-dimethoxy-1,1,4,4-tetramethyl-2,3-dihydronaphthalene **2** (6.50 g, 26.2 mmol), boron tribromide (5.00 mL, 52.7 mmol) in anhydrous dichloromethane (70 mL). 6,7-Dihydroxy-1,1,4,4-tetramethyl-2,3-dihydronaphthalene (5.27 g, 91%) **3** was collected as a white precipitate. Mp: 181 °C (Lit: 182-184 °C <sup>142</sup>);  $\nu_{max}$  (cm<sup>-1</sup>): 3259.70, 2922.16, 1610.56, 1512.19, 1431.18, 1361.74; <sup>1</sup>H NMR (500 MHz, CDCl<sub>3</sub>-*d*)  $\delta$  6.78 (s, 2H, ArH), 4.88 (br s, 2H, OH), 1.64 (s, 4H, CH<sub>2</sub>), 1.22 (s, 12H, CH<sub>3</sub>) ppm; <sup>13</sup>C NMR (126 MHz, CDCl<sub>3</sub>-*d*)  $\delta$  141.10, 137.95, 113.00, 35.04, 33.78, 31.84 ppm.

### Model Compound 1 (M1)



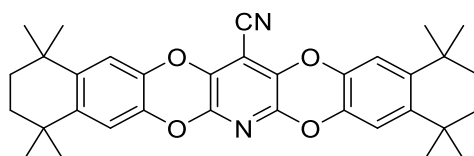
6,7-Dihydroxy-1,1,4,4-tetramethyl-2,3-dihydronaphthalene (5.00 g, 22.7 mmol) dissolved in anhydrous DMF (30 mL) were added to a solution of tetrafluoroterephthalonitrile (2.27 g, 13.0 mmol) dissolved in anhydrous DMF (20 mL). Anhydrous potassium carbonate (12.6 g, 0.0912 mol) was added to the mixture and was left to stir for 24 hours at 80 °C. The mixture was poured into water and stirred. 37% concentrated hydrochloric acid was added to the mixture dropwise until foaming stopped. Precipitates were filtered and washed with acetone. M1 was collected as bright yellow powder (6.66 g, 92%). Mp: above 300 °C;  $\nu_{max}$  (cm<sup>-1</sup>): 2968.45, 2237.43, 1980.89, 1687.71, 1444.68, 1315.45, 1263.37; <sup>1</sup>H NMR (500 MHz, CDCl<sub>3</sub>-*d*):  $\delta$  6.91 (s, 4H, ArH), 1.67 (s, 8H, CH<sub>2</sub>), 1.25 (s, 24H, CH<sub>3</sub>) ppm; <sup>13</sup>C NMR (126 MHz, CDCl<sub>3</sub>-*d*):  $\delta$  143.28, 139.43, 137.54, 114.70, 109.89, 94.30, 34.78, 34.40, 31.82 ppm; HRMS (EI, m/z): calculated C<sub>36</sub>H<sub>36</sub>O<sub>4</sub>N<sub>2</sub>, 560.26696, found 560.26488 [M<sup>+</sup>].

### Amidoxime-functionalised model compound 1 (AO-M1)



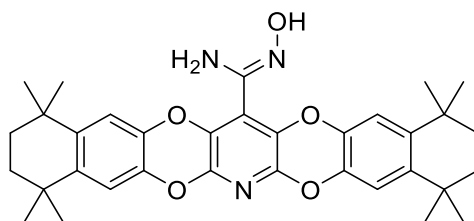
GP 5 was followed using M1 (5.50 g, 9.81 mmol) in THF (100 mL) to obtain a white precipitate (5.50 g, 90%). Mp: above 300 °C;  $\nu_{max}$  ( $\text{cm}^{-1}$ ): 3460.30, 3363.86, 3255.84, 2954.95, 1660.71, 1591.27, 1440.83, 1273.02;  $^1\text{H}$  NMR (500 MHz,  $\text{DMSO-}d_6$ )  $\delta$  9.54 (s, 1.5H, OH), 6.76-6.82 (m, 4H, ArH), 5.84 (s, 3H,  $\text{NH}_2$ ), 1.59 (s, 8H,  $\text{CH}_2$ ), 1.19 (s, 24H,  $\text{CH}_3$ ) ppm;  $^{13}\text{C}$  NMR (126 MHz,  $\text{DMSO-}d_6$ )  $\delta$  143.42, 140.76, 138.37, 135.51, 113.11, 34.30, 33.42, 31.13 ppm. HRMS (EI, m/z): calculated  $\text{C}_{36}\text{H}_{42}\text{O}_6\text{N}_4$ , 626.30989, found 626.30733 [ $\text{M}^+$ ]

### Model Compound 2 (M2)



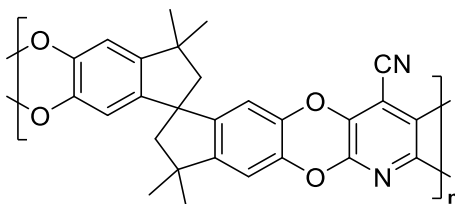
6,7-Dihydroxy-1,1,4,4-tetramethyl-2,3-dihydronaphthalene (1.00 g, 4.54 mmol) dissolved in anhydrous DMF (5 mL) was added dropwise to a solution of 2,3,5,6-tetrafluoro-4-pyridinecarbonitrile (0.40 g, 2.27 mmol) dissolved in anhydrous DMF (5 mL). Anhydrous potassium carbonate (2.50 g, 18.1 mmol) was added to the mixture, and it was stirred for 24 hours at 80 °C. The mixture was poured into water and stirred. 37% concentrated hydrochloric acid was added to the mixture dropwise until foaming stopped. Precipitates were filtered, washed with acetone. M2 was collected as pale-yellow powder (1.11 g, 91%). Mp: above 300 °C;  $\nu_{max}$  ( $\text{cm}^{-1}$ ): 2956.87, 2856.58, 2237.43, 1500.62, 1431.18, 1317.38, 1259.52, 1234.44, 995.27;  $^1\text{H}$  NMR (500 MHz,  $\text{CDCl}_3$ )  $\delta$  6.91 (s, 2H, ArH), 6.87 (s, 2H, ArH), 1.66 (s, 8H,  $\text{CH}_2$ ), 1.24 (s, 12H,  $\text{CH}_3$ ), 1.23 (s, 12H,  $\text{CH}_3$ ) ppm;  $^{13}\text{C}$  NMR (126 MHz,  $\text{CDCl}_3$ )  $\delta$  142.88, 142.76, 141.86, 138.46, 137.53, 135.11, 114.85, 114.30, 109.50, 98.96, 34.86, 34.34, 34.30, 31.83 ppm; NMR (126 MHz,  $\text{DMSO-}d_6$ )  $\delta$  143.42, 140.76, 138.37, 135.51, 113.11, 34.30, 33.42, 31.13 ppm. HRMS (EI, m/z): calculated  $\text{C}_{34}\text{H}_{36}\text{N}_2\text{O}_4$ , 536.26733, found 536.26549 [ $\text{M}^+$ ]

### Amidoxime-functionalised model compound 2 (AO-M2)



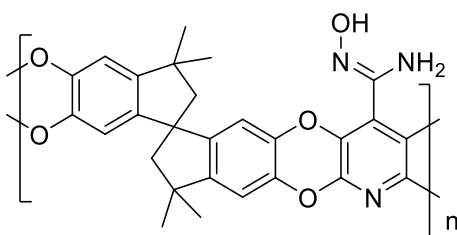
M2 (1.00 g, 1.86 mmol) was added to THF (100 mL). Excess hydroxylamine 50 wt. % H<sub>2</sub>O was then added, and the mixture was refluxed for 48 hours. The mixture was poured into ethanol, filtered and washed with ethanol. A white precipitate (0.94 g, 89%) was collected. Mp: above 300 °C;  $v_{max}$  (cm<sup>-1</sup>): 3448.72, 3354.21, 2953.02, 2860.43, 1639.49, 1597.06, 1502.55, 1431.18, 1319.31, 1267.23; <sup>1</sup>H NMR (500 MHz, CDCl<sub>3</sub>): δ 9.71 (s, 1H, OH), 7.00 (s, 2H, ArH), 6.84 (s, 2H, ArH), 5.95 (s, 2H, NH), 1.6 (s, 8H, CH<sub>2</sub>), 1.2 (s, 24H, CH<sub>3</sub>) ppm; <sup>13</sup>C NMR (126 MHz, CDCl<sub>3</sub>) δ 143.02, 139.17, 137.28, 136.42, 114.36, 109.65, 94.05, 34.57, 34.13, 31.57 ppm; HRMS (EI, m/z): calculated C<sub>34</sub>H<sub>39</sub>N<sub>3</sub>O<sub>5</sub>, 569.28817, found 569.28693 [M<sup>+</sup>]

### PIM-py



GP 4 was followed using 5,5',6,6'-tetrahydroxy-3,3,3',3'-tetramethyl-1,1'-spirobiindane (1.10 g, 3.23 mmol), 2,3,5,6-tetrafluoro-4-pyridinecarbonitrile (0.5689 g, 3.23 mmol) and anhydrous potassium carbonate (2.02 g, 14.62 mmol) in anhydrous DMF (20 mL). The mixture was stirred at 70 °C for 72 hours. PIM-py (1.35 g, 96%) was collected as a bright yellow powder.  $v_{max}$  (cm<sup>-1</sup>): 2954.95, 2856.58, 2162.20, 1431.18, 1307.74, 1238.30, 1107.14, 993.34, 873.75; <sup>1</sup>H NMR (500 MHz, ) : 6.76 (d, J = 29.63 Hz, 2H, ArH), 6.39 (d, J = 28.86 Hz, 2H, ArH), 2.31 (s, 4H, CH<sub>2</sub>), 1.32 (s, 12H, CH<sub>3</sub>) ppm; BET surface area = 736 m<sup>2</sup> g<sup>-1</sup>; total pore volume = 0.517 ml g<sup>-1</sup> at (P/P<sub>0</sub> = 0.98); TGA analysis: initial weight loss due to thermal degradation commences at 495 °C with a 35% loss of mass below 800 °C.

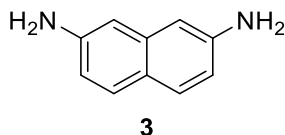
## AO-PIM-py



GP 5 was followed using PIM-py (0.49 g, 1.12 mmol) and an excess hydroxylamine 50% wt. H<sub>2</sub>O solution (10 mL) in THF (50 mL). AO-PIM-py (0.50 g, 94 %) was collected as a pale-yellow powder.  $\nu_{max}$  (cm<sup>-1</sup>): 3845.37, 3361.93, 2953.02, 2862.36, 1653.00, 1487.12, 1408.04, 1309.67, 1288.45, 1246.02, 1107.14, 989.48; <sup>1</sup>H NMR (500 MHz, DMSO- *d*<sub>6</sub>): 9.64 (t, J = 50.49, 50.49 Hz, 1H, OH), 7.05-6.75 (m, 2H, ArH), 6.41-6.14 (m, 2H, ArH), 5.89 (br s, 2H, NH<sub>2</sub>), 2.09 (s, 4H, CH<sub>2</sub>), 1.24 (s, 12H, CH<sub>3</sub>); BET surface area = 254 m<sup>2</sup> g<sup>-1</sup>; total pore volume = 0.204 ml g<sup>-1</sup> at (P/P<sub>0</sub>=0.98); TGA analysis: initial weight loss due to thermal degradation commences at 274 and 474 °C with a 37% loss of mass below 800 °C.

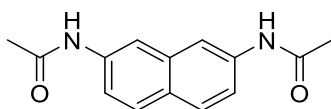
## 9.4 Amine-containing monomer and polymer synthesis

### 2,7-Diaminonaphthalene<sup>166</sup>



A mixture of 2,7-dihydroxynaphthalene (6.00 g, 37.4 mmol) and NaHSO<sub>3</sub> (11.7 g, 112 mmol) in 34% ammonia solution (70 mL) were heated to 170 °C in a pressure reactor for 17 hours. The mixture was then cooled to room temperature and basified with 4M NaOH aq. solution to > pH 12. The solid was filtered and washed with water, dissolved in 2M HCl aq. solution and filtered through Celite®. 4M NaOH aq. solution was added to the solution, precipitates were filtered and washed with water to yield 2,7-diaminonaphthalene as brown solids (5.70 g, 96 %). Mp: 159 °C (Lit: 158 °C<sup>166</sup>);  $\nu_{max}$  (cm<sup>-1</sup>): 3296.35, 3196.05, 1616.35, 1517.98, 1290.38, 1220.94, 827.46; <sup>1</sup>H NMR (500 MHz, CDCl<sub>3</sub>): δ 7.50 (d, 2H, ArH), 6.75 (s, 2H, ArH), 6.70 (d, 2H, ArH), 3.76 (s, 4H, NH<sub>2</sub>) ppm; <sup>13</sup>C NMR (126 MHz, CDCl<sub>3</sub>) δ 144.76, 136.57, 129.21, 122.77, 114.98, 107.03 ppm.

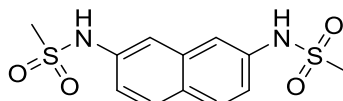
### ***N,N'*-2,7-Naphthalenebis(acetamide)**



4

Anhydrous sodium acetate (10.0 g, 126 mmol) was added to a stirred solution of 2,7-naphthalenediamine (1.00 g, 6.32 mmol) in acetic anhydride (10 mL). The reaction mixture was stirred at room temperature for 8 hours. The reaction mixture was then cooled in an ice bath, whilst iced water was added. 2,7-Naphthalenebisacetamide (1 g, 65.3%) was collected as purple solid via filtration. Mp: 168 °C;  $\nu_{max}$  (cm<sup>-1</sup>): 3288.63, 1653.00, 1525.69, 1421.54, 1361.74, 1278.81, 831.32; <sup>1</sup>H NMR (500 MHz, DMSO-*d*<sub>6</sub>):  $\delta$  10.08 (s, 2H, NH), 8.13 (s, 2H, ArH), 7.78-7.65 (m, 2H, ArH), 7.50-7.38 (m, 2H, ArH), 2.09 (s, 6H, CH<sub>3</sub>) ppm; <sup>13</sup>C NMR (126 MHz, DMSO-*d*<sub>6</sub>): 168.65, 137.38, 133.95, 128.01, 126.30, 118.39, 114.40, 24.15 ppm.

### ***N,N'*-Bis(mesyl)-2,7-naphthalenediamine**

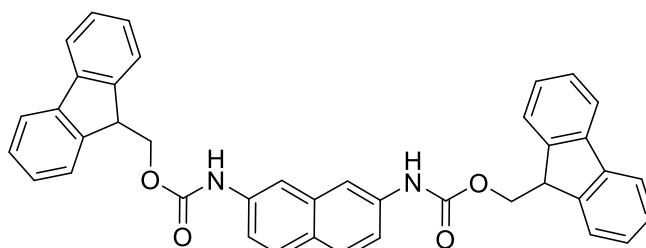


5

To a stirred solution of 2,7-diaminonaphthalene (0.50 g, 3.16 mmol) in pyridine (10 mL) at 0 °C, methanesulfonyl chloride (0.91 g, 7.9 mmol) was added dropwise. The reaction mixture was stirred at room temperature for 3 hours, poured into water and extracted with ethyl acetate. The solution was dried with magnesium sulphate and solvent was removed under vacuum. *N,N'*-Bis(mesyl)-2,7-naphthalenediamine was collected as a brown solid (0.67 g, 67%). Mp: 215 °C;  $\nu_{max}$  (cm<sup>-1</sup>): 3253.91, 1641.42, 1519.91, 1317.38, 1134.14, 970.19, 837.10, 763.81; <sup>1</sup>H NMR (500 MHz, acetone-*d*<sub>6</sub>):  $\delta$  8.77 (s, 2H, NH), 7.89 (dt, *J* = 9.0, 0.7 Hz, 2H, ArH), 7.77-7.75 (m, 2H, ArH), 7.45 (dd, *J* = 8.9, 2.1 Hz, 2H, ArH), 3.07 (s, 6H, CH<sub>3</sub>) ppm; <sup>13</sup>C NMR (126 MHz, acetone-*d*<sub>6</sub>):  $\delta$  150.68, 137.96, 135.58, 130.03, 120.32, 116.26, 39.57 ppm.



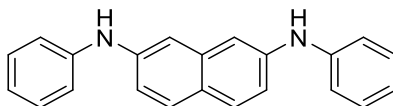
### ***N,N'*-Bis(Fmoc)-2,7-naphthalenecarbamide**



**6**

Fmoc chloride (2.05 g, 7.90 mmol) was added to a stirring solution of naphthalene-2,7-diamine (0.50 g, 3.16 mmol) in water (15 mL). The reaction mixture was heated at 60 °C for 1 day, filtered and washed with water. Solid collected was washed with hot ethanol to yield *N,N'*-Bis(Fmoc)-2,7-naphthalenecarbamide as a grey solid (1.1 g, 61%). Mp: above 300 °C;  $\nu_{max}$  (cm<sup>-1</sup>): 3315.63, 3167.12, 3035.96, 1695.43, 1633.71, 1521.84, 1413.82, 1323.17; <sup>1</sup>H NMR (500 MHz, DMSO-*d*<sub>6</sub>):  $\delta$  9.87 (s, 2H, NH) 7.92 (d, 4H, ArH), 7.91-7.84 (m, 2H, ArH), 7.78 (d, 4H, ArH), 7.72 (d, 2H, ArH), 7.47-7.39 (m, 6H, ArH), 7.39-7.33 (m, 4H, ArH), 4.54 (d, 4H, CH<sub>2</sub>), 4.34 (t, 2H, CH) ppm; <sup>13</sup>C NMR (126 MHz, DMSO-*d*<sub>6</sub>):  $\delta$  153.52, 143.76, 140.81, 137.16, 133.98, 128.08, 127.68, 127.12, 125.68, 125.11, 120.19, 117.76, 113.15, 65.64, 46.64 ppm.

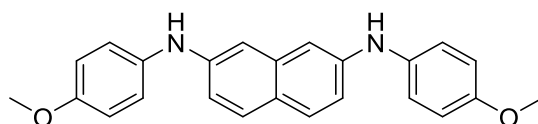
### ***N,N'*-Bis(phenyl)-2,7-naphthalenediamine<sup>168</sup>**



**7**

2,7-Dihydroxynaphthalene (1.50 g, 9.36 mmol), aniline (6 g, 64.5 mmol) and aniline chloride (2.40 g, 18.5 mmol) were heated to 145 °C in microwave reactor for 3h. After cooling, precipitates were filtered and washed with methanol to yield *N,N'*-Bis(phenyl)-2,7-naphthalenediamine as a silver solid (5.70 g, 98%). Mp: 160 °C (Lit: 158-159 °C<sup>168</sup>),  $\nu_{max}$  (cm<sup>-1</sup>): 3394.72, 3034.03, 1627.92, 1595.13, 1500.62, 1301.95, 869.90, 729.09; <sup>1</sup>H NMR (500 MHz, acetone-*d*<sub>6</sub>):  $\delta$  7.64 (d, *J* = 8.7 Hz, 2H, ArH), 7.51 (br s, 2H, NH), 7.34 (d, *J* = 2.2 Hz, 2H, ArH), 7.30-7.20 (m, 8H, ArH), 7.09 (dd, *J* = 8.7, 2.2 Hz, 2H, ArH) ppm; <sup>13</sup>C NMR (126 MHz, acetone-*d*<sub>6</sub>):  $\delta$  144.54, 142.95, 137.17, 130.04, 129.52, 125.30, 121.28, 118.66, 117.98, 109.96 ppm;

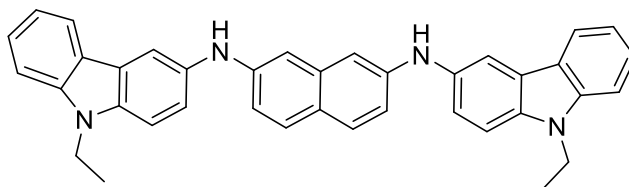
***N,N'*-Bis(4-methoxyphenyl)-2,7-naphthalenediamine**<sup>168</sup>



8

GP 2 was followed using 2,7-dihydroxynaphthalene (2.00 g, 12.5 mmol), *p*-anisidine (3.08 g, 25.0 mmol) and iodine (0.23 g, 0.892 mmol) in xylene (25 mL). Precipitates collected were recrystallized in toluene to yield *N*<sup>2</sup>,*N*<sup>7</sup>-bis(4-methoxyphenyl)-2,7-naphthalenediamine as silver solids (1.55 g, 33%). Mp: 165 °C (Lit: 161-163 °C<sup>169</sup>);  $\nu_{max}$  (cm<sup>-1</sup>): 3412.08, 3012.81, 2949.16, 2835.36, 1627.92, 1508.33, 1242.16, 1031.92, 821.68, 520.78; <sup>1</sup>H NMR (400 MHz, DMSO-*d*<sub>6</sub>):  $\delta$  7.92 (s, 2H, NH), 7.51 (d, *J* = 8.7 Hz, 2H, ArH), 7.16-7.08 (m, 4H, ArH), 6.94 (d, *J* = 2.2 Hz, 2H, ArH), 6.92-6.84 (m, 6H, ArH), 3.73 (s, 6H, CH<sub>3</sub>) ppm; <sup>13</sup>C NMR (126 MHz, DMSO-*d*<sub>6</sub>):  $\delta$  153.93, 143.32, 135.95, 128.40, 122.22, 120.83, 115.25, 114.53, 105.18, 55.19 ppm.

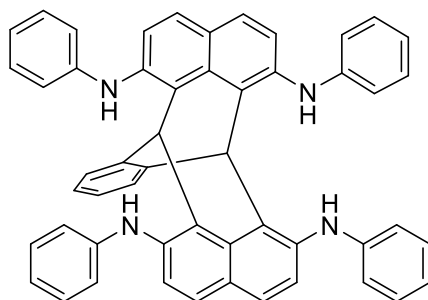
***N*<sup>2</sup>, *N*<sup>7</sup>-Bis(9-ethylcarbazole)-2,7-naphthalenediamine**<sup>218</sup>



9

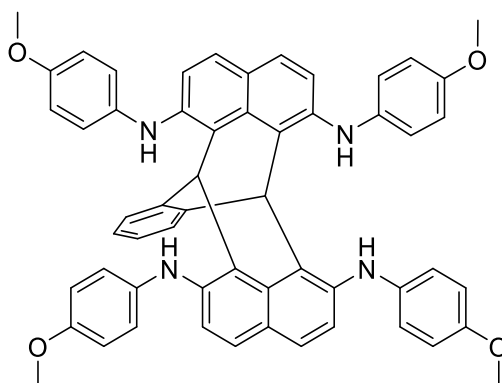
GP 2 was followed using 2,7-dihydroxynaphthalene (2.00 g, 12.5 mmol), 3-amino-9-ethylcarbazole (5.25 g, 25.0 mmol) and iodine (0.23 g, 0.892 mmol) in 1,2-dichlorobenzene (20 mL). Precipitates collected were recrystallized in toluene to yield *N*<sup>2</sup>, *N*<sup>7</sup>-bis(9-ethylcarbazole)-2,7-naphthalenediamine (2.73 g, 40%) as white powder. Mp: 230 °C (Lit: 232-234.5 °C<sup>218</sup>);  $\nu_{max}$  (cm<sup>-1</sup>): 3390.86, 3051.39, 2974.23, 1622.13, 1510.26, 1469.76, 1344.38, 1301.95, 1222.87; <sup>1</sup>H NMR (400 MHz, DMSO-*d*<sub>6</sub>):  $\delta$  8.20 (s, 2H, NH), 8.00 (d, *J* = 7.5 Hz, 2H, ArH), 7.88 (d, *J* = 1.8 Hz, 2H, ArH), 7.47 (d, *J* = 8.7 Hz, 2H, ArH), 7.42 (d, *J* = 8.7 Hz, 4H, ArH), 7.39-7.36 (m, 2H, ArH), 7.32 (dd, *J* = 8.7, 1.8 Hz, 2H, ArH), 7.12-7.07 (m, 2H, ArH), 6.97 (d, *J* = 1.9 Hz, 2H, ArH), 6.95 (dd, *J* = 8.7, 1.9 Hz, 2H, ArH), 4.35 (q, *J* = 7.2 Hz, 4H, CH<sub>2</sub>), 1.36 (t, *J* = 7.2 Hz, 6H, CH<sub>3</sub>); <sup>13</sup>C NMR (126 MHz, DMSO-*d*<sub>6</sub>):  $\delta$  144.21, 139.92, 136.29, 135.49, 134.82, 128.44, 125.56, 122.67, 122.13, 121.92, 120.41, 120.39, 118.23, 114.94, 111.58, 109.59, 108.96, 104.89, 36.93, 13.72 ppm.

### Tetra(aniline) naphthopleiadene (NNP1)



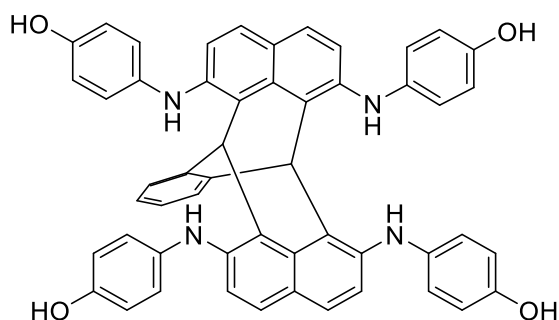
GP 3 was followed using  $N^2,N^7$ -bis(phenyl)-2,7-naphthalenediamine (1.00 g, 3.22 mmol), phthalaldehyde(0.22 g, 1.64 mmol) in ethanol (20 mL). Product (1.41 g ,61%) was collected as a grey powder. Mp: above 300 °C,  $\nu_{max}$  ( $\text{cm}^{-1}$ ): 3331.07, 3041.74, 1595.13, 1492.90, 1334.74, 1290.38, 1271.09, 835.18, 742.59, 690.52;  $^1\text{H}$  NMR (500 MHz,  $\text{DMSO-}d_6$ ):  $\delta$  8.80 (s, 4H, NH), 7.64 (d, 4H, ArH), 7.30 (d, 4H, ArH), 7.25-7.12 (m, 9H, ArH), 6.93-6.85 (m, 12H, ArH), 6.84-6.81 (m, 2H, ArH), 6.52 (s, 2H, bridge-H), 6.50-6.47 (m, 2H, ArH) ppm.  $^{13}\text{C}$  (126 MHz,  $\text{DMSO-}d_6$ ):  $\delta$  145.95, 139.94, 138.58, 133.21, 129.54, 129.16, 129.15, 129.11, 128.97, 126.57, 121.85, 120.29, 117.52, 44.11 ppm. HRMS (EI, m/z): calculated  $\text{C}_{52}\text{H}_{38}\text{N}_4$ , 718.30910, found 718.306106 [ $\text{M}^+$ ].

### Tetra(4-methoxyphenyl) naphthopleiadene (NNP2)



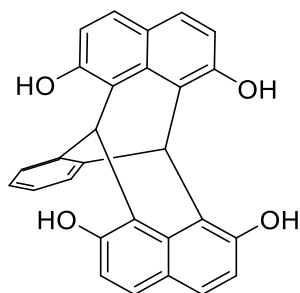
GP 3 was followed using  $N^2,N^7$ -bis(4-methoxyphenyl)-2,7-naphthalenediamine (2.00 g, 5.40 mmol), phthalaldehyde(0.222 g, 2.70 mmol) in ethanol (10 mL). Precipitates were filtered and washed with acetone to afford tetra(methoxyphenyl) naphthopleiadene (1.54 g, 68%) as light brown solid. Mp: above 300 °C;  $\nu_{max}$  ( $\text{cm}^{-1}$ ): 3309.85, 2947.23, 2829.57, 1614.42, 1504.48, 1336.67, 1234.44, 1033.85, 823.60;  $^1\text{H}$  NMR (500 MHz,  $\text{DMSO-}d_6$ ):  $\delta$  8.68 (s, 4H, NH), 7.56 (d, 4H, ArH), 7.20 (d, 4H, ArH), 6.92-6.86 (m, 8H, ArH), 6.86-6.82 (m, 8H, ArH), 6.35-6.29 (m, 4H, ArH and bridge-H) ppm;  $^{13}\text{C}$  NMR (126 MHz,  $\text{DMSO-}d_6$ ):154.19, 140.04, 139.87, 139.09, 133.58, 128.83, 128.59, 128.17, 126.71, 126.35, 120.45, 119.98, 114.64, 55.30, 43.95 ppm. HRMS (EI, m/z): calculated  $\text{C}_{56}\text{H}_{47}\text{N}_4\text{O}_4$ , 839.35918, found 839.3556 [ $\text{M}^+$ ].

### Tetra(4-hydroxyphenyl) naphthopleiadene (NNP3)



GP 3 was followed using tetra(4-methoxyphenyl) naphthopleiadene (1.00 g, 1.19 mmol), boron tribromide (2.38 g, 9.52 mmol) in anhydrous dichloromethane (20 mL) to afford product (0.86 g, 92%) as a pale-purple solid. Mp: above 300 °C;  $\nu_{max}$  (cm<sup>-1</sup>): 3383.14, 3261.63, 1616.35, 1506.41, 1346.31, 1240.23, 829.39, 700.16; <sup>1</sup>H NMR (500 MHz, acetone-*d*<sub>6</sub>):  $\delta$  8.09 (s, 4H, NH), 7.97 (s, 4H, OH), 7.51 (d, 4H, ArH), 7.20 (d, 4H, ArH), 6.92-6.84 (m, 8H, ArH), 6.80-6.78 (m, 2H, ArH), 6.78-6.72 (m, 8H, ArH), 6.48-6.45 (m, 2H, ArH), 6.43 (s, 2H, bridge-H) ppm; <sup>13</sup>C NMR (126 MHz, acetone-*d*<sub>6</sub>):  $\delta$  153.60, 141.54, 139.11, 135.29, 129.55, 129.28, 127.17, 122.89, 120.26, 116.74, 45.62 ppm; HRMS (EI, m/z): calculated C<sub>52</sub>H<sub>38</sub>N<sub>4</sub>O<sub>4</sub>, 782.28931, found 782.2754 [M<sup>+</sup>].

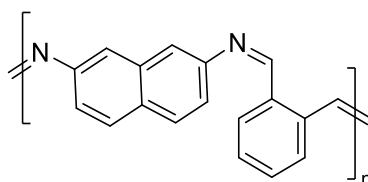
### Tetrahydroxy-naphthopleiadene<sup>165</sup>



8

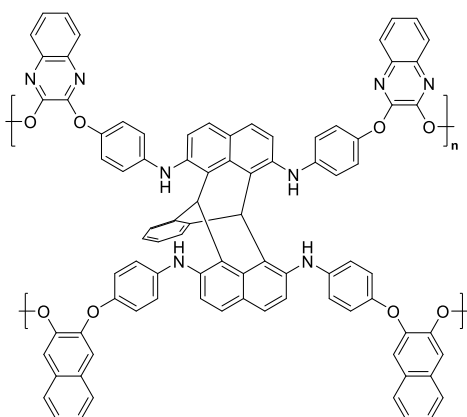
2,7-Dihydroxynaphthalene (1.91 g, 11.9 mmol) and phthalaldehyde (0.80 g, 5.97 mmol) were dissolved in dry methanol (100 mL) and refluxed under inert atmosphere. A few drops of concentrated HCl were added to the reaction mixture and the reaction continued for 3 hours. The reaction mixture was then cooled to room temperature and poured into water. The resulting precipitate was filtered, washed with water and cold methanol to yield the tetrahydroxy naphthopleiadene (1.75 g, 70%) as a greyish green powder. Mp: above 300 °C;  $\nu_{max}$  (cm<sup>-1</sup>): 3200.32, 2978.95, 2868.43, 1611.12, 1509.06, 1423.80; <sup>1</sup>H NMR (500 MHz, DMSO-*d*<sub>6</sub>):  $\delta$  9.94 (s, 4H, OH), 7.74 (d, 4H, ArH), 7.37 (dd, 2H, ArH), 7.16 (dd, 2H, ArH), 6.96 (d, 4H, ArH), 6.82 (s, 2H, bridge-H); <sup>13</sup>C NMR (126 MHz, DMSO-*d*<sub>6</sub>)  $\delta$  151.96, 141.95, 133.90, 129.09, 128.46, 127.63, 125.30, 120.41, 115.63 ppm.

### Imine Schiff base polymeric product (CP1)



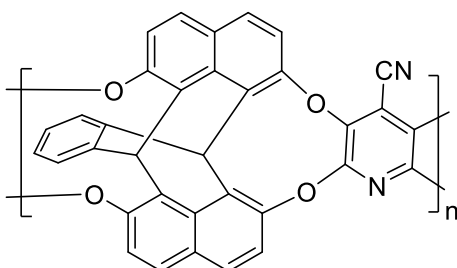
GP 3 was followed using 2,7-diaminonaphthalene (1 g, 6.32 mmol) and phthalaldehyde (0.424 g, 3.16 mmol). The reaction was refluxed for 24 hr, and the resulting polymeric product was washed with water, acetone, and methanol to yield a dark red solid (0.74 g, 91 %).  $\nu_{max}$  ( $\text{cm}^{-1}$ ): 3377.36, 3057.17, 1728.58, 1616.35, 1508.33, 1381.03, 1103.28, 833.25;  $^{13}\text{C}$  NMR (76 MHz, solid state):  $\delta$  166.04, 143.82, 128.07 ppm; BET surface area =  $12 \text{ m}^2 \text{ g}^{-1}$ ; total pore volume =  $0.0374 \text{ ml g}^{-1}$  at ( $P/P_0=0.98$ ); TGA analysis: initial weight loss due to thermal degradation commences at  $383 \text{ }^\circ\text{C}$  with a 29% loss of mass below  $800 \text{ }^\circ\text{C}$ .

### NNP3-crosslinked polymer (CP2)



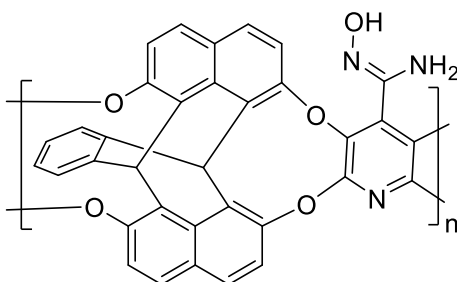
GP 4 was followed using NNP3 (1 g, 1.41 mmol) and 2,3-dichloroquinoxaline (0.282 g, 1.41 mmol). The reaction was carried out for 24 h, the resulting mixture was acidified and filtered, then washed with water, acetone, and methanol respectively. Purple solids (1.83 g, 96%) were collected.  $\nu_{max}$  ( $\text{cm}^{-1}$ ): 2980.02, 1604.77, 1496.76, 1427.32, 1328.95, 1192.01, 1055.06, 829.39, 756.10;  $^{13}\text{C}$  NMR (76 MHz, solid state):  $\delta$  144.62, 137.75, 126.64 ppm; BET surface area =  $0 \text{ m}^2 \text{ g}^{-1}$ ; total pore volume =  $0.0372 \text{ ml g}^{-1}$  at ( $P/P_0=0.98$ ); TGA analysis: initial weight loss due to thermal degradation commences at  $453 \text{ }^\circ\text{C}$  with a 39% loss of mass below  $800 \text{ }^\circ\text{C}$ .

### PIM-NP-py



GP 4 was followed using tetrahydroxy-naphthopoleiadene (1.19 g, 2.84 mmol), 2,3,5,6-tetrafluoro-4-pyridinecarbonitrile (0.5000 g, 2.84 mmol) and anhydrous potassium carbonate (3.14 g, 22.7 mmol) in anhydrous DMF (65 mL). The solution was heated to 65 °C and left to react for 4 days. Due the insoluble nature of the polymer, no reprecipitation step was carried out. PIM-NP-py (1.36 g, 93%) was collected as a bright yellow powder.  $v_{max}$  ( $\text{cm}^{-1}$ ): 2214.28, 2002.11, 1614.42, 1506.41, 1400.32, 1323.17, 1176.58, 983.70, 835.18;  $^{13}\text{C}$  NMR (76 MHz, solid state):  $\delta$  151.34, 139.85, 131.15, 128.18, 120.18, 39.20 ppm; BET surface area = 514  $\text{m}^2 \text{g}^{-1}$ ; total pore volume = 0.0582  $\text{ml g}^{-1}$  at ( $P/P_0=0.98$ ); TGA analysis: initial weight loss due to thermal degradation commences at 355 °C with a 27% loss of mass below 800 °C.

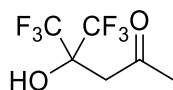
### AO-PIM-NP-py



Trip-py (0.50 g, 0.97 mmol) was dispersed in THF (50 mL), excess hydroxylamine 50% wt.  $\text{H}_2\text{O}$  solution (10 mL) was added, and the solution was heated to reflux for 12 hours. The solution was cooled to room temperature and poured into ethanol. The precipitates were filtered and washed further with ethanol to afford AO-PIM-NP-py (0.51 g, 96%) as pale-yellow powder.  $v_{max}$  ( $\text{cm}^{-1}$ ): 3479.58, 3369.64, 1676.14, 1610.56, 1508.33, 1394.53, 1182.36, 835.18;  $^{13}\text{C}$  NMR (76 MHz, solid state):  $\delta$  162.67, 151.29, 140.13, 128.18, 120.08, 59.48, 52.41, 39.21 ppm; BET surface area = 1  $\text{m}^2 \text{g}^{-1}$ ; total pore volume = 0.00293  $\text{ml g}^{-1}$  at ( $P/P_0=0.98$ ); TGA analysis: initial weight loss due to thermal degradation commences at 258 and 439 °C with a 34% loss of mass below 800 °C.

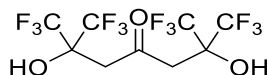
## 9.5 Fluorinated monomer and polymer synthesis

### 5,5,5-Tri-fluoro-4-hydroxy-4-(trifluoromethyl)pentan-2-one



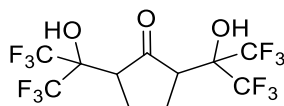
Perfluoroacetone sesquihydrate (59.2 mL, 259 mmol) and acetone (9.6 mL, 130 mmol) and pentane (20 mL) were added to a high-pressure reactor. Pentane (30 mL) were added in order to maintain high pressure in the system. The mixture was heated at 150 °C for 9 hours. Solvents were removed under reduced pressure to leave behind a colourless oil. Vacuum distillation was performed, and 5,5,5-Tri-fluoro-4-hydroxy-4-(trifluoromethyl)pentan-2-one (21.3 g, 73%) was distilled off and collected as a clear oil.  $\nu_{max}$  (cm<sup>-1</sup>): 3292.49, 1701.22, 1207.44, 1151.50, 1062.78, 937.40, 721.38; <sup>1</sup>H NMR (500 MHz, CDCl<sub>3</sub>):  $\delta$  6.75 (s, 1H, OH), 2.96 (s, 2H, CH<sub>2</sub>), 2.32 (s, 3H, CH<sub>3</sub>) ppm; <sup>13</sup>F NMR (500 MHz, CDCl<sub>3</sub>):  $\delta$  -78.9 (s, 6F, CF<sub>3</sub>).

### 1,1,1,7,7,7-Hexafluoro-2,6-dihydroxy-2,6-bis(trifluoromethyl)-4-heptanone



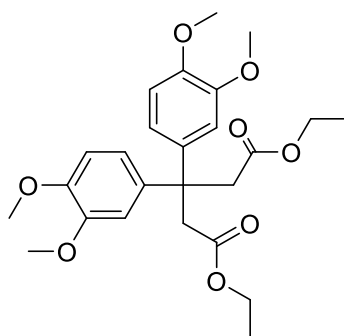
1,1,1,7,7,7-hexafluoro-2,6-dihydroxy-2,6-bis(trifluoromethyl)-4-heptanone (10 g, 20%) was collected as white solids after vacuum distillation. Mp: 78 °C;  $\nu_{max}$  (cm<sup>-1</sup>): 3460.30, 1712.79, 1404.18, 1234.44, 1165.00, 134.14, 1060.85, 767.67, 705.95; <sup>1</sup>H NMR (500 MHz, CDCl<sub>3</sub>):  $\delta$  5.36 (s, 2H, OH), 3.15 (s, 4H, CH<sub>2</sub>) ppm; <sup>13</sup>C NMR (500 MHz, CDCl<sub>3</sub>):  $\delta$  207.69, 123.35, 121.06, 40.14 ppm; <sup>19</sup>F NMR (500 MHz, CDCl<sub>3</sub>): -77.82 (s, 12F, CF<sub>3</sub>) ppm.

### 2,5-Bis(1,1,1,3,3,3-hexafluoro-2-hydroxypropan-2-yl)cyclopentan-1-one



Perfluoroacetone sesquihydrate (38.3 mL, 168 mmol) and cyclopentan-1-one (4.80 mL, 67.1 mmol) were added together into a Dean-Stark set-up. The solution was heated to 140 °C, an excess of potassium hydroxide pellets was added to the mixture in small aliquots. The reaction was allowed to react for 1 week. The product was collected by filtration and washed with water to obtain white crystals (12.8 g, 46%). Mp: 78 °C;  $\nu_{max}$  (cm<sup>-1</sup>): 3377.36, 1718.58, 1249.87, 1203.58, 1145.72, 1134.14, 1051.20, 960.55; <sup>1</sup>H NMR (500 MHz, DMSO-*d*<sub>6</sub>):  $\delta$  8.00 (s, 2H, OH), 3.05-2.98 (m, 2H, CH), 2.30-2.17 (m, 2H, CH<sub>2</sub>); <sup>13</sup>C NMR (500 MHz, DMSO-*d*<sub>6</sub>):  $\delta$  203.92, 123.37 (q,  $J_{C-F}$  = 21.8 Hz, CF<sub>3</sub>), 49.89, 48.87, 22.69 ppm; <sup>19</sup>F NMR (500 MHz, DMSO-*d*<sub>6</sub>):  $\delta$  -71.67 (q,  $J_{C-F}$  = 9.40, 9.81 Hz, 3F, CF<sub>3</sub>), -73.07 (q,  $J_{C-F}$  = 9.61 Hz, 3F, CF<sub>3</sub>) ppm. HRMS (EI, m/z): calculated C<sub>11</sub>H<sub>8</sub>F<sub>12</sub>O<sub>3</sub>, 416.02763, found 416.97550 [M<sup>+</sup>].

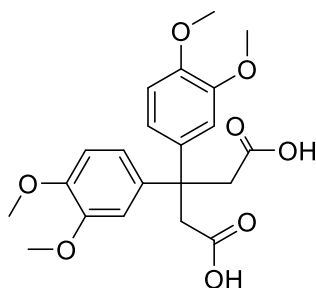
### Diethyl-3,3-bis(3,4-dimethoxyphenyl) pentanedioate<sup>115</sup>



10

Veratrole (22.2 mL, 176 mmol) and diethyl-1,3-acetone dicarboxylate (4.00 mL, 22.0 mmol) were added together and stirred at 0 °C. Concentrated sulphuric acid (10 mL) were added to the stirring mixture dropwise and continued to stir at room temperature for 20 hours. The mixture was then poured into ice water and stirred until gel-like product formed. Water was removed, and the gel-like product was then stirred in hexane to obtain product as a white powder (8.92 g, 88%). Mp: 83-84 °C (Lit: 84-86 °C<sup>115</sup>);  $\nu_{max}$  (cm<sup>-1</sup>): 2974.23, 1728.22, 1508.33, 1342.46, 1247.94, 1141.86, 1016.49; <sup>1</sup>H NMR (500 MHz, CDCl<sub>3</sub>):  $\delta$  6.81-6.75 (m, 4H, ArH), 6.63 (d, J = 1.8 Hz, 2H, ArH), 3.91 (q, J = 7.2 Hz, 4H, CH<sub>2</sub>), 3.88 (s, 6H, OCH<sub>3</sub>), 3.77 (s, 6H, OCH<sub>3</sub>) ppm; <sup>13</sup>C NMR (500 MHz, CDCl<sub>3</sub>):  $\delta$  171.62, 148.48, 147.67, 139.09, 119.68, 111.54, 110.41, 60.19, 56.06, 55.93, 46.61, 42.89, 14.15 ppm.

### 3,3-Bis(3,4-dimethoxyphenyl) pentanedioic acid<sup>115</sup>



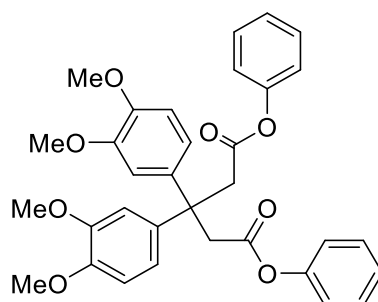
11

Diethyl-3,3-bis(3,4-dimethoxyphenyl) pentanedioate (2.00 g, 4.34 mmol) were dissolved in ethanol (25 mL) and stirred. 40% aqueous sodium hydroxide (25 mL) were added to the mixture dropwise, the reaction was allowed to continue for 2 days at 40 °C. Water (25 mL) were added to the reaction mixture and washed with diethyl ether. The aqueous layer was collected and cooled to 0 °C, concentrated hydrochloric acid were added dropwise until the pH became acidic. Pale yellow precipitates were collected and washed with water. Recrystallisation from diethyl ether yielded 3,3-bis(3,4-dimethoxyphenyl) pentanedioic acid (1.08 g, 54%) as a white solid. Mp: 110 °C (Lit: 110-112 °C<sup>115</sup>);  $\nu_{max}$  (cm<sup>-1</sup>): 2960.73, 1734.01, 1510.26, 1442.75, 1411.89, 1247.94, 1141.86, 1022.27, 804.31; <sup>1</sup>H



NMR (400 MHz, CDCl<sub>3</sub>): 6.77-6.69 (m, 4H, ArH), 6.57 (d, J = 2.0 Hz, 2H, ArH), 3.84 (s, 6H, OCH<sub>3</sub>), 3.71 (s, 6H, OCH<sub>3</sub>), 3.53 (s, 4H, CH<sub>2</sub>) ppm; <sup>13</sup>C NMR (400 MHz, CDCl<sub>3</sub>): δ 176.88, 148.59, 147.78, 138.69, 119.45, 111.28, 110.57, 56.03, 55.86, 45.83, 42.10 ppm.

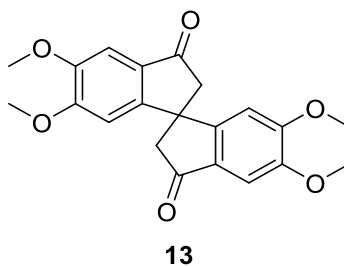
**3,3-Bis(3,4-dimethoxyphenyl) phenyl ester**<sup>208</sup>



**12**

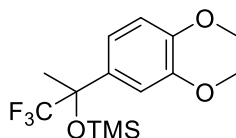
3,3-Bis(3,4-dimethoxyphenyl) pentanedioic acid (1.00 g, 2.47 mmol), phenol (0.26 g, 2.72 mmol) and 4-dimethylaminopyridine (0.14 g, 1.112 mmol) were added together. Under nitrogen atmosphere, anhydrous dichloromethane (10 mL) was added to the flask, and N,N'-diisopropylcarbodiimide (0.342 g, 2.72 mmol) was added to the mixture dropwise at 0 °C. The mixture was allowed to warm to room temperature after 10 minutes and left to stir overnight. The solution was washed with 0.1 M hydrochloric acid, 1 M sodium hydroxide solution, saturated sodium hydrogen carbonate solution and brine respectively. Solvent was removed under vacuum, and the crude product was purified by column chromatography hexane/ethyl acetate (1:1, v/v) to yield product as white powder (0.35 g, 25%). Mp: 179 °C;  $\nu_{max}$  (cm<sup>-1</sup>): 2974.23, 1728.22, 1508.33, 1342.46, 1247.94, 1141.86, 1016.49, 815.89; <sup>1</sup>H NMR (500 MHz, CDCl<sub>3</sub>): δ 7.30-7.24 (m, 4H, ArH), 7.18-7.13 (m, 2H, ArH), 6.89 (dd, J = 8.5, 2.2 Hz, 2H, ArH), 6.85 (d, J = 8.5 Hz, 2H, ArH), 6.73 (d, J = 2.2 Hz, 2H, ArH), 6.71-6.66 (m, 4H, ArH), 3.90 (s, 6H, OCH<sub>3</sub>), 3.79 (s, 4H, CH<sub>2</sub>), 3.77 (s, 6H, OCH<sub>3</sub>) ppm; <sup>13</sup>C NMR (500 MHz, CDCl<sub>3</sub>): δ 170.28, 150.42, 148.80, 148.07, 129.42, 125.94, 121.63, 119.82, 111.65, 110.72, 56.15, 42.84, 42.39 ppm; HRMS (FT-MALDI, m/z): calculated: 556.20972 found: 579.19337 [M<sup>+</sup>+Na].

### 5,6,5',6'-Tetramethoxy-1,1'-spirobisindane-3,3'-dione<sup>115</sup>



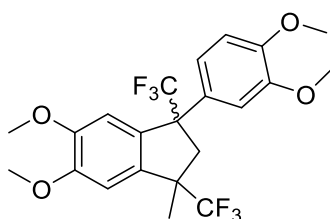
3,3-Bis(3,4-dimethoxyphenyl) pentanedioic acid (1.00 g, 2.47 mmol) was added in small aliquots to polyphosphoric acid heated at 80 °C and the mixture was allowed to stir overnight. The solution was poured into an ice water bath and stirred until white precipitates crashed out. The crude product was filtered and recrystallized in acetic acid/methanol (4:1, v/v), and the product was collected as a white powder (0.46 g, 48%). Mp: 247 °C (Lit: 245-250 °C<sup>115</sup>);  $\nu_{max}$  (cm<sup>-1</sup>): 2929.87, 1687.71, 1591.27, 1496.76, 1290.38, 1124.50, 1055.06, 850.61; <sup>1</sup>H NMR (500 MHz, CDCl<sub>3</sub>):  $\delta$  203.13, 156.45, 154.07, 150.63, 129.20, 105.21, 103.87, 56.89, 56.64, 53.27, 47.80 ppm.

### ((2-(3,4-Dimethoxyphenyl)-1,1,1-trifluoropropan-2-yl)oxy)-trimethylsilane<sup>209</sup>



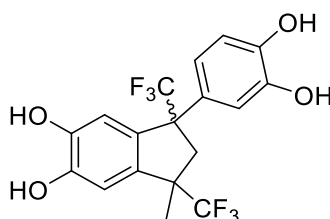
3,4-Dimethoxyacetophenone (2 g, 11.1 mmol) and potassium carbonate (3.07 g, 22.2 mmol) were added to anhydrous DMF (20 mL). Trimethyl(trifluoromethyl)silane (9.84 mL, 66.6 mmol) was added to the solution slowly at 0 °C. The mixture was allowed to stir at room temperature for 15 hours, poured into a mixture of saturated ammonium chloride solution (40 mL) and 1M hydrochloric solution (10 mL) and extracted using diethyl ether. Solvent was removed under vacuum. The crude product was purified by column chromatography hexane/ethyl acetate (7:3, v/v) to yield the product as a mixture of enantiomers (2.42 g, 68%) in the form of an orange oil.  $\nu_{max}$  (cm<sup>-1</sup>): 2958.80, 1666.50, 1514.12, 1257.59, 1145.72, 1026.13, 842.89; <sup>1</sup>H NMR (400 MHz, CDCl<sub>3</sub>):  $\delta$  7.13-7.07 (m, 2H, ArH), 7.01 (s, 1H, ArH), 7.00 (s, 1H, ArH), 6.85-6.78 (m, 2H, ArH), 3.86 (s, 6H, OCH<sub>3</sub>), 3.85 (s, 6H, OCH<sub>3</sub>), 2.00 (s, 3H, CH<sub>3</sub>), 1.78 (s, 3H, CH<sub>3</sub>), 0.13 (s, 18H, Si(CH<sub>3</sub>)) ppm; <sup>13</sup>C NMR (400 MHz, CDCl<sub>3</sub>):  $\delta$  149.17, 148.45, 132.62, 125.37 (q, J<sub>C-F</sub> = 285.6 Hz, CF<sub>3</sub>), 119.31, 110.61, 110.43, 76.96 (q, J<sub>C-F</sub> = 29.4 Hz, CF<sub>3</sub>), 55.84, 55.82, 22.6, 1.97 ppm; <sup>19</sup>F NMR (400 MHz, CDCl<sub>3</sub>):  $\delta$  -81.82 (s, CF<sub>3</sub>) ppm.

### Tetra(methoxy)-bis(trifluoromethyl) indane (FI-1)<sup>213</sup>



(2-(3,4-Dimethoxyphenyl)-1,1,1-trifluoropropan-2-yl)oxy)-trimethylsilane (2 g, 6.2 mmol) was stirred in concentrated sulphuric acid (5 mL) at room temperature for 30 minutes. The mixture was poured into ice water, stirred for 1 hour and extracted with ethyl acetate. The solvent was removed under vacuum. The crude product was purified by column chromatograph hexane/ethyl acetate (7:3, v/v) to obtain a mixture of *cis/trans* isomers of the product as a near-colourless oil (1.15 g, 40%).  $\nu_{max}$  ( $\text{cm}^{-1}$ ): 3005.10, 2937.59, 1604.77, 1508.33, 1463.97, 1222.87, 1126.43, 1091.71, 1026.13, 869.90;  $^1\text{H}$  NMR (400 MHz,  $\text{CDCl}_3$ ):  $\delta$  6.98 (s, 1H, ArH), 6.88 (s, 1H, ArH), 6.87 (d,  $J = 2.1$  Hz, 1H, ArH), 6.76 (d,  $J = 0.8$  Hz, 1H, ArH), 6.73 (dd,  $J = 8.5, 2.1$  Hz, 1H, ArH), 3.91 (s, 3H, OCH<sub>3</sub>), 3.90 (s, 3H, OCH<sub>3</sub>), 3.83 (s, 3H, OCH<sub>3</sub>), 3.79 (s, 3H, OCH<sub>3</sub>), 3.12 (d,  $J = 13.5$  Hz, 1H, CH<sub>2</sub>), 2.44 (d,  $J = 13.5$  Hz, 1H, CH<sub>2</sub>), 1.14 (s, 3H, CH<sub>3</sub>) ppm (*cis*-isomer); 6.90 (s, 1H, ArH), 6.84 (s, 1H, ArH), 6.83-6.80 (m, 2H, ArH), 6.78 (s, 1H, ArH), 3.92 (s, 3H, OCH<sub>3</sub>), 3.84 (s, 3H, OCH<sub>3</sub>), 3.84 (s, 3H, OCH<sub>3</sub>), 3.75 (s, 3H, OCH<sub>3</sub>), 2.82 (d,  $J = 15.2$  Hz, 1H, CH<sub>2</sub>), 2.73 (d, 15.2 Hz, 1H, CH<sub>2</sub>), 1.56 (s, 3H, CH<sub>3</sub>) ppm (*trans*-isomer);  $^{13}\text{C}$  NMR (400 MHz,  $\text{CDCl}_3$ ):  $\delta$  150.77, 150.69, 150.26, 149.90, 148.94, 148.84, 148.80, 148.47, 135.71, 135.57, 132.87, 132.12, 131.48, 130.26, 129.37, 129.23, 129.00, 128.62, 127.13, 126.99, 126.75, 126.37, 120.89, 120.20, 111.43, 110.80, 110.66, 108.89, 108.78, 106.70, 106.40, 60.56 (q,  $J_{\text{C-F}} = 25.78$  Hz, CCF<sub>3</sub>), 59.66 (q,  $J_{\text{C-F}} = 26.41$  Hz, CCF<sub>3</sub>), 56.33, 56.29, 56.13, 56.02, 55.92, 55.91, 52.22 (q,  $J_{\text{C-F}} = 26.86$  Hz, CCF<sub>3</sub>), 52.18 (q,  $J_{\text{C-F}} = 26.91$  Hz, CCF<sub>3</sub>), 46.09, 44.36, 23.11, 22.50 ppm;  $^{19}\text{F}$  NMR (400 MHz,  $\text{CDCl}_3$ ):  $\delta$  -69.59 (s, CF<sub>3</sub>), -70.00 (s, CF<sub>3</sub>), -75.51 (s, CF<sub>3</sub>), -75.60 (s, CF<sub>3</sub>) ppm.

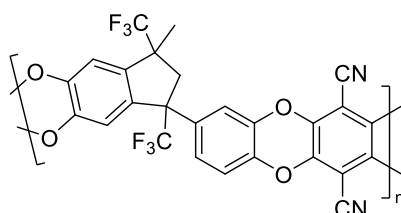
### Tetra(hydroxy)-bis(trifluoromethyl) indane (FI-2)



GP 1 was followed using **FI-1** (1 g, 2.15 mmol), boron tribromide (2.45 mL, 25.8 mmol) in anhydrous dichloromethane (10 mL). The crude product was obtained as dark-red oil and purified by repeated reprecipitation in hexane to obtain an off-white powder (0.62 g, 71%). Mp: 51 °C;  $\nu_{max}$  ( $\text{cm}^{-1}$ ): 2958.80, 1668.43, 1514.12, 1257.59, 1145.72, 1026.13, 842.89 ppm;  $^1\text{H}$  NMR (400 MHz,  $\text{CDCl}_3$ ):  $\delta$  7.02 (s, 1H,

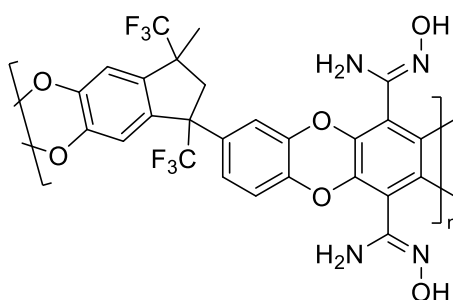
ArH), 6.94-6.87 (m, 3H, ArH), 6.85 (dd,  $J = 2.13, 11.52$  Hz, 2H, ArH), 6.81-6.77 (m, 3H, ArH), 6.74 (dd,  $J = 2.27, 8.50$ , 1H, ArH), 3.07 (d,  $J = 13.56$ , 1H, ArH), 2.82 (d,  $J = 15.10$ , 1H, ArH), 2.68 (d, 15.12, 1H, 1H, ArH), 2.42 (d,  $J = 13.51$ , 1H, ArH), 1.52 (s, 3H, CH<sub>3</sub>), 1.08 (s, 3H, ArH) ppm; <sup>13</sup>C NMR (400 MHz, CDCl<sub>3</sub>):  $\delta$  145.47, 145.27, 144.66, 144.36, 143.46, 143.21, 143.10, 132.93, 132.88, 132.31, 121.12, 120.79, 115.69, 115.50, 115.28, 115.14, 113.32, 113.11, 111.26, 110.77, 51.68 (m, CCF<sub>3</sub>), 45.86, 44.09, 23.15, 22.49 ppm; <sup>19</sup>F NMR (400 MHz, CDCl<sub>3</sub>):  $\delta$  -70.26 (s, CF<sub>3</sub>), -70.50 (s, CF<sub>3</sub>), -75.62 (s, CF<sub>3</sub>), -75.77 (s, CF<sub>3</sub>) ppm.

### PIM-FI



GP 4 was followed, using FI-2 (0.79 g, 1.93 mmol), TFTP (0.387 g, 1.93 mmol), and anhydrous K<sub>2</sub>CO<sub>3</sub> (2.14 g, 15.5 mmol), in 15 ml of anhydrous DMF. The reaction mixture was stirred at 75 °C for 5 days under N<sub>2</sub> atmosphere. The reaction mixture was filtered and washed with water and methanol; the resulting polymer was collected as a dark yellow powder (0.8 g, 78%).  $\nu_{max}$  (cm<sup>-1</sup>): 2214.28, 2002.11, 1614.42, 1506.41, 1400.32, 1323.17, 1176.58, 983.70, 835.18; <sup>1</sup>H NMR (500 MHz, acetone-*d*<sub>6</sub>):  $\delta$  7.49-6.83 (m, 4H, ArH), 3.26-2.58 (m, 3H, CH<sub>3</sub>), 1.84-1.50 (m, 1H, CH<sub>2</sub>), 1.42-1.01 (m, 1H, CH<sub>2</sub>) ppm; <sup>13</sup>C NMR (400 MHz, acetone-*d*<sub>6</sub>): 141.80, 141.68, 141.18, 140.93, 140.57, 140.00, 139.67, 139.26, 136.43, 136.05, 135.65, 125.84, 116.97, 115.12, 113.86, 108.89, 94.23, 59.92, 51.95, 44.78, 21.77, 21.39 ppm; <sup>19</sup>F NMR (400 MHz, acetone-*d*<sub>6</sub>):  $\delta$  -71.20, -71.29, -75.66, -76.14 ppm; BET surface area = 436 m<sup>2</sup> g<sup>-1</sup>; total pore volume = 0.313 ml g<sup>-1</sup> at (P/P<sub>0</sub>=0.98); TGA analysis: initial weight loss due to thermal degradation commences at 451 °C with a 46% loss of mass below 800 °C.

### AO-PIM-FI

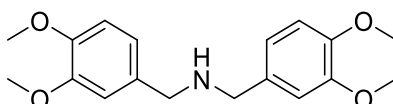


GP 5 was followed, using PIM-FI (0.5 g, 1.22 mmol). The mixture was precipitated in water and washed with acetone, the polymer was collected as a dark brown solid (0.73 g, 94%).  $\nu_{max}$  (cm<sup>-1</sup>): <sup>1</sup>H NMR (500 MHz, MeOD):  $\delta$  7.26-6.52 (m, 4H, ArH), 3.14-2.26 (m, 3H, CH<sub>3</sub>), 1.64-1.39 (m, 1H, CH<sub>2</sub>), 1.25-0.93 (m,

<sup>1</sup>H, CH<sub>2</sub>) ppm; <sup>13</sup>C NMR (400 MHz, acetone-*d*<sub>6</sub>): δ 146.42, 145.60, 140.68, 136.21, 133.75, 124.40, 115.97, 111.74, 103.10, 95.20, 67.49, 51.66, 43.43, 21.56, 21.05 ppm; <sup>19</sup>F NMR (400 MHz, MeOD): δ -71.63, -71.78, -76.82, -77.14 ppm; BET surface area = 0 m<sup>2</sup> g<sup>-1</sup>; total pore volume = 0.005 ml g<sup>-1</sup> at (P/P<sub>0</sub>=0.98); TGA analysis: weight loss due to thermal degradation commences at 253, 412 °C with a 47% loss of mass below 800 °C.

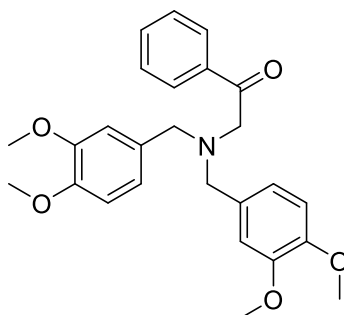
## 9.6 Future work

### Bis(3,4-dimethoxybenzyl)amine <sup>214</sup>



3,4-Dimethoxybenzaldehyde (5.00 g, 32.6 mmol) and 3,4-dimethoxybenzylamine (5.45 g, 32.6 mmol) were dissolved in ethanol (100 mL) and refluxed for 5 hours. The reaction mixture was then cooled to room temperature, sodium borohydride (1.51 g, 40 mmol) was added in small aliquots. The reaction was allowed to continue for another 2 hours. The sodium borohydride was filtered, and the solvent was removed under vacuum. The solid was then dissolved in ethyl acetate, washed with saturated ammonium chloride, water and brine consecutively. The solvent was dried with magnesium sulphate and removed under vacuum. Crude product was obtained as a yellow oil which was then washed in hexane, to afford purified product as a white solid (6.75 g, 65%). Mp: 69 °C (Lit: 69 °C<sup>214</sup>);  $\nu_{max}$  (cm<sup>-1</sup>): 3007.25, 2980.17, 1681.54, 1593.65, 1452.97, 1275.03, 1249.45, 1234.36, 1020.11; <sup>1</sup>H NMR (400 MHz, CDCl<sub>3</sub>): δ 7.00 (d, J = 1.4 Hz, 2H, ArH), 6.91-6.82 (m, 4H, ArH), 3.79 (s, 6H, CH<sub>3</sub>), 3.78 (s, 6H, CH<sub>3</sub>), 3.69 (s, 4H, CH<sub>2</sub>) ppm; <sup>13</sup>C NMR (126 MHz, CDCl<sub>3</sub>): δ 149.04, 148.07, 133.10, 120.28, 111.47, 111.10, 55.90, 52.95 ppm.

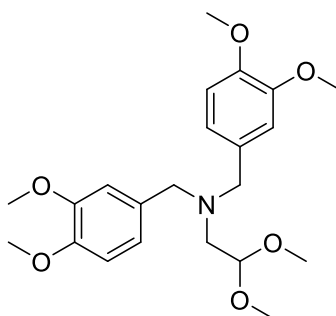
### Bis(3,4-dimethoxybenzyl)phenacylamine <sup>219</sup>



Bis(3,4-dimethoxybenzyl)amine (6.50 g, 20.5 mmol), phenacyl bromide (4.08 g, 20.5 mmol) were dissolved in anhydrous dichloromethane (100 mL) at room temperature. Anhydrous potassium carbonate (0.708 g, 5.12 mmol) was added to the mixture and reacted for 4 hours. The solvent was

removed under vacuum, the solid obtained was redissolved in diethyl ether and washed with water. The organic layer was dried under vacuum. Column chromatography was run to collect the product as an orange oil (2.05 g, 23%).  $\nu_{max}$  (cm<sup>-1</sup>): 3068.21, 2925.44, 1694.58, 1556.70, 1539.21, 1476.53, 1303.21, 1019.26; <sup>1</sup>H NMR (400 MHz, CDCl<sub>3</sub>):  $\delta$  7.27 (d, J = 2.1 Hz, 2H, ArH), 6.92 (d, J = 2.1 Hz, 1H, ArH), 6.90 (d, J = 2.0 Hz, 1H, ArH), 6.79 (s, 1H, ArH), 6.77 (s, 1H, ArH), 3.94 (s, 6H, CH<sub>3</sub>), 3.82 (t, J = 5.4 Hz, 4H, CH<sub>2</sub>), 3.79 (s, 6H, CH<sub>3</sub>) ppm; <sup>13</sup>C NMR (126 MHz, CDCl<sub>3</sub>):  $\delta$  149.96, 149.57, 123.26, 121.93, 113.47, 111.05, 56.66, 55.93, 48.74 ppm.

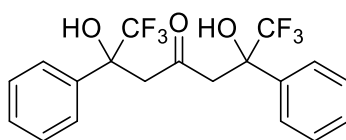
## 2-[Bis(3,4-dimethoxyphenyl)methylamino]-1-phenylethanone



17

3,4-Dimethoxybenzaldehyde (1.00 g, 6.00 mmol) and aminoacetaldehyde dimethyl acetyl (0.633 g, 6.00 mmol) were dissolved in chloroform (50ml). NaBH(OAc)<sub>3</sub> (1.90 g, 9 mmol) were added and the mixture was stirred for 2 hours at room temperature. Another aliquot of 3,4-dimethoxybenzaldehyde (1.00 g, 6.00 mmol) and NaBH(OAc)<sub>3</sub> (1.90 g, 9.00 mmol) was added to the mixture, and the reaction was allowed to stir for a further 8 hours, at room temperature. The reaction mixture was then quenched with sat. NaHCO<sub>3</sub> and the aqueous layer was extracted with EtOAc. The mixture was recrystallised in Et<sub>2</sub>O, to obtain the pure product as a white solid (1.31 g, 27%). Mp: 69 °C <sup>1</sup>H NMR (400 MHz, CDCl<sub>3</sub>):  $\delta$  6.96 (d, J = 1.88 Hz, 2H, ArH), 6.86 (dd, J = 1.86, 8.14 Hz, 2H, ArH), 6.79 (d, J = 8.19 Hz, 2H, ArH), 4.47 (t, J = 5.23 Hz, 1H, CH), 3.88 (s, 3H, CH<sub>3</sub>), 3.86 (s, 3H, CH<sub>3</sub>), 3.59 (s, 4H, CH<sub>2</sub>) ppm; <sup>13</sup>C NMR (126 MHz, CDCl<sub>3</sub>):  $\delta$  148.97, 148.12, 132.30, 121.03, 112.16, 110.94, 103.70, 58.69, 56.05, 55.89, 54.93, 53.45 ppm.

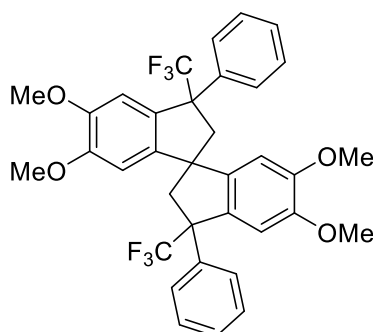
### 1,1,1,7,7,7-Hexafluoro-2,6-dihydroxy-2,6-diphenyl-heptan-4-one



18

2,2,2-Trifluoroacetonephenone (22 mL, 100 mmol), acetone (2 mL, 44.0 mmol) and 1,8-diazabicyclo[5.4.0]undec-7-ene (1.34 g, 8.80 mmol) were added together and stirred under inert atmosphere. Two more additions of acetone (2 mL, 44.0 mmol) were added after 2 days and 4 days of reaction, the reaction mixture was allowed to react for a total of 1 week to obtain a gel-like mixture. Vacuum distillation was carried out and 1,1,1,7,7,7,-hexafluoro-2,6-dihydroxy-2,6-diphenyl-heptan-4-one (5.20 g, 29%) was distilled off initially as a clear oil, which then solidified into creamy-white solids Mp: 74 °C;  $\nu_{max}$  (cm<sup>-1</sup>): 3460.30, 3066.82, 1712.79, 1404.18, 1340.53, 1165.00, 1134.14, 1060.85, 705.95; <sup>1</sup>H NMR (400 MHz, acetone-*d*<sub>6</sub>):  $\delta$  7.70-7.64 (m, 4H, ArH), 7.44-7.34 (m, 6H, ArH), 5.85 (br s, 2H, OH), 3.64 (d, J = 17.0 Hz, 2H, CH<sub>2</sub>), 3.32 (d, J = 17.0 Hz, 2H, CH<sub>2</sub>) ppm; <sup>13</sup>C NMR (400 MHz, acetone-*d*<sub>6</sub>):  $\delta$  207.95, 206.12, 138.70, 129.35, 129.02, 127.48, 124.61, 76.77 (q, J = 26.8 Hz), 46.33, 31.72 ppm; <sup>19</sup>F NMR (400 MHz, acetone-*d*<sub>6</sub>):  $\delta$  -81.1 (s, 6F, CF<sub>3</sub>) ppm; HRMS (EI, m/z): calculated C<sub>19</sub>H<sub>16</sub>F<sub>6</sub>O<sub>3</sub>, 406.09982, found 406.098877 [M<sup>+</sup>].

### Diphenyl-bis(trifluoromethyl) bisindane monomer (FI-3)



Compound **18** (0.50 g, 1.23 mmol) and veratrole (0.34 g, 2.46 mmol) were dissolved in minimal amount of anhydrous DCM, and the mixture was then added to a stirred solution containing catalytic amount of triflic acid in 3 ml TFA acid. The reaction was stirred at room temperature for 24 hours, then poured into water, and extracted with DCM. The organic layer was then extracted with water again, followed by NaHCO<sub>3</sub>. The mixture was dried over MgSO<sub>4</sub>, and the solvent were removed under vacuum. The crude product was stirred in hexane, a white solid was collected with a yield of 23%. Mp: 91 °C;  $\nu_{max}$  (cm<sup>-1</sup>): <sup>1</sup>H NMR (400 MHz, CDCl<sub>3</sub>):  $\delta$  7.52-7.46 (m, 2H, ArH), 7.33 (td, J = 1.66, 7.32 Hz, 2H, ArH), 7.30-7.22 (m, 2H, ArH), 6.96-6.89 (m, 2H, ArH), 6.82 (dd, J = 2.13, 8.37 Hz, 2H, ArH), 6.78 (d, J = 8.39 Hz, 2H,

*ArH*), 6.63 (d,  $J = 2.13$ , 2H, *ArH*), 3.84 (s, 6H,  $-OCH_3$ ), 3.77 (s, 6H,  $-OCH_3$ ), 1.74 (s, 4H,  $CH_2$ ) ppm;  $^{13}C$  NMR (400 MHz,  $CDCl_3$ ): 153.25, 149.11, 148.43, 147.78, 136.87, 132.87, 131.76 (q,  $J_{C-F} = 34.27$  Hz,  $CF_3$ ), 128.55, 126.81, 123.46, 121.16, 118.32, 111.44, 110.15, 56.10, 56.02, 56.01, 22.47 ppm;  $^{19}F$  NMR (400 MHz,  $CDCl_3$ ):  $\delta$  -64.52 (s, 6F,  $CF_3$ ) ppm; HRMS (EI,  $m/z$ ): calculated  $C_{35}H_{30}F_6O_4$ , 628.20483, found 668.1754 [ $M^+ + K$ ].



## References

- 1 J. Rouquerol, D. Avnir, C. W. Fairbridge, D. H. Everett, J. M. Haynes, N. Pernicone, J. D. F. Ramsay, K. S. W. Sing and K. K. Unger, *Pure Appl. Chem.*, 1994, **66**, 1739–1758.
- 2 R. M. Firdaus, A. Desforges, A. Rahman Mohamed and B. Vigolo, *J. Clean. Prod.*, 2021, **328**, 129553.
- 3 X. Li, L. Zhang, Z. Yang, P. Wang, Y. Yan and J. Ran, *Sep. Purif. Technol.*, 2020, **235**, 116213.
- 4 W. S. Chai, J. Y. Cheun, P. S. Kumar, M. Mubashir, Z. Majeed, F. Banat, S.-H. Ho and P. L. Show, *J. Clean. Prod.*, 2021, **296**, 126589..
- 5 S. De Gisi, G. Lofrano, M. Grassi and M. Notarnicola, *Sustain. Mater. Technol.*, 2016, **9**, 10–40.
- 6 M. Atif, H. Z. Haider, R. Bongiovanni, M. Fayyaz, T. Razzaq and S. Gul, *Surf. Interfaces.*, 2022, **31**, 102080.
- 7 Y. He, L. Yin, N. Yuan and G. Zhang, *J. Chem. Eng.*, 2024, **481**, 148754.
- 8 S. Karimi, M. Tavakkoli Yarak and R. R. Karri, *Renewable Sustainable Energy Rev.*, 2019, **107**, 535–553.
- 9 H. Bashiri and S. Orouji, *Theor Chem Acc.*, 2014, **134**, 1594.
- 10 K. S. W. Sing, *Pure Appl. Chem.*, 1985, **57**, 603–619.
- 11 K. S. W. Sing, *Advances in Colloid and Interface Science.*, 1998, **76–77**, 3–11.
- 12 K. K. Mohanty, *AIChE Journal.*, 1992, **38**, 1303–1304.
- 13 R. W. Smithwick, *Powder Technol.*, 1982, **33**, 201–209.
- 14 I. Langmuir, *J. Am. Chem. Soc.*, 1917, **39**, 1848–1906.
- 15 M. E. Davis, *Nature.*, 2002, **417**, 813–821.
- 16 T. D. Bennett, F.-X. Coudert, S. L. James and A. I. Cooper, *Nat. Mater.*, 2021, **20**, 1179–1187.
- 17 A. G. Slater and A. I. Cooper, *Science.*, 2015, **348**, aaa8075.
- 18 K. Chen, S. Hesam Mousavi, R. Singh, R. Q. Snurr, G. Li and P. A. Webley, *Chem. Soc. Rev.*, 2022, **51**, 1139–1166.
- 19 N. Prasetya, N. F. Himma, P. D. Sutrisna, I. G. Wenten and B. P. Ladewig, *Chem. Eng. J.*, 2020, **391**, 123575.
- 20 S. J. Allen, L. Whitten and G. McKay, *Dev. Chem. Eng. Mineral Process.*, 1998, **6**, 231–261.
- 21 T. Cam Quyen Ngo, T. Kim Ngan Tran, H. Dung Chau and B. Ngoc Hoang, *Materials Today: Proceedings.*, 2023, **03**, 511.
- 22 A. Ahmadpour and D. D. Do, *Carbon*, 1996, **34**, 471–479.
- 23 M. Danish and T. Ahmad, *Renewable and Sustainable Energy Reviews.*, 2018, **87**, 1–21.
- 24 Z. Heidarinejad, M. H. Dehghani, M. Heidari, G. Javedan, I. Ali and M. Sillanpää, *Environ Chem Lett.*, 2020, **18**, 393–415.

- 25 *Activated Carbon Progress and Applications*, ed. C. Verma and M. A. Quraishi, The Royal Society of Chemistry, 2023, pp. P001-P004.
- 26 P. J. F. Harris, Z. Liu and K. Suenaga, *J. Phys.: Condens. Matter*, 2008, **20**, 362201.
- 27 C. S. Allen, F. Ghamouss, O. Boujibar and P. J. F. Harris, *Proc. R. soc. Lond. Ser. A-Contain.*, 2022, **478**, 20210580.
- 28 W. Gu and G. Yushin, *WIREs Energy and Environment*, 2014, **3**, 424–473.
- 29 J. Lan, B. Wang, C. Bo, B. Gong and J. Ou, *J. Ind. Eng. Chem.*, 2023, **120**, 47–72.
- 30 M. Lewoyehu, *J. Clean. Prod.* 2021, **159**, 105279.
- 31 S. Wong, N. Ngadi, I. M. Inuwa and O. Hassan, *J. Clean. Prod.*, 2018, **175**, 361–375.
- 32 A. A. Abd, M. R. Othman and J. Kim, *Environ Sci Pollut Res.*, 2021, **28**, 43329–43364.
- 33 A. F. Masters and T. Maschmeyer, *Microporous and Mesoporous Mater.*, 2011, **142**, 423–438.
- 34 S.M. Alexa-Stratulat, I. Olteanu, A.-M. Toma, C. Pastia, O.-M. Banu, O.C. Corbu and I.-O. Toma, *Coatings*, 2024, **14**, 18.
- 35 A. Corma, M. J. Díaz-Cabañas, J. Martínez-Triguero, F. Rey and J. Rius, *Nature*, 2002, **418**, 514–517.
- 36 B. M. Weckhuysen and J. Yu, *Chem. Soc. Rev.*, 2015, **44**, 7022–7024.
- 37 T. Nakano and Y. Nozue, *JCM*, 2008, **7**, 443–462.
- 38 A. Campanile, B. Liguori, C. Ferone, D. Caputo and P. Aprea, *Sci Rep.*, 2022, **12**, 3686.
- 39 T. A. Aragaw and A. A. Ayalew, *Water pract.*, 2018, **14**, 145–159.
- 40 R. de A. Bessa, L. de S. Costa, C. P. Oliveira, F. Bohn, R. F. do Nascimento, J. M. Sasaki and A. R. Loiola, *Microporous and Mesoporous Mater.*, 2017, **245**, 64–72.
- 41 F. Collins, A. Rozhkovskaya, J. G. Outram and G. J. Millar, *Microporous and Mesoporous Mater.*, 2020, **291**, 109667.
- 42 L. F. de Magalhães, G. R. da Silva and A. E. C. Peres, *Adsorption Science & Technol.*, 2022, **2022**, e4544104.
- 43 S. Montalvo, C. Huiliñir, R. Borja, E. Sánchez and C. Herrmann, *Bioresour. Technol.*, 2020, **301**, 122808.
- 44 J. Shi, Z. Yang, H. Dai, X. Lu, L. Peng, X. Tan, L. Shi and R. Fahim, *Water Sci Technol.*, 2018, **2017**, 621–635.
- 45 L. Wu, W. Fan, X. Wang, H. Lin, J. Tao, Y. Liu, J. Deng, L. Jing and H. Dai, *Catalysts*, 2023, **13**, 604.
- 46 Z. Magyarová, M. Králik and T. Soták, *Monatsh Chem.*, 2023, **154**, 815–835.
- 47 Y. Li and J. Yu, *Nat Rev Mater.*, 2021, **6**, 1156–1174.
- 48 H. Pan, C. Yu, X. Suo, L. Yang, X. Cui and H. Xing, *Mater. Chem. Front.*, 2023, **7**, 6463–6482..

- 49 C. C. H. Lin, K. A. Dambrowitz and S. M. Kuznicki, *The Canadian Journal of Chemical Engineering*, 2012, **90**, 207–216.
- 50 O. M. Yaghi, G. Li and H. Li, *Nature*, 1995, **378**, 703–706.
- 51 H. Li, M. Eddaoudi, M. O’Keeffe and O. M. Yaghi, *Nature*, 1999, **402**, 276–279.
- 52 M. Ding, X. Cai and H.-L. Jiang, *Chem Sci.*, 2019, **10**, 10209–10230.
- 53 A. J. Howarth, Y. Liu, P. Li, Z. Li, T. C. Wang, J. T. Hupp and O. K. Farha, *Nat Rev Mater.*, 2016, **1**, 1–15.
- 54 O. M. Yaghi, M. O’Keeffe, N. W. Ockwig, H. K. Chae, M. Eddaoudi and J. Kim, *Nature*, 2003, **423**, 705–714.
- 55 B. Li, H.M. Wen, Y. Cui, W. Zhou, G. Qian and B. Chen, *J. Adv. Mater.*, 2016, **28**, 8819–8860.
- 56 D. Ongari, L. Talirz and B. Smit, *ACS Cent. Sci.*, 2020, **6**, 1890–1900.
- 57 X. Zhang, Z. Chen, X. Liu, S. L. Hanna, X. Wang, R. Taheri-Ledari, A. Maleki, P. Li and O. K. Farha, *Chem Soc Rev.*, 2020, **49**, 7406–7427.
- 58 T. A. Goetjen, J. Liu, Y. Wu, J. Sui, X. Zhang, J. T. Hupp and O. K. Farha, *ChemComm.*, 2020, **56**, 10409–10418.
- 59 A. Bavykina, N. Kolobov, I. S. Khan, J. A. Bau, A. Ramirez and J. Gascon, *Chem Rev.*, 2020, **120**, 8468–8535.
- 60 Iad Pascanu, Greco González Miera, A. Ken Inge, and Belén Martín-Matute, *J. Am. Chem. Soc.*, **2019** *141* (18), 7223–7234.
- 61 H. Li, K. Wang, Y. Sun, C. T. Lollar, J. Li and H.-C. Zhou, *Mater. Today Chem.*, 2018, **21**, 108–121.
- 62 H. Daglar, H. C. Gulbalkan, G. Avci, G. O. Aksu, O. F. Altundal, C. Altintas, I. Erucar and S. Keskin, *Angew. Chem. Int. Ed.*, 2021, **60**, 7828–7837.
- 63 J. Cao, X. Li and H. Tian, *Curr. Med. Chem.*, 2020, **27**, 5949–5969.
- 64 K. Suresh and A. J. Matzger, *Angew. Chem. Int. Ed.*, 2019, **58**, 16790–16794.
- 65 M.X. Wu and Y.-W. Yang, *Adv. Mater.*, 2017, **29**, 1606134.
- 66 E. A. Dolgoplova, A. M. Rice, C. R. Martin and N. B. Shustova, *Chem. Soc. Rev.*, 2018, **47**, 4710–4728.
- 67 W. Cheng, X. Tang, Y. Zhang, D. Wu and W. Yang, *Trends Food Sci. Tech.*, 2021, **112**, 268–282.
- 68 L. J. Small, S. E. Henkelis, D. X. Rademacher, M. E. Schindelholz, J. L. Krumhansl, D. J. Vogel and T. M. Nenoff, *Adv. Funct. Mater.*, 2020, **30**, 2006598.
- 69 A. P. Côté, A. I. Benin, N. W. Ockwig, M. O’Keeffe, A. J. Matzger and O. M. Yaghi, *Science*, 2005, **310**, 1166–1170.
- 70 H. M. El-Kaderi, J. R. Hunt, J. L. Mendoza-Cortés, A. P. Côté, R. E. Taylor, M. O’Keeffe and O. M. Yaghi, *Science*, 2007, **316**, 268–272.

- 71 M. Alharbi, R. Aljohani, R. Alzahrani, Y. Alsufyani and N. Alsmami, *Comput. Chem.*, 2023, **11**, 53–66.
- 72 M.-X. Wu and Y.-W. Yang, *Chin. Chem. Lett.*, 2017, **28**, 1135–1143.
- 73 Y. Yusran, H. Li, X. Guan, Q. Fang and S. Qiu, *EnergyChem.*, 2020, **2**, 100035.
- 74 S. Kumar, B. Z. Dholakiya and R. Jangir, *ACS Appl. Mater. Interfaces.*, 2024, **16**, 1, 1553–1563
- 75 S. Jiang, L. Meng, W. Ma, G. Pan, W. Zhang, Y. Zou, L. Liu, B. Xu and W. Tian, *Mater. Chem. Front.*, 2021, **5**, 4193–4201.
- 76 X. Liu, D. Huang, C. Lai, G. Zeng, L. Qin, H. Wang, H. Yi, B. Li, S. Liu, M. Zhang, R. Deng, Y. Fu, L. Li, W. Xue and S. Chen, *Chem Soc Rev.*, 2019, **48**, 5266–5302.
- 77 Y. Zhou, Z. Wang, P. Yang, X. Zu and F. Gao, *J. Mater. Chem.*, 2012, **22**, 16964–16970.
- 78 N. Sinha and S. Pakhira, *ACS Appl. Electron. Mater.*, 2021, **3**, 720–732.
- 79 M. P. Tsyurupa, Z. K. Blinnikova, N. A. Proskurina, A. V. Pastukhov, L. A. Pavlova and V. A. Davankov, *Nanotechnol Russia.*, 2009, **4**, 665–675.
- 80 M. P. Tsyurupa and V. A. Davankov, *React. Funct. Polym.*, 2002, **53**, 193–203.
- 81 L. Tan and B. Tan, *Chem Soc Rev.*, 2017, **46**, 3322–3356.
- 82 B. C. Pan, Y. Xiong, A. M. Li, J. L. Chen, Q. X. Zhang and X. Y. Jin, *React. Funct. Polym.*, 2002, **53**, 63–72.
- 83 S. S. Reddy, R. M. N. Kalla, A. Varyambath and I. Kim, *Catal. Commun.*, 2019, **126**, 15–20.
- 84 A. Hu, X. Yang, Q. You, Y. Liu, Q. Wang, G. Liao and D. Wang, *J Mater Sci.*, 2019, **54**, 2712–2728.
- 85 H. Masoumi, A. Ghaemi and H. G. Gilani, *Separation and Purification Technol.*, 2021, **260**, 118221.
- 86 G. Ji, Z. Yang, X. Yu, Y. Zhao, F. Zhang and Z. Liu, *ACS Sustainable Chem. Eng.*, 2020, **8**, 16320–16326.
- 87 O. Manaenkov, L. Nikoshvili, A. Bykov, O. Kislitsa, M. Grigoriev, M. Sulman, V. Matveeva and L. Kiwi-Minsker, *Mol.*, 2023, **28**, 8126.
- 88 J. Gu, Y. Yuan, T. Zhao, F. Liu, Y. Xu and D.-J. Tao, *Separation and Purification Technol.*, 2022, **301**, 121971.
- 89 L. Shao, S. Wang, M. Liu, J. Huang and Y.-N. Liu, *J. Chem. Eng.*, 2018, **339**, 509–518.
- 90 P. M. Budd, B. S. Ghanem, S. Makhseed, N. B. McKeown, K. J. Msayib and C. E. Tattershall, *ChemComm.*, 2004, **0**, 230–231.
- 91 N. B. McKeown, *Polym J*, 2020, **202**, 122736.
- 92 T. M. Long and T. M. Swager, *Adv. Mater.*, 2001, **13**, 601–604.
- 93 G. Genduso, B. Ghanem, Y. Wang and I. Pinnau, *Polym. J.*, 2019, **11**, 361.
- 94 M. Heuchel, D. Fritsch, P. M. Budd, N. B. McKeown and D. Hofmann, *J. Membr. Sci.*, 2008, **318**, 84–99.
- 95 C. Pathak, A. Gogoi, A. Devi and S. Seth, *Chem. Eur. J.*, 2023, **29**, e202301512.

- 96 N. B. McKeown, *Int. Sch. Res. Notices.*, **2012**, e513986.
- 97 C. Grazia Bezzu, M. Carta, M.-C. Ferrari, J. C. Jansen, M. Monteleone, E. Esposito, A. Fuoco, K. Hart, T. P. Liyana-Arachchi, C. M. Colina and N. B. McKeown, *J. Mater. Chem.*, 2018, **6**, 10507–10514.
- 98 X. Ma, O. Salinas, E. Litwiller and I. Pinnau, *Macromol.*, 2013, **46**, 9618–9624.
- 99 I. Rose, M. Carta, R. Malpass-Evans, M.-C. Ferrari, P. Bernardo, G. Clarizia, J. C. Jansen and N. B. McKeown, *ACS Macro Lett.*, 2015, **4**, 912–915.
- 100 B. S. Ghanem, M. Hashem, K. D. M. Harris, K. J. Msayib, M. Xu, P. M. Budd, N. Chaukura, D. Book, S. Tedds, A. Walton and N. B. McKeown, *Macromol.*, 2010, **43**, 5287–5294.
- 101 I. Rose, C. G. Bezzu, M. Carta, B. Comesaña-Gándara, E. Lasseuguette, M. C. Ferrari, P. Bernardo, G. Clarizia, A. Fuoco, J. C. Jansen, K. E. Hart, T. P. Liyana-Arachchi, C. M. Colina and N. B. McKeown, *Nature Mater.*, 2017, **16**, 932–937.
- 102 C.-H. Chou, D. S. Reddy and C.-F. Shu, *J. Polym. Sci.*, 2002, **40**, 3615–3621.
- 103 H. Sanaeepur, A. Ebadi Amooghin, S. Bandehali, A. Moghadassi, T. Matsuura and B. Van der Bruggen, *Prog. Polym. Sci.*, 2019, **91**, 80–125.
- 104 S. Sridhar, R. S. Veerapur, M. B. Patil, K. B. Gudasi and T. M. Aminabhavi, *J. Appl. Polym. Sci.*, 2007, **106**, 1585–1594.
- 105 B. S. Ghanem, N. B. McKeown, P. M. Budd, N. M. Al-Harbi, D. Fritsch, K. Heinrich, L. Starannikova, A. Tokarev and Y. Yampolskii, *Macromol.*, 2009, **42**, 7881–7888.
- 106 Ö. V. Rúnarsson, J. Artacho and K. Wärnmark, *EurJOC*, 2012, **2012**, 7015–7041.
- 107 Carta M, Malpass-Evans R, Croad M, Rogan Y, Jansen JC, Bernardo P, Bazzarelli F, McKeown NB. *Science*. 2013, **339**, 303-307.
- 108 M. Lee, C. G. Bezzu, M. Carta, P. Bernardo, G. Clarizia, J. C. Jansen and N. B. McKeown, *Macromol.*, 2016, **49**, 4147–4154.
- 109 H. Guo, X. Hu, T. Zheng, Z. Wang and J. Yan, *Eur. Polym. J.*, 2023, **193**, 112100.
- 110 H. Zhou and W. Jin, *Membranes.*, 2019, **9**, 3.
- 111 P. M. Budd, K. J. Msayib, C. E. Tattershall, B. S. Ghanem, K. J. Reynolds, N. B. McKeown and D. Fritsch, *J. Membr. Sci.*, 2005, **251**, 263–269.
- 112 P. Agarwal, R. E. Hefner, S. Ge, I. Tomlinson, Y. Rao and T. Dikic, *J. Membr. Sci.*, 2020, **595**, 117501.
- 113 F. Topuz, B. Satilmis and T. Uyar, *Polym. J.*, 2019, **178**, 121610.
- 114 N. B. McKeown, *Curr. Opin. Chem. Eng.*, 2022., **36**, 100785.
- 115 M. Carta, K. J. Msayib, P. M. Budd and N. B. McKeown, *Org. Lett.*, 2008, **10**, 2641–2643.
- 116 P. Yanaranop, B. Santoso, R. Etzion and J. Jin, *Polym. J.*, 2020, **194**, 122392.

- 117 M. Tian, S. Rochat, H. Fawcett, A. D. Burrows, C. R. Bowen and T. J. Mays, *Adsorption*, 2020, **26**, 1083–1091.
- 118 N. Du, H. B. Park, G. P. Robertson, M. M. Dal-Cin, T. Visser, L. Scoles and M. D. Guiver, *Nature Mater.*, 2011, **10**, 372–375.
- 119 B. Satilmis and P. M. Budd, *J. Colloid Interface Sci.*, 2017, **492**, 81–91.
- 120 M. Carta, M. Croad, R. Malpass-Evans, J. C. Jansen, P. Bernardo, G. Clarizia, K. Friess, M. Lanč and N. B. McKeown, *Adv Mater.*, 2014, **26**, 3526–3531.
- 121 B. Comesaña-Gándara, J. Chen, C. Grazia Bezzu, M. Carta, I. Rose, M.-C. Ferrari, E. Esposito, A. Fuoco, J. C. Jansen and N. B. McKeown, *Energy Environ Sci*, 2019, **12**, 2733–2740.
- 122 C. Ma and J. Urban, *Proceedings of the Nature Research Society*, 2018, **2**, 02002.
- 123 M. A. Abdulhamid and G. Szekely, *Curr. Opin. Chem. Eng.*, 2022, **36**, 100804.
- 124 D. Ramimoghadam, E. M. Gray and C. J. Webb, *Int. J. Hydrogen Energy.*, 2016, **41**, 16944–16965.
- 125 F. Topuz, M. H. Abdellah, P. M. Budd and M. A. Abdulhamid, *Polym Rev.*, 2023, **0**, 1–55.
- 126 P. Pullumbi, F. Brandani and S. Brandani, *Curr. Opin. Chem. Eng.*, 2019, **24**, 131–142.
- 127 A. Sattari, A. Ramazani, H. Aghahosseini and M. K. Aroua, *J. CO<sub>2</sub> Util.*, 2021, **48**, 101526.
- 128 L. Zhu, D. Shen and K. H. Luo, *J. Hazard. Mater.*, 2020, **389**, 122102.
- 129 S. Liu, Y. Peng, J. Chen, T. Yan, Y. Zhang, J. Liu and J. Li, *J. Hazard. Mater.*, 2020, **382**, 121103.
- 130 Y. Wang, X. Ma, B. S. Ghanem, F. Alghunaimi, I. Pinnau and Y. Han, *Mater. Today. Nano.*, 2018, **3**, 69–95.
- 131 C. R. Mason, L. Maynard-Atem, K. W. J. Heard, B. Satilmis, P. M. Budd, K. Friess, M. Lanč, P. Bernardo, G. Clarizia and J. C. Jansen, *Macromol.*, 2014, **47**, 1021–1029.
- 132 C. R. Mason, L. Maynard-Atem, N. M. Al-Harbi, P. M. Budd, P. Bernardo, F. Bazzarelli, G. Clarizia and J. C. Jansen, *Macromol.*, 2011, **44**, 6471–6479.
- 133 D. Saha and M. J. Kienbaum, *Microporous and Mesoporous Mater.*, 2019, **287**, 29–55.
- 134 L. Spessato, V. A. Duarte, J. M. Fonseca, P. A. Arroyo and V. C. Almeida, *J. CO<sub>2</sub> Util.*, 2022, **61**, 102013.
- 135 H. A. Patel and C. T. Yavuz, *Chem. Commun.*, 2012, **48**, 9989–9991.
- 136 Yu. S. Simanenko, T. M. Prokop'eva, I. A. Belousova, A. F. Popov and E. A. Karpichev, *Theor. Exp. Chem.*, 2001, **37**, 288–295.
- 137 V. G. Snider and C. L. Hill, *J. Hazard. Mater.*, 2023, **442**, 130015.
- 138 D. Jung, K. O. Kirlikovali, Z. Chen, K. B. Idrees, A. Atilgan, R. Cao, T. Islamoglu and O. K. Farha, *ACS Materials Lett.*, 2021, **3**, 320–326.
- 139 E. Madrid, D. J. Lowe, K. J. Msayib, N. Mckeown, Q. Song, G. A. Attard, T. Duren and F. Marken, *ChemElectroChem.*, 2019, **6**, 252.

- 140 N. Mehio, M. A. Lashely, J. W. Nugent, L. Tucker, B. Correia, C.-L. Do-Thanh, S. Dai, R. D. Hancock and V. S. Bryantsev, *J. Phys. Chem. B.*, 2015, **119**, 3567–3576.
- 141 T. M. Prokop'eva, Yu. S. Simanenko, E. A. Karpichev, V. A. Savelova and A. F. Popov, *Russ J Org Chem*, 2004., **40**, 1617–1629.
- 142 R. G. D. Taylor, C. G. Bezzu, M. Carta, K. J. Msayib, J. Walker, R. Short, B. M. Kariuki and N. B. McKeown, *Chemistry A European J.*, 2016, **22**, 2466–2472.
- 143 L. Chen, L. Bromberg, T. A. Hatton and G. C. Rutledge, *Polym. J.*, 2007, **48**, 4675–4682.
- 144 A. Głębocka, E. D. Raczyńska, A. Chylewska and M. Makowski, *J. Phys. Org. Chem.*, 2016, **29**, 326–335.
- 145 L. Yao, A. Grishaev, G. Cornilescu and A. Bax, *J. Am. Chem. Soc.*, 2010, **132**, 10866–10875.
- 146 A. S. Novikov and D. S. Bolotin, *J. Phys. Org. Chem.*, 2018, **31**, 3772.
- 147 B. Petrovic, M. Gorbounov and S. Masoudi Soltani, *Microporous and Mesoporous Mater.*, 2021, **312**, 110751.
- 148 N. Bhardwaj and S. C. Kundu, *Biotechnol. Adv.* 2010, **28**, 325–347.
- 149 A. Baji, K. Agarwal and S. V. Oopath, *Polym J.*, 2020, **12**, 492.
- 150 R. Haddad, A. Roostaie, M. Haddad and M. Mogharabi, *Iran. J. Chem. Chem. Eng.*, 2023, **5**, 123–130.
- 151 Y. Li, J. Zhu, H. Cheng, G. Li, H. Cho, M. Jiang, Q. Gao and X. Zhang, *Adv. Mater. Technol.*, 2021, **6**, 2100410.
- 152 A. Arabi Shamsabadi, M. Rezakazemi, F. Seidi, H. Riazi, T. Aminabhavi and M. Soroush, *PECS*, 2021, **84**, 100903.
- 153 L. M. Robeson, *J. Membr. Sci.*, 1991, **62**, 165–185.
- 154 L. M. Robeson, *J. Membr. Sci.*, 2008, **320**, 390–400.
- 155 R. Swaidan, B. Ghanem and I. Pinnau, *ACS Macro Lett.*, 2015, **4**, 947–951.
- 156 F. H. Allen, O. Kennard, D. G. Watson, L. Brammer, A. G. Orpen and R. Taylor, *J. Chem. Soc., Perkin Trans. 2*, 1987, S1–S19.
- 157 *Gas Separation Membranes: Polymeric and Inorganic*, Ed. A. Ismail, K. Khulbe and T. Matsuura, 2015, Springer International Publishing Switzerland.
- 158 M. Liu, X. Lu, M. D. Nothling, C. M. Doherty, L. Zu, J. N. Hart, P. A. Webley, J. Jin, Q. Fu and G. G. Qiao, *ACS Materials Lett.*, 2020, **2**, 993–998.
- 159 R. Swaidan, B. Ghanem, E. Litwiller and I. Pinnau, *Macromol.*, 2015, **48**, 6553–6561.
- 160 R. Castaldo, G. Gentile, M. Avella, C. Carfagna and V. Ambrogio, *Polym J.*, 2017, **9**, 651.
- 161 N. B. McKeown and P. M. Budd, *Macromol.*, 2010, **43**, 5163–5176.
- 162 Y. Jiao, F. H. Stillinger and S. Torquato, *Phys. Rev. Lett.*, 2008, **100**, 245504.

- 163 Y. Jiao, F. H. Stillinger and S. Torquato, *Phys. Rev. E.*, 2009, **79**, 041309.
- 164 C. G. Bezzu, A. Fuoco, E. Esposito, M. Monteleone, M. Longo, J. C. Jansen, G. S. Nichol and N. B. McKeown, *Adv. Funct. Mater.*, 2021, **31**, 2104474.
- 165 M. K. Amin, C. Ye, S. Pang, Y. Liu, G. Nichol and N. McKeown, *ChemRxiv*. 2023.
- 166 P. Zhang, H. Chu, X. Li, W. Feng, P. Deng, L. Yuan and B. Gong, *Org. Lett.*, 2011, **13**, 54–57.
- 167 E. Romero, S. Oueslati, M. Benchekroun, A. C. A. D'Hollander, S. Ventre, K. Vijayakumar, C. Minard, C. Exilie, L. Tlili, P. Retailleau, A. Zavala, E. Elisée, E. Selwa, L. A. Nguyen, A. Pruvost, T. Naas, B. I. Iorga, R. Dodd and K. Cariou, 2020.
- 168 V. I. Maslennikova, L. V. Shelenkova, O. S. Serkova, L. K. Vasyanina and E. E. Nifantiev, *Arkivoc.*, **2012**, 136–149.
- 169 S.-H. Hsiao and J.-S. Han, *J. Polym. Sci. Part A: Polym. Chem.*, 2017, **55**, 1409–1421.
- 170 C. Hansch, *Chem. rev.*, Vol.91(2), p.165-195.
- 171 A. Devarajan, E. D. Asuquo, M. Z. Ahmad, A. B. Foster and P. M. Budd, *ACS Appl. Polym. Mater.*, 2021, **3**, 3485–3495.
- 172 C. Wang, F. Guo, H. Li, J. Xu, J. Hu, H. Liu and M. Wang, *J. Membr. Sci.*, 2020, **598**, 117677.
- 173 R. Swaidan, B. S. Ghanem, E. Litwiller and I. Pinnau, *J. Membr. Sci.*, 2014, **457**, 95–102.
- 174 S. Beveridge, C. A. McAnally, G. S. Nichol, A. R. Kennedy, E. J. Cussen and A. J. Fletcher, *Cryst.*, 2020, **10**, 548.
- 175 H. Marsh and W. F. K. Wynne-Jones, *Carbon*, 1964, **1**, 269–279.
- 176 V. Presser, J. McDonough, S.-H. Yeon and Y. Gogotsi, *Energy Environ. Sci.*, 2011, **4**, 3059–3066.
- 177 A. Yurduşen, A. Yürüm and Y. Yürüm, *CrystEngComm.*, 2020, **22**, 932–944.
- 178 N. Chanut, S. Bourrelly, B. Kuchta, C. Serre, J.-S. Chang, P. A. Wright and P. L. Llewellyn, *ChemSusChem.*, 2017, **10**, 1543–1553.
- 179 Y. Gensterblum, A. Busch and B. M. Krooss, *Fuel.*, 2014, **115**, 581–588.
- 180 C.-H. Yu, C.-H. Huang and C.-S. Tan, *Aerosol Air Qual. Res.*, 2012, **12**, 745–769.
- 181 E. Lasseguette, M. Carta, S. Brandani and M.-C. Ferrari, *Int. J. Greenhouse Gas Control.*, 2016, **50**, 93–99.
- 182 G. Kupgan, A. G. Demidov and C. M. Colina, *J. Membr. Sci.*, 2018, **565**, 95–103.
- 183 V. F. Cardoso, D. M. Correia, C. Ribeiro, M. M. Fernandes and S. Lanceros-Méndez, *Polym. J.*, 2018, **10**, 161.
- 184 V. H. Dalvi and P. J. Rossky, *Proc Natl Acad Sci USA*, 2010, **107**, 13603–13607.
- 185 J. S. Murray, P. G. Seybold and P. Politzer, *J. Chem. Thermodyn.*, 2021, **156**, 106382.
- 186 A. H. Alahmed, M. E. Briggs, A. I. Cooper and D. J. Adams, *J. Mater. Chem.*, 2019, **7**, 549–557.
- 187 C. Wang, J. Zhang and Z. Wang, *ACS Appl. Nano Mater.*, 2021, **4**, 14060–14068.



- 188 H. Chen, Z. Yang, C.-L. Do-Thanh and S. Dai, *ChemSusChem.*, 2020, **13**, 6182–6200.
- 189 M. G. Dhara and S. Banerjee, *Prog. Polym. Sci.* 2010, **35**, 1022–1077.
- 190 T. Furuya, A. S. Kamlet and T. Ritter, *Nature*, 2011, **473**, 470–477.
- 191 X. Lu, D. Jin, S. Wei, M. Zhang, Q. Zhu, X. Shi, Z. Deng, W. Guo and W. Shen, *Nanoscale.*, 2015, **7**, 1002–1012.
- 192 N. Du, G. P. Robertson, J. Song, I. Pinnau, S. Thomas and M. D. Guiver, *Macromol.*, 2008, **41**, 9656–9662.
- 193 S. Banerjee, G. Maier and M. Burger, *Macromol.*, 1999, **32**, 4279–4289.
- 194 K. Hu, Q. Ye, Y. Fan, J. Nan, F. Chen, Y. Gao and Y. Shen, *Eur. Polym. J.*, 2021, **157**, 110566.
- 195 C. Chen, CN110041212A, 2019.
- 196 H. Zhou, CN110105189A, 2019.
- 197 H. Zhou, CN111410617A, 2020.
- 198 T. Komata, K. Matsunaga, Y. Hirotsu, S. Akiba and K. Ogura, *J. Fluor. Chem.*, 2007, **128**, 902–909.
- 199 A. Dei and L. Sorace, *Dalton Trans.*, 2003, **0**, 3382–3386.
- 200 V. K. Pandey and P. Anbarasan, *J. Org. Chem.*, 2014, **79**, 4154–4160
- 201 K. Sato, M. Higashinagata, T. Yuki, A. Tarui, M. Omote, I. Kumadaki and A. Ando, *J. Fluor. Chem.*, 2008, **129**, 51–55.
- 202 T. L. Andrew and T. M. Swager, *J. Org. Chem.*, 2011, **76**, 2976–2993.
- 203 J. S. Ward, A. Danos, P. Stachelek, M. A. Fox, A. S. Batsanov, A. P. Monkman and M. R. Bryce, *Mater. Chem. Front.*, 2020, **4**, 3602–3615.
- 204 T. Ishihara, H. Shinjo, Y. Inoue and T. Ando, *J. Fluor. Chem.*, 1983, **22**, 1–19.
- 205 X. Liu, C. Xu, M. Wang and Q. Liu, *Chem. Rev.*, 2015, **115**, 683–730.
- 206 K. Takahashi, Y. Ano and N. Chatani, *Chem Commun (Camb).*, 2020, **56**, 11661–11664.
- 207 M. S. Said, N. S. Khonde, P. Kumar and J. M. Gajbhiye, *Org. Lett.*, 2023, **25**, 1094–1098.
- 208 R. Craig, S.A. Loscot, J.T. Mohr, D.C. Behenna, A.M. Harned, B.M. Stolz, *Org. Lett.*, 2015, **17**, 5160–5163.
- 209 S. Yamada, K. Kinoshita, S. Iwama, T. Yamazaki, T. Kubota and T. Yajima, *RSC Adv.*, 2013, **3**, 6803–6806.
- 210 B. Cui, H. Sun, Y. Xu, L. Duan and Y.-M. Li, *Tetrahedron Lett.*, 2017, **73**, 6754–6762.
- 211 George. A. Olah, G. K. S. Prakash, Q. Wang, X.-Y. Li, M. Sánchez-Roselló, C. del Pozo Losada and J. L. Aceña, in *e-EROS.*, John Wiley & Sons, Ltd, 2009.
- 212 L. A. Babadzhanova, N. V. Kirij, Yu. L. Yagupolskii, W. Tyrra and D. Naumann, *Tetrahedron Lett.*, 2005, **61**, 1813–1819.

- 213 Olesya V. Khoroshilova, Irina A. Boyarskaya, and Aleksander V. Vasilyev, *J. Org. Chem.*, 2022, **87**, 15845–15862.
- 214 T. Reuillon, A. Bertoli, R. J. Griffin, D. C. Miller and B. T. Golding, *Org. Biomol. Chem.*, 2012, **10**, 7610.
- 215 N. Coşun and L. Büyükuysal, *Heterocycl. Chem.*, 1998, **1**, 53–59.
- 216 D. Zhang and F. Tanaka, *ACS*, 2015, **357**, 3458–3462.
- 217 M. F. Boehm, L. Zhang, B. A. Badea, S. K. White, D. E. Mais, E. Berger, C. M. Suto, M. E. Goldman and R. A. Heyman, *J. Med. Chem.*, 1994, **37**, 2930–2941.
- 218 R. Degutyte, M. Daskeviciene, J. Stumbraite and V. Getautis, *Arkivoc.*, **2009**, 115–122.
- 219 N. Coşkun and F. Tirli, *Synth. Commun.*, 1997, **27**, 1–9.